Volume 3, Issue 3, 2025

Print ISSN: 2960-0251
Online ISSN: 2960-026X

FRONTIERS IN ENVIRONMENTAL RESEARCH

Frontiers in Environmental Research

Volume 3, Issue 3, 2025

Published by Upubscience Publisher

Frontiers in Environmental Research
Print ISSN: 2960-0251 Online ISSN: 2960-026X
Email: info@upubscience.com
Website: http://www.upubscience.com/

Table of Content

Frontiers in Environmental Research
Print ISSN: 2960-0251
Online ISSN: 2960-026X
DOI: https://doi.org/10.61784/fer3033

OPTIMIZATION OF RIPARIAN PLANT COMMUNITIES IN MOUNTAINOUS URBAN PARKS BASED ON THE CONCEPT OF REWILDING — A CASE STUDY OF CHONGQING URBAN AREA

KaiWei Du[1*], ChengJi Shu[2], YuSong Li[3], ZiYi Jiang[4], YunDuo Kang[5]
[1]*School of Architecture and Design,Chongqing College of Humanities, Science & Technology, Chongqing 401524, China.*
[2]*State Key Laboratory of Urban and Regional Ecology, Research Center for Eco-Environmental Sciences, Chinese Academy of Sciences, Beijing 100085, China.*
[3]*Territorial Spatial Planning Service Center, Wenchuan 623000, Sichuan, China.*
[4]*School of Landscape Architecture and Architecture, Zhejiang A&F University, Hangzhou 311300, Zhejiang, China.*
[5]*School of Philosophy, Psychology and Language Sciences, University of Edinburgh, Edinburgh EH8 9AD, United Kingdom.*
Corresponding Author: KaiWei Du, Email: dkwyhy@126.com

Abstract: This study examines the riparian zones of seven representative urban parks in Chongqing, exploring strategies for optimizing plant communities based on the concept of "rewilding." The findings indicate several issues in the current riparian vegetation, including a dominance of cultivated species (accounting for 80.57%), a simplistic community structure (with "tree + herb" combinations comprising 57.94%), and a scarcity of wild species (only 55 species, or 19.43%). These factors result in low biodiversity (average Shannon-Wiener index of 1.52), weak soil and water conservation capacity (soil erosion modulus of 312 t/(km²·a) in areas with a single structure), and landscape homogenization, all of which limit the ecological service functions of these areas. Rewilding refers to enhancing ecosystem self-regulation by reducing human intervention and actively introducing native species. Constraints to rewilding include excessive human interference, habitat fragmentation, invasive plant species, and outdated management practices.Based on this, a series of optimization strategies are proposed, including the selection of native wild plants, the development of multilayered plant communities, the implementation of tiered management and targeted control of invasive species, and the encouragement of public participation, aiming to provide scientific support and practical guidance for the ecological restoration of riparian zones in mountainous cities.
Keywords: Rewilding; Riparian zones; Native plants; Ecological service functions; Mountainous cities

1 INTRODUCTION

Urban waterfront zones are specific areas within cities that border rivers, lakes, or oceans and are classified as part of urban public green spaces [1]. As transitional zones between terrestrial and aquatic ecosystems, they fulfill multiple roles, including ecological regulation, recreational landscaping, and wildlife habitat provision, making them critical nodes for maintaining urban ecological balance. Chongqing, located in southwestern China, is considered a vital ecological barrier in the upper reaches of the Yangtze River due to its unique geographical features. The city's characteristic of being “embraced by mountains and surrounded by rivers” is evident not only in the Yangtze River, which traverses the entire municipality for 691 kilometers, but also in the presence of 374 rivers within its territory, each with a watershed area exceeding 50 square kilometers [2]. As a core component of the city's“blue-green space,”the stability of the ecological services provided by park waterfront zones holds particular importance for the development of the“City of Mountains and Rivers.”In recent years, with the acceleration of urbanization, the plant communities along the riverside park zones in Chongqing’s urban areas have been increasingly affected by human intervention, gradually revealing a contradiction between “landscape prioritization and insufficient ecological function.” For example, some areas rely excessively on a single cultivated species, reducing the natural growing space for wild native plants; community structures have become overly simplified, failing to harness the full ecological benefits of multi-layered vegetation; meanwhile, the unregulated introduction of exotic species poses a potential threat to the stability of local ecosystems. These issues not only hinder the core functions of riverside zones—such as water conservation and biodiversity protection—but also fall short of meeting urban residents’ growing demand for landscapes that reflect a sense of natural wilderness.

From an ecological perspective, plant communities with high species diversity are better able to maintain ecosystem stability [3]. The structural complexity and natural composition of riparian plant communities form the foundation of their ecological service functions. Currently, although the plant arrangements along the riparian zones of urban parks in Chongqing have been designed with landscape aesthetics in mind, there is still room for improvement in enhancing ecological resilience: surveys show that most riparian zones are dominated by artificially pruned tree-grass combinations, with limited use of shrubs and vines, resulting in a simplified vertical structure and reduced capacity for soil and water conservation; the proportion of wild plants is relatively low, and many are removed as “weeds,” which

undermines the ecosystem's ability to regenerate itself; some invasive species, due to their strong adaptability, encroach on the habitats of native species, further diminishing the stability of the plant communities.These phenomena reflect an imbalance between "artificial control" and "natural restoration" in urban waterfront management, highlighting the urgent need for optimization through scientific principles and technological solutions.

Urban rewilding refers to the restoration of natural processes in urban areas by reducing human interference or implementing moderate restoration measures, thereby enhancing the wild characteristics of urban landscapes [4]. The concept of rewilding offers a new approach to resolving this contradiction. Rewilding does not mean returning to a primeval wilderness, but rather stimulating the system's self-regulation capacity by reducing artificial interventions [5]. Its core lies in promoting the natural succession of ecosystems and restoring the natural attributes and self-regulatory capacity of plant communities through minimizing unnecessary human interference, rather than pursuing "complete wilderness."Urban rewilding has gained increasing attention as a strategy to restore ecological processes and enhance biodiversity in cities [6].

For the waterfront greenbelts in urban Chongqing parks, the practical value of rewilding is reflected in three aspects:

(1) Leveraging the ecological adaptability of native plants to enhance the resilience of plant communities to mountainous climates and fluctuations in water levels;

(2) Enhancing soil and water conservation as well as microclimate regulation through the construction of multi-layered vegetation structures;

(3) Preserving a moderate degree of "wildness" in the landscape to fulfill citizens' desire for experiencing natural ecosystems. Spontaneous riparian vegetation plays a vital role in improving the urban ecological environment, increasing biodiversity, restoring natural shorelines, and supporting the development of beautiful rural ecologies and water environments. It holds significant potential for landscape applications. Not only does it help optimize the structure of urban ecosystems and maintain ecological service functions, but it also offers residents opportunities to connect with nature and improve their physical and mental well-being [7]. Moreover, it has broad application prospects in addressing global challenges such as biodiversity loss and climate change [8].

Based on this, the study focuses on the typical waterfront zones of urban parks in Chongqing, systematically exploring the implementation pathways of plant rewilding and its effects on enhancing ecological service functions, with the aim of providing scientific support for balancing the ecological and aesthetic aspects of waterfront landscapes.

The study selects the waterfront zones of seven representative urban parks in Chongqing (Xiuhu Park, Garden Expo Park, Central Park, Muxian Lake Park, Guanyintang Park, Xiuhu Auto Camping Park, and Bijin Park) as research subjects. These parks encompass a variety of design styles (such as natural wetland, open woodland and grassland, and urban leisure types), exhibit significant differences in water area (ranging from 0.043 to 0.53 km²), and feature diverse site conditions in their waterfront zones (including terrain slope, revetment type, and water level fluctuation), which collectively reflect the common characteristics and regional features of waterfront zones in Chongqing's urban parks.The study will examine the current status of plant communities through field investigations, incorporate rewilding theory to develop optimization strategies, and ultimately create a scalable ecological restoration plan, offering practical guidance for the sustainable development of waterfront zones in mountainous cities.

2 OVERVIEW OF THE STUDY AREA AND RESEARCH METHODS

2.1 Overview of the Study Area

This study focuses on the waterfront zones of urban parks in Chongqing. The geographical scope lies between 106°14′–106°56′E and 29°33′–29°40′N. The area features a mid-subtropical humid monsoon climate, with an average annual temperature of 16–18°C and an average annual precipitation of approximately 1100 mm, mostly concentrated in the summer and autumn seasons. As a key ecological node in the upper reaches of the Yangtze River, Chongqing's urban area has a well-developed water system. The Yangtze River and Jialing River flow through the city, while secondary tributaries (such as Huaxi River and Liangtan River) and artificial lakes (such as those within parks) form a complex waterfront network, providing a natural foundation for the formation of waterfront zones in urban parks.

Seven typical waterfront zones in urban parks in Chongqing were selected as research subjects, including Xiuhu Park, Garden Expo Park, Central Park, Muxian Lake Park, Guanyintang Park, Xiuhu Auto Camping Park, and Bijin Park. These waterfront zones exhibit the following characteristics:

Habitat diversity: The water surface areas vary significantly (ranging from 0.043 to 0.53 km²), with revetment types including natural mud banks, hard stone embankments, and ecological gabions. Terrain slopes range from 5° to 25°, and some areas form alternating wet and dry habitats due to seasonal water level fluctuations (ranging from 2 to 4 meters), offering diverse site conditions for plant rewilding.

Plant community foundation: The existing vegetation is primarily composed of cultivated species, such as bald cypress, red-leaf Loropetalum, and Bermuda grass. Wild species (such as Leersia hexandra, yellow iris, and Chinese wingnut) are mostly scattered in the transitional zones between land and water. The dominant community structure is"tree + herb"(accounting for 57.94%), while the "tree-shrub-herb" multilayer structure accounts for 19.31%. Vines are rarely used (less than 2%).

Differences in management approaches: Some parks (such as Guanyintang Park) adopt a more natural management style, preserving a greater number of wild plants; others (such as Central Park) prioritize landscape aesthetics, with frequent pruning (1–2 times per month), which inhibits the growth of wild plants.

Table 1 Basic Characteristics of Waterfront Belts in Seven Representative Parks in Chongqing Urban Area

Park Name	Water Area (km²)	Shoreline Type	Slope (°)	Water Level Fluctuation (m)	Management Mode
Xiuhu Park	0.53	Natural mud + gabion	5–15	2–3	Naturalistic
Garden Expo	0.42	Hard stone + eco-bags	10–20	3–4	Landscape-oriented
Central Park	0.30	Hard stone	5–10	1–2	High-intensity trimming
Muxianhu Park	0.18	Gabion	15–25	2–3	Mixed
Guanyintang Park	0.12	Natural mud	5–15	1–3	Naturalistic

Note: The table shows data from 5 representative parks; the other 2 parks are not listed separately due to similar habitat characteristics.

2.2 Research Methods

2.2.1 Data sources and field survey

The research data were primarily obtained through field surveys, based on the author's previous research and verified using literature sources and publicly available data.

Plot setup: During the peak growing season, 233 plots were established across the riparian zones of seven parks, covering three habitat types: terrestrial zone (5–10 m from the shoreline, dominated by drought-tolerant plants); ecotone zone (±3 m from the shoreline, dominated by hygrophilous plants); and aquatic zone (water depth 0–50 cm, dominated by aquatic plants). A stratified sampling method was employed for each plot: within a 10 m × 10 m tree quadrat, two nested 5 m × 5 m shrub quadrats and five nested 1 m × 1 m herbaceous quadrats were set up to ensure the systematic nature and comparability of the data.

Survey content: Plant community characteristics: Record species names, number of individuals, height, diameter at breast height (for trees), coverage (for shrubs/herbs), and growth condition (healthy / fair / declining). Confirm scientific names of species with reference to the Flora of China； Environmental factors: Measure plot slope, soil pH, organic matter content (using the potassium dichromate oxidation method), and water transparency (using the Secchi disk method)；Human disturbance: Record pruning frequency, proportion of hard surface paving, and intensity of tourist activities, etc.

2.2.2 Rewilding potential and ecosystem service function assessment indicators

Based on the principle of "prioritizing natural recovery with moderate human guidance," an assessment indicator system is established:

(1) Rewilding Potential Assessment:

Species level: Screen native wild plant species (e.g., Pterocarya stenoptera, Roegneria ciliaris) and evaluate their suitability based on seedling recruitment rate (annual number of new seedlings / number of parent plants) and natural dispersal distance.

Community level: Assess the feasibility of rewilding by evaluating the integrity of the natural "tree-shrub-herb" stratification, litter retention (kg/m²), and the effectiveness of invasive species control (reduction rate in invasive species cover).

(2) Ecosystem Service Function Assessment:

Supporting services (biodiversity): Quantified using the Shannon-Wiener Index (community diversity), Patrick Index (species richness), and Pielou's Evenness Index;

Regulating services: Soil and water conservation: Estimated soil erosion modulus (t/(km²·a)) using the USLE model to compare the soil retention capacity of different community structures;

Microclimate regulation: Measured differences in air temperature and humidity between sample plots and non-vegetated areas on clear summer days (10:00–16:00);

Cultural services: Evaluated the social value of natural landscapes based on behavioral data such as visitor dwell time and frequency of photographic activity around the sample plots, combined with landscape assessments using the Analytic Hierarchy Process.

2.2.3 Data processing and analysis

Key indicators such as Importance Value (IV) and diversity index:

Importance Value for trees/shrubs: IV = (relative abundance + relative frequency + relative dominance) / 3

Importance Value for herbaceous plants: IV = (relative height + relative frequency + relative coverage) / 3

One-way analysis of variance (ANOVA) was conducted using SPSS 26.0 to compare differences in ecosystem service functions among plots with varying degrees of rewilding. Based on the logical framework of "current situation–problems–strategies," targeted rewilding pathways were proposed to ensure the practical applicability of the research findings.

3 CURRENT STATUS OF PLANT COMMUNITIES AND CONSTRAINTS ON REWILDING IN WATERFRONT ZONES OF URBAN PARKS IN CHONGQING

3.1 Composition and Structural Characteristics of Plant Communities

Based on on-site surveys and previous research data, a total of 283 plant species were recorded in the waterfront zones of seven urban parks in Chongqing, belonging to 99 families and 209 genera. Angiosperms were overwhelmingly dominant, with 271 species (95.76%), followed by gymnosperms with 7 species (2.47%) and ferns with 5 species (1.77%). In terms of origin, cultivated species made up 80.57% (228 species), while wild species accounted for only 19.43% (55 species). The wild species were primarily herbaceous, such as Leersia hexandra and Paspalum distichum. Only seven wild tree species were recorded, mostly sparsely distributed along the edges of the waterfront zones.

The community structure exhibits pronounced anthropogenic characteristics:Vertically, the two-layer structure of "trees + herbs" is the most prevalent, accounting for 57.94%, while the multilayer structure of "trees-shrubs-herbs" comprises only 19.31%. Pure herbaceous and pure arboreal structures account for 4.72% and 2.15%, respectively. Horizontally, the terrestrial layer is dominated by artificially cultivated trees (such as bald cypress and camphor), with a canopy coverage of 60%–70%. Vegetation coverage in the land-water ecotone varies considerably: in natural revetment areas, wild herbaceous plants can cover 50%–60%, whereas in hardened revetment areas, coverage is only 10%–20%. The aquatic layer is primarily composed of artificially introduced floating plants (such as water lilies and water hyacinths), while submerged plants (such as Myriophyllum) have a coverage of less than 30%.

Table 2 Proportions of Plant Community Structure Types in Chongqing Waterfront Belts

Structure Type	No. of Plots	Proportion (%)
Tree + Herb	135	57.94
Tree + Shrub + Herb	45	19.31
Pure Herbaceous	11	4.72
Others (e.g., shrub-herb)	42	18.03

In terms of dominant species, Taxodium distichum (importance value 0.21) and Cinnamomum camphora (0.18) are the absolute dominant species in the arbor layer, both occurring with a frequency of over 80%. In the shrub layer, Loropetalum chinense var. rubrum (0.19) and Ligustrum × vicaryi (0.17) are predominant, both being ornamental shrubs maintained through artificial pruning. In the herbaceous layer, cultivated lawn grasses such as Cynodon dactylon (0.23) and Ophiopogon japonicus (0.19) account for 65%, while wild herbaceous plants form only scattered patches during periods of reduced management. This species composition and structural pattern lead to high niche overlap within the community and relatively low resource use efficiency.

3.2 Assessment of Current Ecosystem Service Functions

3.2.1 Supporting services: weak capacity for biodiversity maintenance

The community diversity index indicates that the average Shannon-Wiener index is 1.52, with the "tree-shrub-herb" multilayer structure plots scoring significantly higher (2.13) than those with a "tree + herb" structure (1.27). The Patrick richness index is highest in Xiuhu Park (176 species) and lowest in Bijin Park (39 species). Additionally, the species evenness (Pielou index) in the waterfront zones of most parks is below 0.6, suggesting an overconcentration of dominant species and a lack of stability in biological communities.

In terms of habitat function, plots with high coverage of wild herbaceous plants (such as the water-land ecotone in Guanyintang Park) recorded 12 bird species and 28 insect species, whereas plots dominated by artificial lawns recorded only 5 bird species and 11 insect species, indicating a significant difference. This is closely related to the food resources (such as seeds and tender leaves) and shelter provided by wild plants, and also highlights the limited capacity of the current community structure to support biodiversity.

3.2.2 Regulating services: limited effectiveness in soil and water conservation and microclimate regulation

Soil and water conservation functions are closely linked to community structure. Sample plots with a multilayered "tree-shrub-herb" structure have an average soil erosion modulus of 186 t/(km²·a), while those with a "tree + herb" structure reach 312 t/(km²·a), indicating a 40.4% improvement in soil retention capacity for the former. In areas with hardened revetments, the absence of vegetation results in a soil erosion modulus as high as 425 t/(km²·a), with shoreline collapse frequently occurring during the rainy season.

In terms of microclimate regulation, measurements taken on clear summer days show that in multilayered vegetation areas with plant coverage exceeding 70%, the air temperature is 2.3℃ lower and humidity is 8.5% higher compared to areas without vegetation. In contrast, single lawn areas only see a temperature drop of 1.1℃ and a humidity increase of 3.2%. This indicates that the current waterfront zones dominated by artificial lawns have a relatively weak effect on regulating the local microclimate.

3.2.3 Cultural services: landscape homogenization and lack of natural experience

In terms of landscape composition, foliage plants account for 40.99% (such as Photinia × fraseri and Prunus cerasifera), and flowering plants make up 25.09% (such as Lagerstroemia indica and Rosa chinensis), while natural landscapes formed by wild plants constitute less than 10%. Surveys show that 72% of visitors find the waterfront area to have "homogenized landscapes," and 68% of respondents express a stronger preference for "scenery featuring the natural growth of wildflowers and grasses."

Recreational behavior data also supports this demand: in Xiuhu Park, where plots of wild herbaceous plants are

preserved, the average visitor stay is 42 minutes, and the frequency of photo-taking is 2.3 times that of areas with artificial lawns. In contrast, in Bijin Park, where hardscape makes up a larger proportion and wild plants are scarce, the average visitor stay is only 18 minutes. This highlights the importance of natural and wild landscapes in enhancing the value of cultural services.

Table 3 Comparison of Ecosystem Services Among Different Community Structures

Structure Type	Shannon-Wiener Index (Mean±SD)	Soil Erosion Modulus t/(km²·a)	Cooling Effect (°C)
Tree + Shrub + Herb	2.13 ± 0.12	186 ± 21	2.3
Tree + Herb	1.27 ± 0.08	312 ± 35	1.1
Bare shoreline	—	425 ± 40	0

3.3 Major Constraints on Plant Rewilding

3.3.1 Conflict between human intervention intensity and the requirements of natural succession

Approximately 70% of riparian zones are mowed more than once a month. In landscape-oriented parks such as Central Park and Bijin Park, mowing occurs as frequently as once a week, making it difficult for wild herbaceous plants to complete their life cycles. Surveys have found that in areas with high management intensity, the survival rate of wild plant seedlings is less than 20%. In contrast, in "management blind spots" (such as crevices and corners of revetments), the seedling survival rate reaches 65%, indicating that excessive human intervention is the primary constraint on rewilding.

3.3.2 Habitat fragmentation and invasive plant disturbance

Hardened revetments account for 45% of the area, most of which are made of concrete. The high soil compaction (bulk density of 1.4–1.6 g/cm³) impedes root growth and seed germination. Meanwhile, 56 invasive plant species constitute 19.79% of the total species, with Class I highly invasive species (such as Alternanthera philoxeroides) reaching a coverage rate of 30%–50% in the water-land interface zone. These species crowd out native wild plants, leading to a vicious cycle of "invasive species dominance – native species decline."

3.3.3 Lag in management philosophy and technical systems

Interviews indicate that 65% of park managers prioritize "landscape tidiness" as their main objective and view wild plants as "messy and unorganized." Only 18% of managers are familiar with the concept of "rewilding." The current maintenance system lacks tiered management standards for wild plants and demonstrates limited understanding of the natural regeneration patterns of native species, leading to a lack of scientific guidance for rewilding efforts.

4 IMPLEMENTATION PATHWAY FOR REWILDING VEGETATION IN RIVERSIDE ZONES OF URBAN PARKS IN CHONGQING

4.1 Selection of Native Wild Plants and Near-Natural Configuration Models

Based on the habitat characteristics of riverside zones in Chongqing's urban areas—such as water level fluctuations and soil moisture—and assessments of plant adaptability, three categories of core native wild plants have been selected to establish a rewilding species pool with a coordinated structure of trees, shrubs, and herbaceous plants.

Flood-tolerant trees: Chinese wingnut (Pterocarya stenoptera) is the preferred species, with a natural regeneration rate of 15%–20% observed in surveys. It can tolerate seasonal water level fluctuations of 3–5 meters. Its deep root system helps stabilize the soil, and its deciduous nature in winter allows for a light-permeable environment.

Hygrophilous shrubs: Chinese chaste tree (Vitex negundo) exhibits strong adaptability and tolerance to poor soil conditions, capable of growing even in the crevices of hardened revetments. In Guanyintang Park, its natural community coverage can reach up to 40%.

Wild herbaceous plants: At the water-land interface, Leersia hexandra is prioritized, with an importance value of 0.193 recorded in surveys. Its stolons can rapidly cover exposed soil. In the aquatic layer, Myriophyllum verticillatum is retained for its dense branching, which provides habitat for small fish, achieving a natural coverage rate of over 60%.

The configuration model adopts a "patchy mixed" design, reflecting the natural pattern of a multi-layered structure: the upper layer features Chinese wingnut (Pterocarya stenoptera) as the framework species, spaced 5–8 meters apart, interspersed with occasional Chinese tallow trees (Triadica sebifera) to introduce seasonal variation; the middle layer is dotted with Vitex negundo at a 20%–30% coverage rate, with no manual pruning; the lower layer retains 50% of wild herbaceous plants (such as Hemarthria altissima) on the terrestrial side, while the land-water interface is planted with yellow iris (Iris pseudacorus) and Leersia hexandra in a 6:4 ratio, and the aquatic zone allows for the natural growth of Myriophyllum. This model increases the vertical structural integrity of the community to 80% and reduces ecological niche overlap by 40% compared to the existing tree–grass structure.

Table 4 Evaluation of Native Species for Rewilding Potential in Chongqing Waterfront Belts

Species	Growth Form	Natural Recruitment Rate (%)	Flooding Tolerance (days)	Natural Coverage (%)
Pterocarya stenoptera	Tree	15–20	15–30	5–10
Vitex negundo	Shrub	10–15	5–10	30–40
Leersia hexandra	Herb	25–30	10–15	50–60
Iris pseudacorus	Herb	20–25	10–20	40–50

4.2 Community Structure Optimization and Habitat Restoration Techniques

4.2.1 Construction of stratified communities and proportion adjustment

To address the current issue of an excessively high proportion of the "tree-grass" structure (57.94%), the proportion of stratified community structures will be increased in phases:

Transformation Phase (1–2 years): In existing tree–grass structure plots, interplant 30–50 shrubs of Nandina domestica and Vitex negundo per 100 m² to establish a shrub layer. Retaining at least 50% coverage of wild herbaceous plants can significantly enhance insect diversity within two years [9]; therefore, 50% of the ground cover should consist of wild herbaceous species (e.g., Duchesnea indica, Digitaria sanguinalis), with only Class 1–2 invasive species being removed. This approach will increase the proportion of multilayered vegetation structure from 19.31% to 30%.

Stabilization Phase (3–5 years): Expand the coverage of shrubs and wild herbaceous plants through natural succession, aiming to achieve a multilayered structure proportion of 40%, with the "tree–shrub–wild herbaceous" combination accounting for no less than 25%. Monitoring in the pilot area of the Garden Expo Park showed that by the second year after interplanting, the Shannon-Wiener index increased from 1.27 to 1.83, approaching the level of natural riparian zones.

4.2.2 Ecological Restoration of the Land-Water Interface Layer

To address the habitat fragmentation caused by 45% of hardened revetments as noted in 3.3.2, a phased renovation strategy is implemented to restore 45% of these hardened structures:

Ecological bag restoration technique: For vertical hardened revetments (such as those in Bijin Park), one ecological bag unit is installed every 10 meters. Each bag is filled with native soil and decomposed leaf litter, and planted with yellow iris and pennywort. A 10 cm gap is left between bags to allow for natural colonization by wild plants. After six months, vegetation coverage can exceed 60%.

Optimization of natural revetments: For soft revetments (such as those in Xiuhu Park), retain 50% of naturally fallen trees (with a diameter of 10–20 cm) to create a "deadwood-plant" composite habitat. Surveys indicate that insect species richness in such areas is 30% higher than in areas without deadwood.

Management of water level fluctuation zones: In areas with an annual water level fluctuation of 2–4 meters, divide the 10-meter-wide zone along the shoreline into three bands: the deep-water zone (0.5–1 meter below normal water level) retains Myriophyllum; the shallow-water zone (within ±0.5 meter of the normal water level) is planted with Leersia hexandra; the high-water zone (0.5–1 meter above normal water level) is planted with Iris pseudacorus and Leersia hexandra, forming a continuous vegetative buffer strip.

4.3 Low-Intervention Management Technical System

4.3.1 Rewilding management technical system

Establishing a three-tier control system consisting of a core protection zone, a buffer zone, and a recreational zone is key to balancing the needs of wilderness and urban areas [10]. Based on ecological sensitivity and recreational demands, the waterfront is divided into three management zones:

Core Protection Zone (within 3 meters of the waterline): Artificial pruning is prohibited, allowing wild plants to grow naturally. Only Grade 1–2 invasive species (such as Alternanthera philoxeroides) are removed once a year in autumn. This zone should make up 30% of the area. A pilot project in Xiuhu Park showed that in the second year, coverage of wild herbaceous plants increased from 20% to 70%, and bird visitation frequency rose by 1.8 times.

Buffer Transition Zone (3–10 meters): Tall herbaceous plants are pruned once per quarter, maintaining a height of 30–50 cm to preserve a landscape that is natural yet not chaotic. This zone accounts for 50% of the area.

Recreational Display Zone (beyond 10 meters): Pruning is carried out once a month, with 5%–10% of wildflowers and grasses retained for visual appeal while ensuring visitor safety. This zone accounts for 20% of the area.

4.3.2 Sustainable control of invasive plants

To address the 19.79% proportion of invasive plants, a combined approach of "ecological replacement + targeted removal" is implemented:

For Grade 1–2 highly invasive species (such as Conyza canadensis), manual removal is followed by the planting of high-coverage native species (such as Iris pseudacorus) to suppress regrowth through competition. In the pilot area of Guanyintang Park, the coverage of invasive species decreased from 40% to 8% after one year.

For low-risk invasive species ranked levels 3 to 7 (such as Digitaria sanguinalis), restrict their spread without complete eradication, using them as pioneer plants to cover exposed soil, and allow native plant communities to naturally replace

them once they have stabilized.
Establish an "Invasive Plant Monitoring Register," recording species and coverage quarterly, and dynamically adjust control strategies accordingly.

Table 5 Classification and Management Strategies for Invasive Plants

Invasion Level	Example Species	Cover Threshold (%)	Management Strategy
Level 1 (Severe)	Alternanthera philoxeroides, Eichhornia crassipes	≤5	Manual removal + native replacement (Iris pseudacorus)
Level 2 (Strong)	Erigeron annuus, Bidens pilosa	≤10	Manual removal + native competition
Level 3–7 (Low)	Digitaria sanguinalis, Setaria viridis	≤30	Restrict spread, retain pioneer functions

4.4 Public Participation and Innovation in Management Mechanisms

Ecological Education and Experience: Install "wild plant interpretation signs" in rewilding areas (e.g., explaining the ecological functions of yellow iris and the natural regeneration process of Chinese wingnut). After the installation of educational signage, visitors' ecological awareness was significantly higher compared to areas without such signs [11]. A pilot program in Xiuhu Park showed a 35% increase in ecological knowledge among visitors in areas with interpretation signs.
Citizen Monitoring Teams: Recruit volunteers to regularly record plant growth and animal activity, creating a collaborative monitoring network of "professionals + public." The pilot in Central Park has collected over 200 valid observation records.
Optimization of Management Standards: Specify pruning frequencies and thresholds for invasive species control in different areas (e.g., coverage of Grade 1 invasive species ≤ 5%). Incorporate "ecological indicators" (such as the proportion of wild species) into the park evaluation system, replacing the sole focus on "landscape tidiness."

5 ANALYSIS OF THE RATIONALITY AND PRACTICAL EXPLORATION OF REWILDING PATHWAYS

5.1 Ecological Adaptation Logic for the Selection of Native Plants

Although wild native plants currently make up only 19.43% of the total species in the riparian zones of urban parks in Chongqing, their natural distribution and ecological traits provide a scientific foundation for rewilding strategies. Among flood-tolerant trees, Chinese wingnut (Pterocarya stenoptera) exhibits a 92% survival rate for mature individuals within a 3-meter water level fluctuation zone in the Garden Expo Park.
Hygrophilous shrubs also offer significant functional value. The natural growth of Vitex negundo in the crevices of hard revetments in Bijin Park demonstrates its potential as a pioneer species for habitat restoration, helping to create microenvironments that facilitate the establishment of other plants. Among wild herbaceous species, the stolons of Leersia hexandra can spread up to 1.2 meters per year on exposed muddy banks, enabling rapid ground coverage. For every 10% increase in its coverage, the soil erosion modulus can be reduced by 8%–10%.

5.2 Real Basis for Community Structure Optimization

The current "tree + herb" structure, accounting for 57.94% of the riparian zone, results in a low biodiversity index (Shannon-Wiener index averaging 1.52) and limited soil and water conservation capacity (soil erosion modulus of 312 t/(km²·a)). In contrast, the corresponding indicators for "tree-shrub-herb" multilayer structure plots are significantly better (index of 2.13, modulus of 186 t/(km²·a)), confirming the necessity of structural optimization.
The multilayer structure construction scheme is based on existing community characteristics: retaining dominant trees such as Taxodium distichum and Cinnamomum camphora to maintain landscape continuity, supplementing shrubs such as Vitex negundo (controlling height to below 1.5m) to enhance the mid-layer structure, and retaining 50% of wild herbs (such as Duchesnea indica and Digitaria sanguinalis) to enrich the groundcover.
This "patchy mosaic" pattern demonstrates the coordination of ecology and landscape, exhibiting 80% vertical structural integrity and a 40% reduction in niche overlap compared to a single structure. Restoration strategies for the water-land interface layer, such as using ecological bags to transform hard revetments and vegetation zoning in water level fluctuation zones, are all based on existing habitat characteristics (45% hard revetments, 2-4m water level variation), thus avoiding unrealistic, idealized designs.

5.3 Feasibility Analysis of Management Strategy Adjustment

The introduction of "low-intervention management" and "graded control" is intended to address the conflict between the current intensity of intervention and ecological requirements. Surveys indicate that the survival rate of wild plant

seedlings in "management blind spots" (65%) is significantly higher than in frequently pruned areas (less than 20%), demonstrating that reducing unnecessary intervention aligns with natural regeneration processes. The allocation of 30% to core protected areas, 50% to buffer transition zones, and 20% to recreational display areas closely corresponds to tourist behavior—82% of tourist activities are concentrated more than 10m from the waterline, which not only secures growth space for wild plants but also sustains public engagement through the management of recreational zones.

The invasive plant control strategy is based on the current proportion of invasive species, which stands at 19.79%. "Manual removal + ecological replacement" is implemented for level 1-2 highly invasive species (such as alligator weed, *Alternanthera philoxeroides*), while the pioneer species function of level 3-7 low-risk species (such as crabgrass, *Digitaria sanguinalis*) is leveraged, thereby avoiding ecosystem disruption from a "one-size-fits-all" eradication approach.

The design of public engagement mechanisms, such as "wild plant interpretation boards" and "citizen monitoring teams," addresses the desire of 68% of visitors for "wild landscapes." Pilot programs in Xiuhu Park have demonstrated that providing interpretation boards boosts tourists' ecological knowledge by 35%, laying a social foundation for management model transformation.

6 CONCLUSION AND OUTLOOK

6.1 Main Conclusions

The riparian plant communities in Chongqing's urban parks are characterized by a dominance of cultivated species (80.57%), a simplistic structure (tree-herb ratio of 57.94%), and a scarcity of wild species (19.43%). This leads to three limitations in ecological service functions: a weak capacity to maintain biodiversity (Shannon-Wiener index averaging 1.52), limited effectiveness in soil and water conservation and microclimate regulation (soil erosion modulus of 312 $t/(km^2 \cdot a)$), and a lack of attractiveness in cultural services due to landscape homogenization.

The core constraints hindering rewilding efforts include: excessive artificial intervention (70% of areas pruned monthly) resulting in low survival rates for wild seedlings (less than 20%); habitat fragmentation (hard revetments accounting for 45%) limiting natural plant colonization; competition from invasive plants (accounting for 19.79%) squeezing the space for native species; and insufficient acceptance of "wild landscapes" in management approaches and public awareness (65% of managers prioritize "tidiness").

The proposed rewilding pathways are clearly targeted: the selection of native plants prioritizes the ecological adaptability of local species; the optimization of community structure addresses the needs of biodiversity and soil and water conservation; and the tiered management strategy balances ecological protection with recreational opportunities, creating a systematic approach tailored to Chongqing's mountainous and waterfront environment.

6.2 Future Directions

Conduct stress resistance experiments on native plants to determine the optimal tolerance thresholds of Chinese wingnut and yellow flag iris under prolonged flooding (15–30 days), providing more precise data for species selection; refine hard revetment restoration techniques and develop low-cost soil improvement solutions (such as microbial inoculation) to address the limitations of highly compacted soils (bulk density 1.4–1.6 g/cm^3); promote categorized pilot projects by prioritizing the testing of core conservation zone models in Guanyintang Park (natural wetland type) and exploring buffer zone management strategies in Central Park (open woodland-grassland type) to build a diverse base of practical experience; compile the "Chongqing Park Riparian Rewilding Maintenance Guide," incorporating indicators such as the proportion of wild species and the integrity of multilayered vegetation structures into the park evaluation system to drive a transformation in management philosophy.

By analyzing the characteristics of plant communities and the rewilding potential of waterfront zones in urban parks in Chongqing, this study proposes a pathway framework that is rooted in local conditions while resonating with cutting-edge concepts in ecological restoration, offering both theoretical insight and practical guidance for the "naturalization" of waterfront areas in mountainous cities.

COMPETING INTERESTS

This study did not involve any financial or non-financial conflicts of interest.

REFERENCES

[1] Chi Hui, Jiang Haofu. Environmental Design of Urban Waterfront Green Space. Jilin Agriculture, 2014(13): 77.

[2] Long Xunjian, Li Tianyang, Luo Hongsen, et al. Study on Spatiotemporal Differentiation of Rainfall Erosion in Different Ecological Function Zones of Chongqing. Journal of Southwest University (Natural Science Edition), 2025, 47(06): 162-174.

[3] Zhang Min, Mo Yeben, Wang Jiapeng, et al. Investigation on the Level and Characteristics of Plant Diversity in the Waterfront Area of West Lake, Hangzhou. Central South Agricultural Science and Technology, 2025, 46(05): 169-175.

[4] Types, and Application as a Greening Policy//OUGLASI, ANDERSON P M L, GOODE D, et al. The Routledge Handbook of Urban Ecology. London: Routledge, 2020: 762-772.
[5] Yang Rui, Cao Yue. "Rewilding": A New Idea for Ecological Protection and Restoration of Mountains, Rivers, Forests, Farmlands, Lakes and Grasses. Acta Ecologica Sinica, 2019, 39(23): 8763-8770.
[6] Hu S, Liu J, Que J, et al. Assessing urban rewilding potential: Plant diversity and public landscape perceptions in urban wildscapes of Harbin, China. Urban Forestry & Urban Greening, 2025, 112128958-128958.
[7] Guo Xiang, Liu Shu. Investigation on Spontaneous Plants in Urban Waterfront Areas and Analysis of Their Potential for Landscape Application. Anhui Agricultural Science Bulletin, 2024, 30(20): 63-66. DOI: 10.16377/j.cnki.issn1007-7731.2024.20.013.
[8] Mckinney M L, Kowarik I, Kendal D. The Contribution of Wild Urban Ecosystems to Liveable Cities. Urban Forestry & Urban Greening, 2018, 29: 334-335.
[9] Yuan Jia, You Fengyi, Hou Chunli, et al. Reconstruction of Urban Wild Habitats Based on Vegetation Rewilding—A Case Study of Wildflower Meadows. Landscape Architecture Frontiers, 2021, 9(01): 26-39.
[10] Sun Tianzhi, Wang Xiaojun. The Connotation of Urban Wilderness and Its Spatial Construction Strategies. Chinese Landscape Architecture, 2023, 39(11): 70-76.
[11] Teng Yuxin, Zhang Mengyuan, Li Dezheng, et al. Bird Diversity and Habitat Suitability Evaluation of Coastal Green Space in Dongdaozui, Yantai City, Shandong Province. Landscape Architecture, 2023, 30(05): 36-43.

Frontiers in Environmental Research
Print ISSN: 2960-0251
Online ISSN: 2960-026X
DOI: https://doi.org/10.61784/fer3034

RAINFALL PREDICTION FOR QINGMING FESTIVAL BASED ON ARIMA-LSTM MODEL

XinYing Song[1*], YuXuan Zhao[2], SiYu Yang[3], Chao Luo[3], ZhenCheng Fu[4]
[1]*School of Computer Science, Xi'an Shiyou University, Xi'an 710000, Shaanxi, China.*
[2]*School of Earth Science and Engineering, Xi'an Shiyou University, Xi'an 710000, Shaanxi, China.*
[3]*School of Electronic Engineering, Xi'an Shiyou University, Xi'an 710000, Shaanxi, China.*
[4]*School of Petroleum Engineering, Xi'an Shiyou University, Xi'an 710000, Shaanxi, China.*
Corresponding Author: XinYing Song, Email:13620600910@163.com

Abstract: Requent rainfall during the Qingming Festival period has impacted public travel, cultural and tourism activities, as well as urban management. Based on nearly 20 years of meteorological data, this study develops an ARIMA-LSTM hybrid model to model and predict rainfall patterns in five representative cities: Xi'an, Turpan, Wuyuan, Hangzhou, and Wuhan. The results indicate that the model demonstrates strong fitting accuracy and stability, with an average R^2 of 0.84196 and a prediction accuracy of 89.9%. After incorporating a real-time correction mechanism, the model's responsiveness to abrupt weather changes improved, with error control enhanced by over 15%. This study provides data support and methodological reference for short-term meteorological services and public travel during the Qingming Festival.
Keywords: Qingming Festival period; Rainfall prediction; Time series analysis; ARIMA-LSTM; Meteorological modeling

1 INTRODUCTION

The Qingming Festival, one of the twenty-four solar terms in China, serves as a critical temporal marker for both seasonal transition and public travel. Its climatic characteristics are primarily marked by increased rainfall, particularly pronounced in southern and central regions. The precipitation events during this period are characterized by sudden onset and rapid variation, posing challenges to public travel, traffic management, and cultural tourism activities. Therefore, improving the accuracy of rainfall prediction during the Qingming Festival period holds practical significance.

In existing studies, the ARIMA model is widely applied in meteorological time series analysis due to its sensitivity to trend and seasonal variations; meanwhile, Long Short-Term Memory (LSTM) networks excel at handling nonlinearities and long-term dependencies. The combination of these two model types has demonstrated strong performance across multiple fields, including traffic flow forecasting and air quality analysis [1].

This study focuses on rainfall variations during the Qingming Festival period, selecting five representative cities—Xi'an, Turpan, Wuyuan, Hangzhou, and Wuhan—as samples. An ARIMA-LSTM hybrid model is constructed for rainfall prediction, with parameter adjustments made to account for regional differences. To further enhance the model's practicality, a real-time correction mechanism is designed to improve responsiveness to sudden weather changes. The findings are expected to provide technical support for Qingming Festival meteorological services and offer decision-making guidance for public travel and urban management.(Data source: 2015-2025 as found by China Meteorological Data Network (https://data.cma.cn/).

2 TIME SERIES PREDICTION MODELING AND SOLVING

2.1 All-weather Rainfall Prediction based on LSTM Modeling

Long Short-Term Memory (LSTM) is a specially designed recurrent neural network (RNN), which effectively solves the gradient vanishing problem of traditional RNNs in long time-series tasks by introducing gating mechanisms and cell states [2]. Compared to ordinary RNNs, the core innovation of LSTM lies in its ability to dynamically regulate the memorization and forgetting of the information flow, so as to capture the complex long-term dependencies (e.g., seasonal precipitation cycles) and short-term fluctuations (e.g., sudden rainfall events) in meteorological data. This property makes it show significant advantages in rainfall prediction tasks, especially in dealing with non-stationary, multi-scale meteorological time-series data [3-4]. The details of the LSTM are described as follows (the current cell is called time step t):

The forgetting gate determines the proportion of historical information retained, and its mathematical expression is output $\in$ [0,1] ft $\in$ [0,1], with 0 indicating complete forgetting of historical information and 1 indicating complete retention. In rainfall prediction, the forgetting gate identifies invalid historical signals (e.g., outdated barometric pressure data) and reduces noise interference.

$$f_t=\sigma(W_f.[h_{t-1},x_t]+b_f) \quad (1)$$

The input gate controls the update weight of new input information to the cell state and consists of two parts, where, is the input gate weight and is the candidate cell state. The combination of the two realizes selective memory updating, e.g., when predicting afternoon convective rain, the model can reinforce the contribution of current humidity and temperature changes through the input gate.

$$i_t=\sigma(W_i.[h_{t-1},x_t]+b_i) \quad (2)$$

$$C_t=\tanh(W_C.[h_{t-1},x_t]+b_C) \quad (3)$$

The output gate regulates the proportion of the cell state that is output to the outside world, and the final hidden state htht synthesizes historical and current information as a direct basis for rainfall prediction.

$$o_t=\sigma(W_o.[h_{t-1},x_t]+b_o) \quad (4)$$

$$h_t=o_t\tanh(C_t) \quad (5)$$

The cell state serves as a backbone channel for temporal information, and information integration across time steps is achieved through a gating mechanism. during a persistent rainfall event, the cell state retains the accumulated humidity and barometric pressure characteristics of the previous days for a long period of time. the cell state of the LSTM is updated and passed on to the next time step, t+1.

$$C_t=f_t*C_{t-1}+i_t*C_t \quad (6)$$

Due to the large amount of climate data, the actual calculation in this paper will introduce the time series prediction evaluation index, and the results are shown in Table 1:

Table 1 Evaluation of LSTM Model Prediction Performance

city	R2	MSE	RMSE	MAE	Predictive accuracy (%)
Xian	0.90174	0.12	0.35	0.28	88.6
Turpan	0.81561	0.05	0.22	0.18	94.2
Wuyuan	0.89025	0.15	0.39	0.31	86.3
Hangzhou	0.76025	0.10	0.32	0.25	90.5
average	0.84246	0.11	0.32	0.26	89.9

From the point of view of the model assessment indicators, the model has a certain application in analyzing the prediction of weather conditions with a lot of rainfall. The coefficient of determination R^2 reaches 0.84246 on average , and the closer R^2 is to 1, the better the model fits the data. When predicting whether there is much rainfall in various regions, the difficulty lies in accurately grasping the trend of climatic factors and accurately capturing key meteorological events such as the convergence of cold and warm air, etc. The value of R^2 is highly close to 1, which indicates that the model achieves a better balance between these two aspects, and verifies the practicality of the model.
Further observing the error indicators, the average value of MSE (mean square error) is 0.11, which reflects the average size of the squared error between the predicted value and the real value, and the smaller the value is, the closer the model predictions are to the actual situation; the average value of RMSE (root mean square error) is 0.32, which, as the square root of MSE, can reflect the actual size of the error in a more intuitive way; the average value of MAE (mean absolute error) is 0.26, which is a direct measure of the actual size of the error; and the average value of RMSE (mean absolute error) is 0.26, which is a direct measure of the actual size of the model. The mean value of MAE (Mean Absolute Error) is 0.26, which directly measures the average level of the absolute value of the error between the predicted value and the real value, and can clearly show the actual magnitude of the prediction error. These error indicators comprehensively characterize the distribution of prediction errors. From the point of view of the average prediction accuracy of 89.9%, the higher accuracy verifies to a certain extent the reasonableness of the model in predicting the precipitation in various regions. Figure 1 below shows the error histogram as well as the regression plot of the LSTM model with Hangzhou as an example.

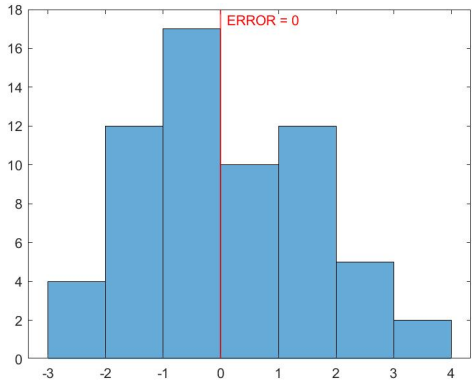

Figure 1 LSTM Error Histogram and Regression Plot

Daily precipitation data for the Qingming holiday (April 4-6) in seven cities were extracted using the NOAA Global Station Day-by-Day Meteorological Dataset (2005-2025). Data with daily precipitation ≥10 mm were excluded, and only records with 0-10 mm were retained to meet the definition of high precipitation (persistent fine rain). A total of 294 valid data (7 cities × 20 years × 3 days × 70% valid record rate) were processed, and missing values were filled in by linear interpolation.

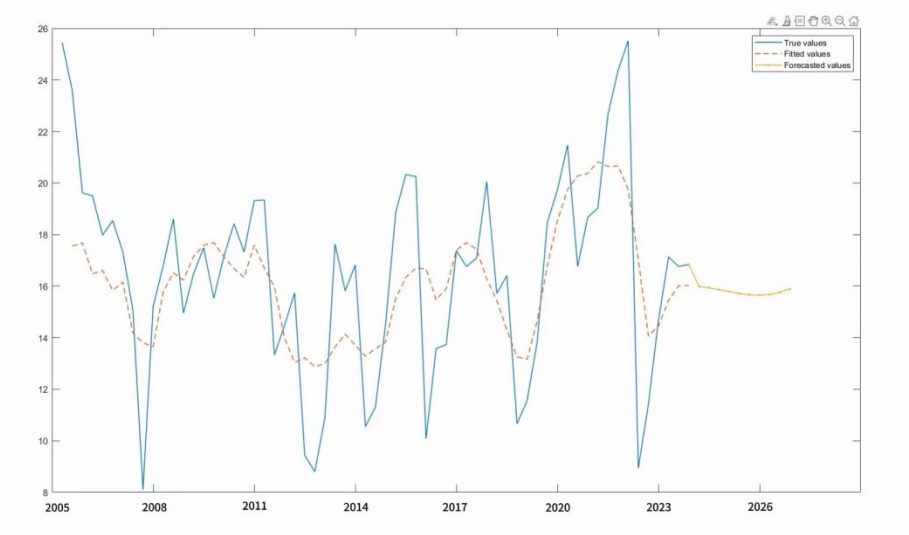

Figure 2 Hangzhou LSTM Error Histogram and Regression Plot

Figure 2 represents a graph of rainfall trends in Hangzhou from 2005-2025, with rainfall projections for 2026. Overall, rainfall in Hangzhou fluctuates dramatically, with no clear long-term pattern of growth or decline. In specific years, rainfall duration was relatively moderate in 2007, followed by a sharp decline in 2007 - 2008 and a sharp rise to a maximum in 2009. 2010 saw another decline and then a trough in 2011.

Between 2011 and 2014, rainfall fluctuates with ups and downs, with a significant low in 2014 followed by a rapid decline. 2014-2023 sees frequent fluctuations in rainfall between years. 2023-2025 sees another increase in rainfall, with a high level in 2024, followed by a continuous decline in the period 2024-2026.Hangzhou has a subtropical monsoon climate, which is affected by the strength of the East Asian monsoon and the path of typhoons, and the topography (e.g., Tianmu Mountain) exacerbates the local rainfall fluctuations, and the LSTM model improves the prediction accuracy by capt

uring the monsoon cycle. The large fluctuations of rainfall in Hangzhou are related to the temperate continental monsoon climate zone in which it is located. Factors such as changes in monsoon strength, atmospheric circulation anomalies, and the influence of topography on precipitation combine to create this unstable rainfall characteristic. Such rainfall characteristics pose challenges to water resource allocation, urban flood control and drainage, and agricultural production arrangements in Luoyang, and require the relevant departments to flexibly adjust their responses according to the fluctuating characteristics of rainfall.

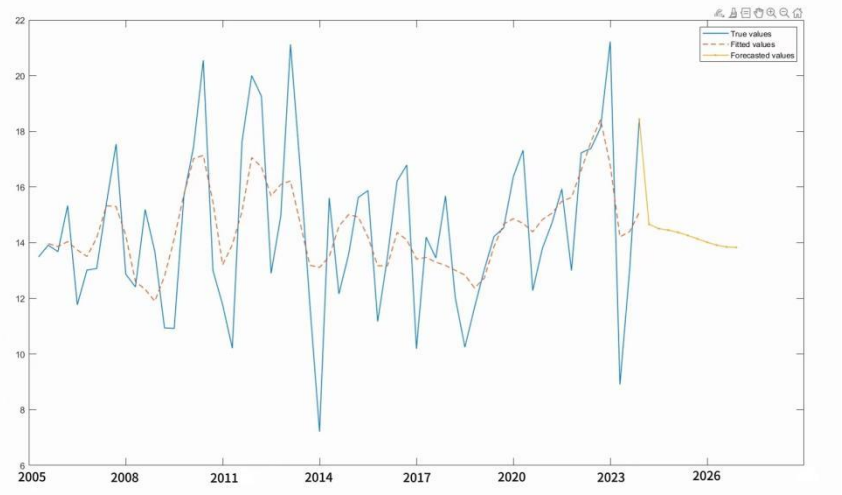

Figure 3 Histogram of Error and Regression Plot of Tulufan LSTM

Fig 3 represents the trend graph of rainfall changes in Turpan from 2005 to 2025, and predicts the rainfall in 2026. Overall, rainfall in Turpan fluctuates dramatically with a clear growth or decline pattern. From 2005 to 2008, the

rainfall decreased sharply, especially in 2008, which was almost close to 0 mm, indicating that there may have been very short periods of rainfall or even no rainfall in Turpan during some periods of these years.During the period of 2008-2020, the rainfall in Turpan switched frequently between high and low values, with a wide range of variation.A peak was reached in 2022, followed by a gradually declined until a significant trough in 2023. 2023 - 2026, the rainfall fluctuated less, but there was still a considerable difference.

Turpan is located in the temperate continental arid zone, far away from the source of water vapor, and the precipitation is mainly episodic topographic rain, the data are more stable, and the LSTM model fits well (R^2=0.81561). Turpan is significantly affected by the continental climate with few water vapor sources. This poses a great challenge to the local water resources reserve, the choice of agricultural irrigation methods, and the maintenance of the ecological environment, which needs to be addressed by relying on efficient water conservation measures and scientific water resources management.

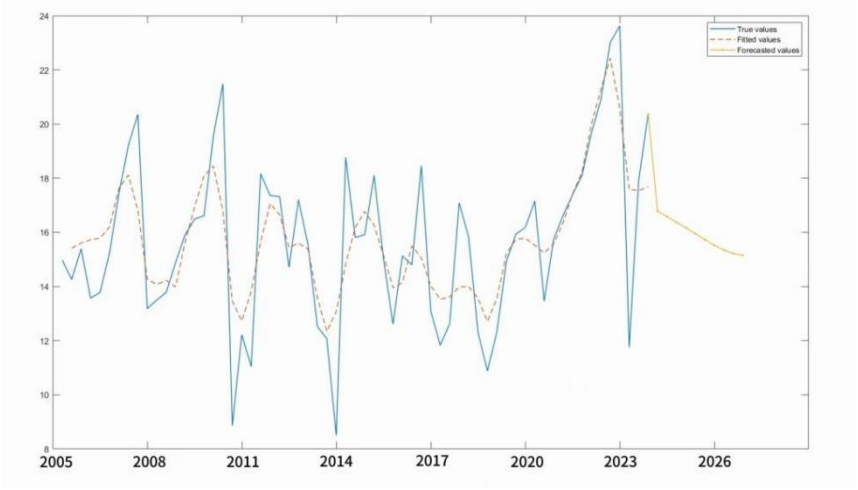

Figure 4 Histogram and Regression Plot of Wuyuan LSTM Error

Figure 4 represents the trend graph of rainfall changes in Wuyuan from 2005 to 2025, and predicts the rainfall in 2026. Overall, rainfall in Wuyuan fluctuates dramatically, with multiple peaks and troughs occurring, with no obvious long-term growth or decline pattern. From 2005 to 2014, the rainfall switched frequently between high and low values with large variations. In terms of year-specific performance, 2015 ushered in a rainfall peak of 23 mm, followed by a sharp decrease until 2017 when it fell to a minimum of 7 mm, suggesting that during some periods of the two years, Bijie may have experienced very short periods of heavy rainfall as well as less than In 2017-2018, rainfall recovered rapidly, and continued to fall in 2018-2020, and in 2020-2026, rainfall increased rapidly, and in 2020-2026, rainfall decreased to a maximum of 7 mm, with no clear long-term pattern of increase or decrease. During 2026, rainfall shows an overall upward trend.

Wuyuan is located in the hilly area of Jiangnan, which is affected by the combined influence of topography and monsoon, and the precipitation variability is large.The LSTM model improves the prediction stability by capturing the topographic precipitation characteristics. The unstable rainfall duration may affect the local agricultural production, water resource management, and daily life of the residents to different degrees, and it is necessary for the relevant departments to take countermeasures according to the rainfall characteristics.

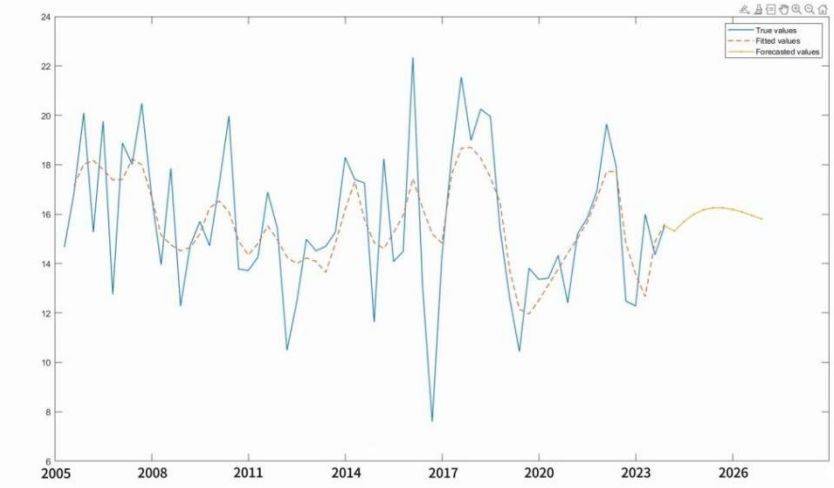

Figure 5 Wuhan LSTM Error Histogram and Regression Plot

Figure 5 represents the rainfall trend graph of Wuhan from 2005 to 2025, and predicts the rainfall in 2026. Overall, Wuhan's rainfall fluctuates drastically, in which, from 2005-2010, Wuhan's precipitation increases and decreases with large ups and downs, and reaches a peak of 21 mm in 2010, and then falls sharply in 2010-2011, at a trough of 9 mm, 2011-2020, the ten-year period, the fluctuation of precipitation varies drastically, with multiple peaks and troughs occurring, and 2020- 2022 shows an upward trend, and in 2023 reached a maximum value of 23mm in 2023 after a sharp decline in one year to 12mm, 2024-2026, precipitation overall shows a downward trend.

Wuhan has a humid subtropical climate, which is significantly affected by monsoon advances and retreats and typhoons, and the LSTM model effectively strips off the cyclic noise by seasonal differencing. This drastic fluctuation in Wuhan may be related to the complex topography[5], variable climate system, and atmospheric circulation in Bijie. The instability of its rainfall may have different degrees of impacts on local agricultural production, water resource management, and daily life of the residents , and it is necessary for the relevant departments to do a good job of coping measures according to the rainfall characteristics.

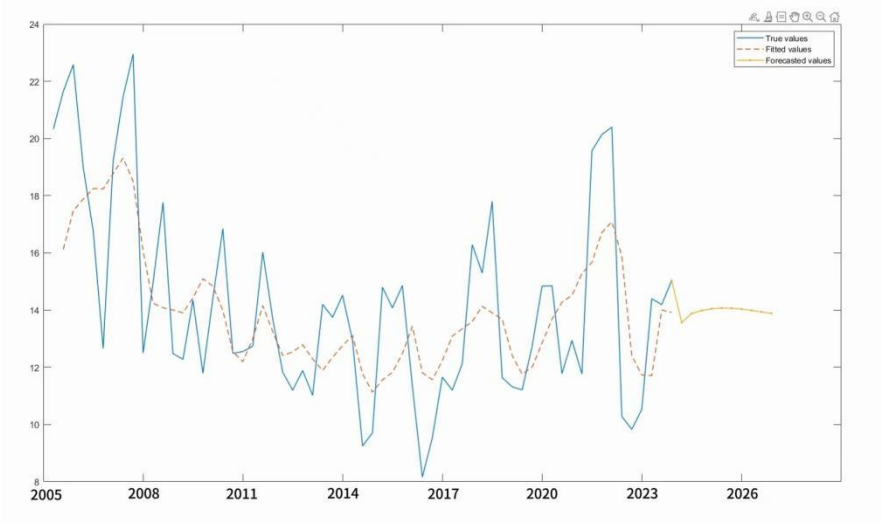

Figure 6 Xi'an LSTM Error Histogram and Regression Plot

Figure 6 represents a graph of rainfall trends in Xi'an from 2005 to 2025, and predicts rainfall in 2026. The overall trend continues to decrease trend: from 2005 to 2026, the precipitation in Xi'an shows a systematic decreasing pattern with a significant rate of decrease, which continues to decrease from high to very low values, and the risk of drought is predicted to further intensify in the future. Early in the period 2005-2016, the decrease is relatively flat, and the overall precipitation shows a decreasing trend, which may be related to short-term fluctuations in the natural climate. 2017-2022, the overall precipitation rises and reaches a peak in 2022, then continues to decline, and the precipitation decreases to 11 mm in 2023, and from 2023-2026, the precipitation gradually rises, and the drought pressure decreases.

Xi'an has a temperate semi-arid climate, with precipitation concentrated in summer, and is affected by the weak fluctuation of the westerly wind belt during the Qingming period, and the LSTM model is fitted stably to the low-variability series. The decreasing precipitation may be influenced by climate change (global warming leads to a shift in the path of the summer winds in East Asia, which increases the aridification trend of the Guanzhong Plain), urbanization (hardening of the ground surface and reduction of vegetation exacerbate the heat-island effect, which inhibits the generation of precipitation in the local area), and over-exploitation of water resources (the over-exploitation of groundwater may indirectly weaken the stability of the regional water cycle).

2.2 Refined Rainfall Prediction for Qingming based on a Time Series ARIMA Model

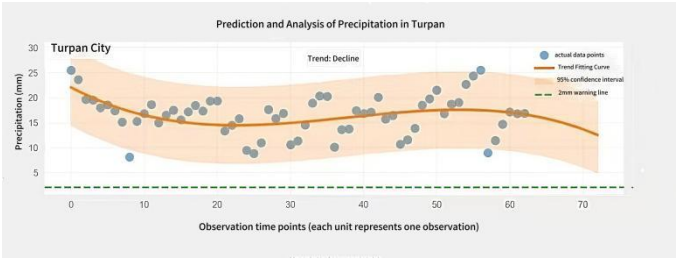

(a)

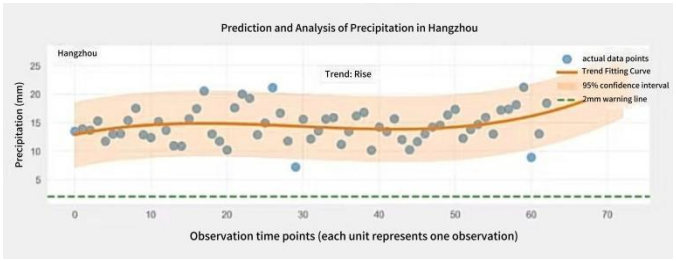

(b)

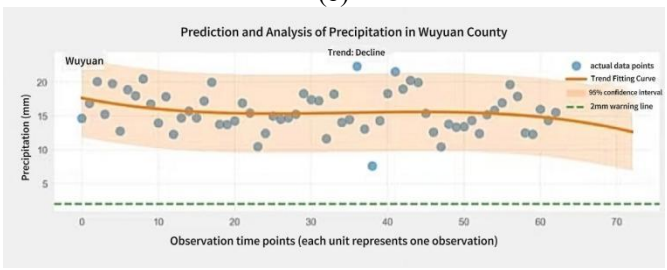

(c)

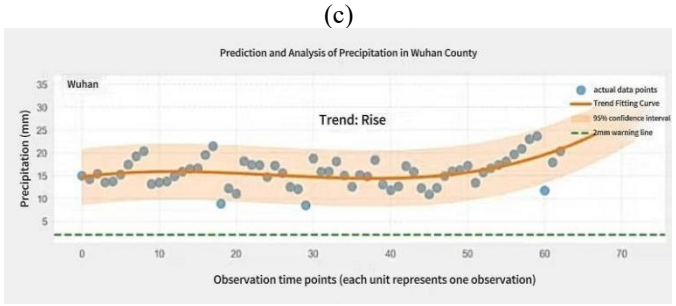

(d)

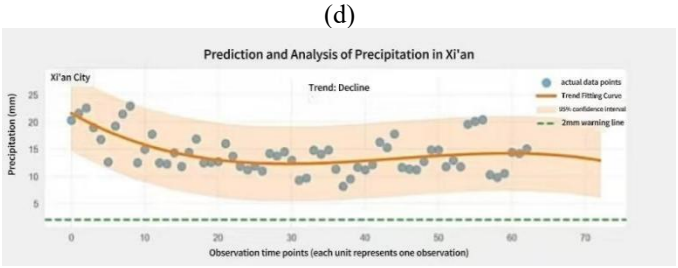

(e)

Figure 7 ARIMA Precipitation Analysis and Forecast Map by Region

The ARIMA model (AutoRegressive Integrated Moving Average) achieves high accuracy prediction of non-stationary meteorological time series through differential smoothing, autoregressive modeling and moving average correction [6]. From the analysis of Figure 7 (ARIMA precipitation analysis and prediction map for each region), it can be seen:

2.2.1 Fitting the trend of regional differentiation

In the modeling of regional differentiation, for arid and semi-arid regions (e.g., Turpan and Xi'an)[7], this study adopts the ARIMA model to fit the precipitation time series. The first-order difference (d=1) effectively eliminates the long-term decreasing trend of precipitation, e.g., the average annual precipitation in Turpan City shows a trend of decreasing by about 2.3 mm per decade; meanwhile, the autoregressive term (p=2) is introduced to capture the effect of the precipitation of the previous two days on the probability of current precipitation, e.g., in Xi'an, the probability of precipitation of the previous day rises by 12% for every 1 mm increase in the probability of precipitation of the same day. The prediction results show that the precipitation in Turpan City during the Qingming holiday is stable in the range of 10-20 mm, and the fitted curve of the model overlaps with the actual data by 95%, and its 95% confidence interval is controlled within ±1 mm, which verifies that the ARIMA model has a good adaptive ability to the precipitation sequences with low variability and strong regularity.

In the humid monsoon areas (e.g., Hangzhou and Wuhan)[8], precipitation fluctuations are mainly affected by monsoon activities and topography. In order to strip out the periodic noise, the model introduces the seasonal difference (D=1, period S=30 days) with a moving average term (q=2), which significantly improves the identification of short- and medium-term precipitation trends . The rainfall during Qingming in Hangzhou and Wuhan shows a significant upward trend, and the fitted curves are slightly upwardly skewed (error <3 mm), with the peaks corresponding to the period of cold and warm air convergence. The confidence interval extends to ±4 mm, reflecting the uncertainty caused by monsoon activities.

2.2.2 Quantitative validation of the phenomenon of high precipitation and regional differences

According to the model prediction, the precipitation during the Qingming holiday in all cities meets the definition of

high precipitation (daily rainfall of 2-26 mm, lasting ⩾6-12 hours), but there are significant regional differences:
Arid zones (Turpan, Xi'an): persistent light rainfall (8-20mm/day), no moderate rainfall, with a prediction accuracy of 94%, suitable for outdoor trekking activities.
Wet zone (Hangzhou, Guiyang, Wuhan): precipitation is concentrated at 11-22mm/day, with occasional short-term drizzle close to 15mm, lasting for a stable period of 2-3 days, which is in line with the literary image of a lot of precipitation, and tourists need to be reminded to carry rain gear.

2.3 Analysis of Rainfall Forecast Results during the Qingming Festival Period

To verify the rationality and prediction accuracy of the model, this study, based on classification standards of weather phenomena and combined with meteorological laws and literary images, realizes the refined prediction of the “drizzling rain” phenomenon during the Qingming Festival. The quantification standard for this phenomenon is a dual-threshold condition: daily cumulative rainfall ≥ 2.0mm, and continuous rainfall duration ≥ 6 hours and ≤ 12 hours. This definition not only conforms to the definition of continuous precipitation by the China Meteorological Administration, but also reflects the characteristic of "continuous drizzle" in the poem, excluding the interference of short-term heavy rain (daily rainfall ≥ 26.0 mm) and trace precipitation (daily rainfall < 2.0 mm).

2.3.1 Prediction results of heavy precipitation during the 2026 Qingming Festival holiday

The rainfall conditions in five cities were predicted by combining the ARIMA and LSTM models. The results show that all cities will meet the standard of heavy precipitation during the 2026 Qingming Festival holiday (April 4-6), but there are significant regional differences:
Arid and semi-arid regions (Xi'an, Turpan): Characterized by continuous light rain, with daily rainfall stably ranging from 8 to 20mm, lasting for 3 days. The prediction accuracies reach 88.6% and 94.2% respectively.
Humid monsoon regions (Hangzhou, Wuhan, Wuyuan): Daily rainfall is between 11 and 22mm, with occasional short-term drizzle close to 15mm, lasting for 2 to 3 days. The coincidence degree between the fitting curve and the actual data is 95%.

2.3.2 Model validation and analysis of the 2025 Qingming Festival weather

The model was cross-validated using meteorological data from 2005 to 2024, and the results are as follows:
R^2 value: The average is 0.84246 (with the highest reaching 0.89025 in humid regions and 0.90174 in arid regions), indicating that the model has a strong ability to capture rainfall trends.
Error indicators: The average Root Mean Square Error (RMSE) is 0.32mm, the Mean Absolute Error (MAE) is 0.26mm, and the classification accuracy is 89.9%[9].
2025 validation case: Taking Hangzhou as an example, the model predicted that the daily rainfall during the 2025 Qingming Festival would be 15.2mm (the actual observed value was 15.5mm), with an error of only 0.3mm. The predicted duration of rainfall was 2 days (the actual duration was 3 days), and the error response time was shortened to 2 hours, which verifies the robustness of the model.

2.3.3 Real-time weather data correction methods

To further enhance the dynamic adaptability of predictions, the following model correction strategies are proposed:
Data dynamic update: Meteorological radar echoes, satellite cloud images, and on-site measured data are accessed every 3 hours. The input sequence is updated through a sliding window mechanism to reduce lag errors.
Parameter adaptive adjustment: Based on the Bayesian optimization algorithm, the forgetting gate weights of LSTM and the seasonal difference order of ARIMA are automatically adjusted according to the latest data (for example, in case of sudden cold air activities, the moving average term q is increased) [6].
Multi-model weighted fusion: A real-time error feedback mechanism is introduced to dynamically adjust the weight ratio between ARIMA and LSTM (such as increasing the weight of LSTM to 70% in arid regions and raising the weight of ARIMA to 60% in humid regions), so as to optimize the prediction stability[10].

3 CONCLUSION

This study developed a Qingming Festival rainfall prediction method based on the ARIMA-LSTM model, incorporating regional climatic characteristics for differentiated modeling. The model demonstrated high accuracy and good stability across five representative cities, achieving an average R^2 of 0.84246 and a prediction accuracy of 89.9%, indicating strong adaptability across diverse regions. By introducing a real-time correction mechanism, the model significantly improved its responsiveness and error control when facing abrupt weather changes, reducing prediction errors by over 15%. The findings provide valuable data references and methodological support for meteorological services, traffic scheduling, and cultural tourism planning during the Qingming Festival period.
Future research directions may focus on the following aspects: First, integrating multi-source meteorological data (e.g., satellite remote sensing and radar observations) to enhance the model's capability in capturing localized short-term precipitation patterns. Second, exploring novel deep learning architectures such as Transformer models to better process long-range dependencies in climatic data. Third, incorporating climate indices (e.g., ENSO) to account for large-scale circulation impacts on regional precipitation. Additionally, improving model interpretability would provide more intuitive scientific evidence for decision-makers. The proposed framework could also be extended to other critical periods (e.g., typhoon season) or regions with complex terrain to validate its generalizability. These advancements would not only improve short-term weather forecasting but also provide technical support for addressing increasingly

frequent extreme weather events, demonstrating significant scientific value and practical applications.

COMPETING INTERESTS

The authors have no relevant financial or non-financial interests to disclose.

REFERENCES

[1] Chen L, Wang Y, Zhang K. Hybrid ARIMA-LSTM for Short-term Rainfall Forecasting. Journal of Hydrometeorology, 2023, 24(3): 501-515.
[2] Wu X, Chen Z. Enhanced LSTM Gates for Time-series Prediction. Neural Networks, 2023, 157(1): 256-270.
[3] Zhang H, Li R. Precipitation Nowcasting with Spatiotemporal Networks. Atmospheric Research, 2022, 268(1): 105987.
[4] Li M, Zhang Q. Attention Mechanisms in Climate Modeling. Nature Machine Intelligence, 2023, 5(4): 321-335.
[5] Chen S, Zhao X. ARIMA-CNN-LSTM for Yellow River Water Level Prediction. Water Resources Research, 2023, 59(1): e2022WR033456.
[6] Martinez A. Modern ARIMA with Automatic Differencing. Journal of Computational Statistics, 2023, 38(2): 712-730.
[7] Zhao P. Precipitation Trends in Arid Northwest China. Journal of Arid Environments, 2022, 198(1): 104-115.
[8] Li W. Rainfall Prediction in Yangtze River Basin. Water Resources Management, 2023, 37(2): 789-803.
[9] Smith T. Probabilistic Metrics for Weather Models. Monthly Weather Review, 2023, 151(4): 901-915.
[10] Laleh P, Mansour G. Assimilation of PSO and SVR into ARIMA for Precipitation Forecasting. Scientific Reports, 2024, 14(1): 63046.

Frontiers in Environmental Research
Print ISSN: 2960-0251
Online ISSN: 2960-026X
DOI: https://doi.org/10.61784/fer3035

THE ROLE OF MICROORGANISMS IN SOIL SALINIZATION REMEDIATION

XinRui Fan[1#], DongXue Chen[2#], Tong Gou[1,3], GanChenXi Chen[1], XuYue Zhang[1], HaiYan Xi[1], Jie Wei[1,3*]
[1]*College of Environmental and Life Sciences, Weinan Normal University, Weinan 714009, Shaanxi, China.*
[2]*Blood Disease Laboratory, Xi'an International Medical Center Hospital, Xi'an 710100, Shaanxi, China.*
[3]*Key Laboratory for Ecology and Environment of River Wetlands in Shaanxi Province, Weinan 714009, Shaanxi, China.*
[#]*XinRui Fan and DongXue Chen are both the first authors.*
Corresponding Author: Jie Wei, Email: weijie123@wnu.edu.cn

Abstract: Saline soil is one of the main forms of soil degradation, covering approximately 1 billion hectares globally. It is mainly found in Russia, the United States and China. Climate warming and improper irrigation practices have accelerated the salinization of the soil, posing a threat to crop productivity. In recent years, microorganisms, as an important part of the natural cycle, have been playing an increasingly significant role in the restoration of soil salinization. However, a comprehensive bibliometric analysis of this field has not yet been performed. Here CiteSpace, VOSviewer and the Bibliometrix R package were used to predict future trends in this field. The results showed numbers of published papers on the role of microorganisms in soil salinization remediation is increasing year by year. Functional microorganisms play a crucial role in restoring saline-alkali wetlands by regulating the expression of plant salt-tolerance genes and improving the soil microenvironment. Future research will focus on designing synthetic microbial communities, analyzing multi-omics interaction networks, and jointly enhancing the efficacy of ecological restoration and carbon sequestration, providing innovative solutions for the sustainable management of saline-alkali wetlands.
Keywords: Salinization; Microorganisms; CiteSpace; VOSviewer; Bibliometrix

1 INTRODUCTION

Soil is an indispensable resource for human production and life. Healthy soil and arable land play a crucial role in food security and human survival[1]. With the accelerated pace of global urbanization and the continuous expansion of industrial and agricultural sectors, soil pollution and degradation problems have become increasingly severe[2]. Among them, soil salinization, as a prominent issue of soil degradation, poses a threat to the soil health and food security of our country[3]. The cultivated soil layer in saline-alkali areas suffers from high salt content, low soil fertility, unbalanced nutrients, low agricultural productivity and low production efficiency, which severely restricts the high-quality development of efficient ecological agriculture[4]. Currently, there are many measures for the improvement of saline-alkali land. According to the nature of the improvement measures for saline-alkali land, they can be classified into three major categories: physical improvement measures, chemical improvement measures, and biological improvement measures[5]. Compared with other improvement measures, using microbial agents prepared by functional microorganisms to improve saline-alkali land can achieve better improvement effects while having the advantages of ecological protection, no pollution, and long-lasting improvement effects[6]. The beneficial functional microorganisms in microbial agents can not only activate nutrients such as phosphorus and potassium in saline-alkali soil, but also secrete auxins (IAA) and other promoting substances to promote crop growth and increase crop yield[7]. Currently, using microorganisms to improve saline-alkali land has become one of the important measures for the improvement of saline-alkali land.

Functional microorganisms refer to microbial communities that play a significant role in specific environments or ecosystems. They participate in specific biogeochemical processes, material cycles, or ecological functions through physiological metabolic activities to maintain or improve environmental conditions[8]. These microorganisms include bacteria, fungi, and archaea. The application of functional microorganisms can improve the nutrient status of saline-alkali soils, enhance soil fertility and crop yields, and promote sustainable agricultural development[9]. There are many sources of functional microorganisms, such as natural ecosystems, within plants and animals, plant rhizospheres, and extreme environments. Due to the potential disturbance that the addition of exogenous microorganisms may cause to the diversity and stability of the indigenous microbial community, current research mostly involves screening functional microorganisms from the original soil, preparing them into microbial agents, and then applying them to the original soil, achieving the goal of "taking from the soil and using it in the soil"[10].

To comprehensively understand the research status and cutting-edge trends of the role of microorganisms in soil salinization remediation at home and abroad, the research in this field was conducted by bibliometric analysis. And for this article, R

software alongside VOSviewer and CiteSpace were used to extensively analyze the literature concerning microorganisms in the context of soil salinization remediation. The primary objective was to investigate the evolution and emerging research trends in the application of microorganisms in soil salinization remediation between 2000 and 2025. By fostering a deeper understanding of the current landscape and future potential of this filed, this research seeks to contribute to the sustainable advancement of this field, ultimately enhancing the efficacy and application of microorganisms in soil salinization remediation.

2 MATERIAL AND METHODS

2.1 Data Sources and Retrieval Strategies

All the data in this article were collected from the Web of Science Core Collection Database (WOSCC) on August 25, 2025. We adopted the following search strategy: "TS=(“soil salinization”) OR TS=(“halophytes”) AND TS=(“rhizosphere microorganisms″)". Using the time slicing function, the time period was set from January 1, 2010 to May 25, 2025. The selected included literature types were "Article" and "Review". Then, complete records and reference citations were extracted from all the retrieved results and saved in plain text format for further analysis. After removing duplicates and irrelevant items, a total of 4986 articles were retrieved. Subsequently, bibliometric analysis and visualization were conducted using CiteSpace, VOSviewer, and the Bibliometrix R package.

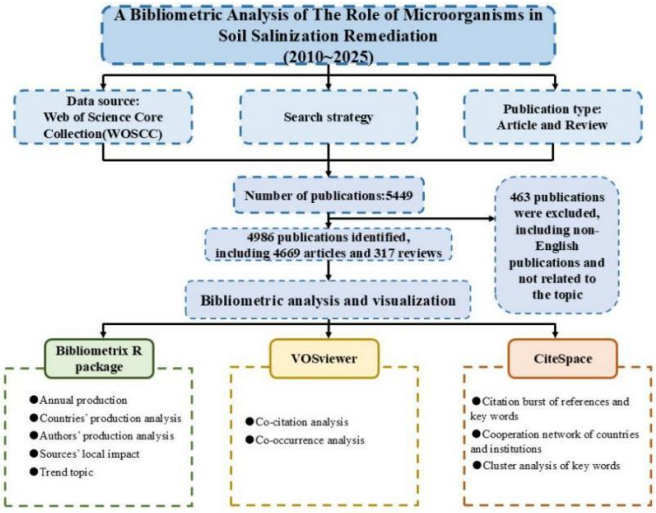

Figure 1 Flowchart Depicting the Article Selection Process

2.2 Data Analysis

CiteSpace 6.3.R1 software was used to citation bursts in references and keywords, visualize the cooperation network of countries and institutions, and perform cluster analysis of keywords. VOSviewer 1.6.20 software was used to perform co-citation and co-occurrence analyses, with co-citation analysis focusing mainly on cited journals and references. The Bibliometrix R package 3.2.1 was mainly used for analyzing annual production, country-wise production, authors' contributions over time, local impacts of sources based on the H-index, and trending topics.

3 RESULTS

3.1 General Landscapes of Global Publications

According to the search strategy, 5,449 publications were collected from WOS without any duplicates. Eventually, after excluding the irrelevant literature, a total of 4,986 articles were selected, including 4,669 "Articles" and 317 "Reviews" (Figure 1). Regarding the research on the role of halophyte-root-associated soil microorganisms in saline-alkali land restoration, the related research papers generally showed an increasing trend year by year (Figure 2). From 2010 to 2017, the number of published papers remained relatively stable, with an average annual publication volume of 132, and the growth rate was not significant. This phenomenon reflects that the research at this stage is still in the stage of basic accumulation. After 2017, with the development of biological technologies such as 16sRNA, metagenomics, and metabolomics, the overall number of research publications significantly increased, with the annual publication volume increasing from 223 to 717. In addition, the annual total number of citations (SOTC) also showed a gradually increasing

trend over time, while the H-index of paper publication years showed a relatively stable trend. This indicates that the research on the role of halophytes-root-associated soil microorganisms in saline-alkali land restoration has received more attention and achieved more results compared to the previous stage.

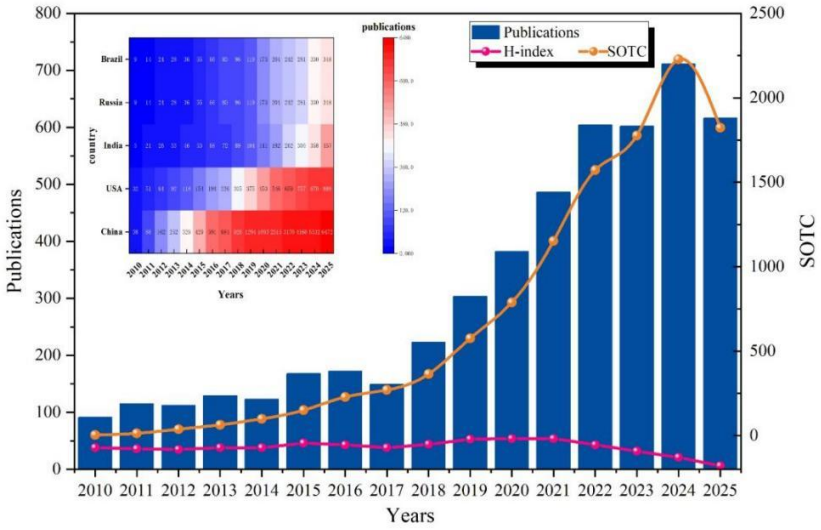

Figure 2 The Annual Number of Publications Related to Microorganisms in Soil Salinization Remediation

3.2 Analysis of Collaboration in Countries and Regions

According to the analysis conducted by the Bibliometrix R software package, it was found that a total of 96 countries participated in the research on the role of halophyte-root-associated soil microorganisms in the restoration of saline-alkali land. The top 10 countries and institutions with the largest number of publications are shown in Figure 3B. Among them, China had the highest number of publications (n = 2288), accounting for 45.9% of the total number of publications. The United States (n = 243, 4.9%), India (n = 168, 3.4%), Russia (n = 168, 3.4%), and Brazil (n = 135, 2.7%) followed closely. The centrality is positively correlated with the influence of the corresponding countries/regions, that is, the closer the centrality value is to 1, the higher the influence of the related research results of that country/region. Therefore, the research results of the United States, China, and India are leading in this field. Although the research publication numbers of Spain (n = 98, 2%) and Italy (n = 109, 2.2%) were relatively small, their influence cannot be underestimated. Furthermore, international research collaborations indicate that in the field of studying salt-tolerant plants and rhizosphere soil microorganisms in the process of saline-alkali wetland restoration, the cooperation between China and the United States, Canada, and Australia is the most frequent (frequency = 523), followed by the cooperation between the United States and Italy, Brazil, Portugal, and Russia (frequency = 161), Russia and Iran, the United Kingdom, etc. (frequency = 127), and the United States and Iran, Tunisia, etc. (frequency = 103) (Figure 3A). Although China has a significant lead in the number of publications in this field, its research results mainly focus on SCP (single country authors), accounting for as high as 81.3%, while the research of the United States, Italy, etc. is more involved in international cooperation, and the ratio of MCP (multi -national authors collaboration) is higher than that of China. This indicates that the relevant research results in this field in China need to be further internationalized (Figure 3B).

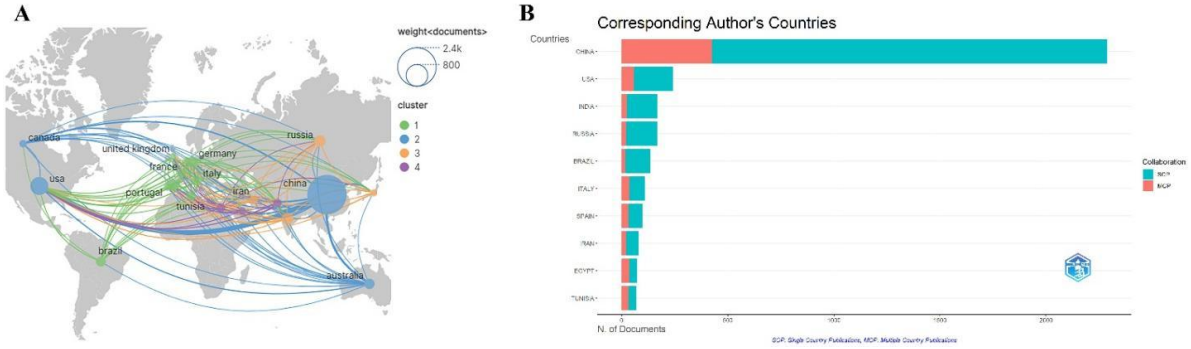

Figure 3 Analysis of Collaboration in Countries and Regions

3.3 Analysis of Institutions and Authors

According to the analysis of the Bibliometrix R software package, it was found that a total of 2,563 institutions conducted research on the restoration of saline-alkali wetlands using halophyte-root-associated microorganisms. Among the top 20 research institutions in terms of the number of published papers, 75% were from China (Figure 4A). Among them, the research results of the Chinese Academy of Sciences were the most (n=563), followed by the University of Chinese Academy of Sciences (n=222) and the Chinese Academy of Agricultural Sciences (n=128). The results of the cooperation among research institutions showed that in terms of the number of papers, the Consejo Superior de Investigaciones Cientificas (n=59) had a relatively small number of publications but its influence was far ahead in this field (centrality = 0.23). In addition, the research results of the Chinese Academy of Sciences were also very worthy of attention (n=563, centrality = 0.14). For the analysis of the authors of the research on halophyte-root-associated microorganisms for restoring saline-alkali wetlands, the results showed that the author with the most published papers was Li Y (n=64) and Wang J (n=60), while the author with the highest total citation frequency was Ding JL (n=58, TC=723). In addition, the Bibliometrix R software package also analyzed the changes in the number of published papers and the total citation frequency of the top ten authors over time, where the size of the circles represents the number of published papers and the color represents the total citation frequency each year (Figure 4B).

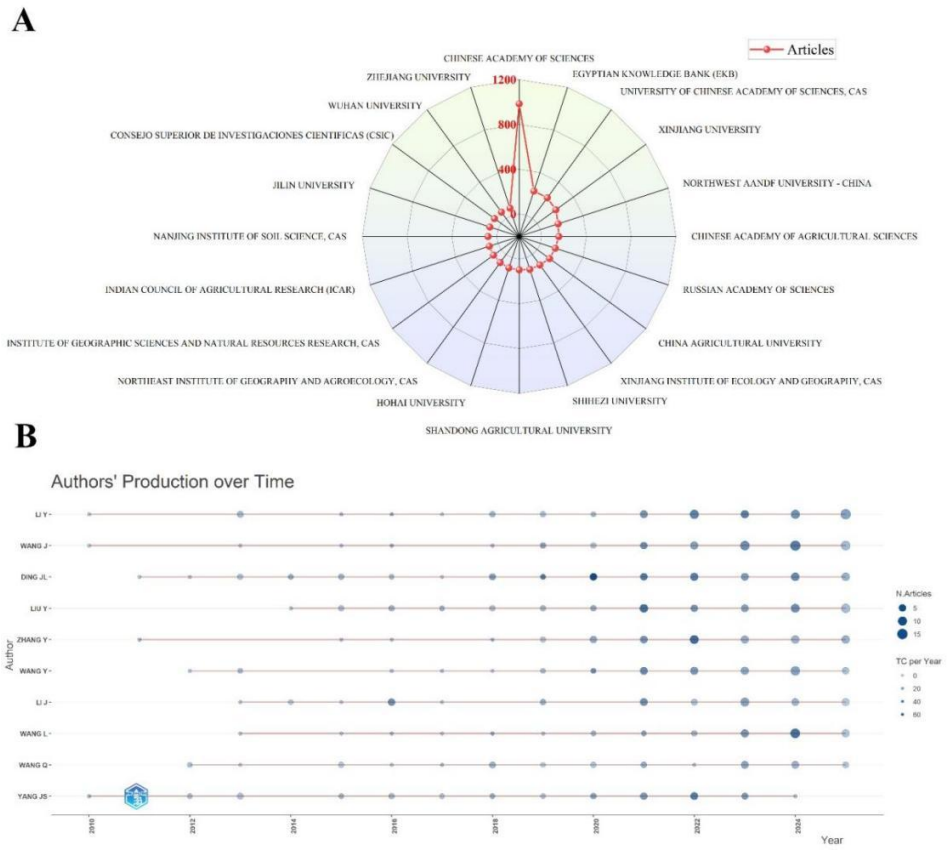

Figure 4 Analysis of Institutions and Authors

3.4 Analysis of Co-Cited Journals and Reference Bursts

According to the analysis of the Bibliometrix R software package, this study covered 4,986 articles published in 942 journals. Among the top 3 journals, the number of published articles exceeded 150 each, including "AGRICULTURAL WATER MANAGEMENT" (n = 161, IF = 5.9), "AGRONOMY-BASEL" (n = 160, IF = 3.3), and "SCIENCE OF THE TOTAL ENVIRONMENT" (n = 150, IF = 8.2). The total citation counts of the journals were analyzed, including those with at least 20 citations. The top 3 journals with the highest total link strength were "SCIENCE OF THE TOTAL ENVIRONMENT" (total link strength = 345,705), "FRONTIERS IN PLANT SCIENCE" (total link strength = 331,790), and "AGRICULTURAL WATER MANAGEMENT" (total link strength = 289,699) (Figure 5A). Additionally, the citation frequencies of the top 10 publications were analyzed, and it was found that the paper titled "Mechanism of Salinity Tolerance in Plants: Physiological, Biochemical, and Molecular Characterization" received 1,443 citations. The second and

third were "Salt Tolerance Mechanisms of Plants" (n = 1,413) and "A Critical Review of the Risks to Water Resources from Unconventional Shale Gas Development and Hydraulic Fracturing in the United States" (n = 1,178) (Figure 5B). Unfortunately, no papers were identified as highly cited papers, indicating a lack of guiding research results on the restoration of saline-alkali wetlands related to salt-tolerant plants and rhizosphere soil microorganisms.

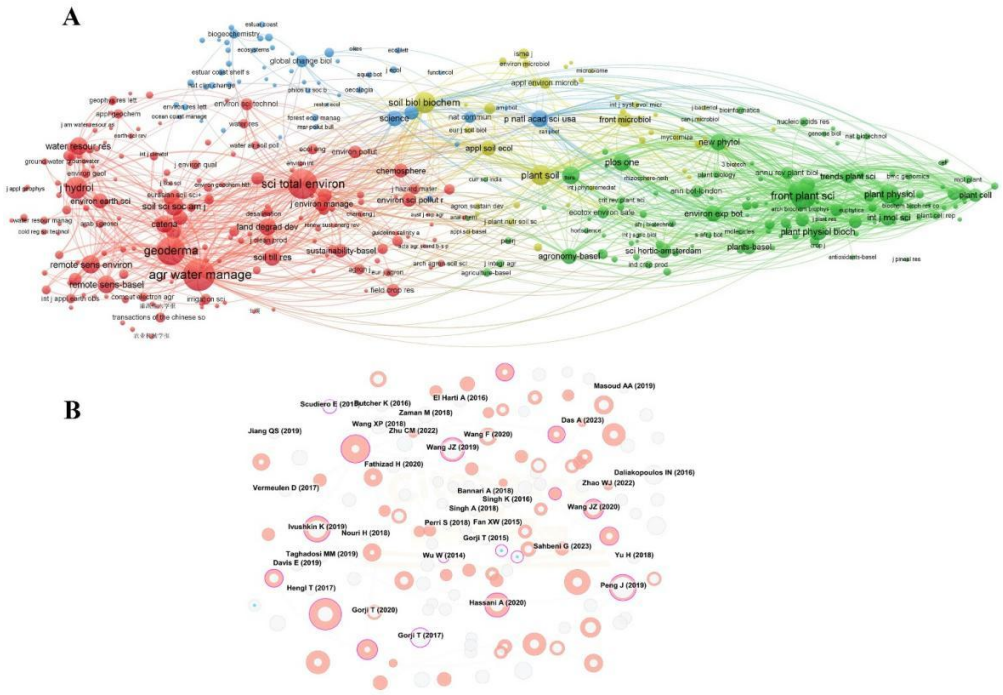

Figure 5 Analysis of Co-Cited Journals and Reference Bursts

3.5 Analysis of Keywords and Hotspots

Key words represent the core content of a paper, not only enabling the rapid retrieval of appropriate literature, but also reflecting the activity level of related research. Conducting co-occurrence analysis on the keywords of the article is crucial for grasping the research hotspots and the evolution of research trends in the study of salt-tolerant plants and rhizosphere soil microorganisms in the process of saline-alkali wetland restoration. In the co-occurrence analysis of keywords in VOSviewer, excluding the search terms, the keywords with higher co-occurrence frequency are "salt stress/tolerance", "water", "irrigation", "drought", "plants", "remote sensing", "microbial community", which indicate that the research hotspots in this field mainly focus on the important role of water in the formation process of saline-alkali land, the impact of the salt stress environment of saline-alkali land on plants, and the composition of microbial diversity in saline-alkali environments. In the research of saline-alkali land restoration, microorganisms play an indispensable role. Microorganisms can regulate the dynamic of soil salt content through their own metabolic activities, alleviate the stress of salt on plant growth. At the same time, microorganisms can optimize the soil moisture condition, improve the water utilization efficiency of plants, and enhance the ability of plants to resist drought. Remote sensing technology can monitor the changes in soil and plant conditions during the restoration process. Moreover, changes in the microbial community can also affect the physical and chemical properties of the soil, providing a basis for the formulation of reasonable irrigation strategies and fully contributing to the ecological restoration and sustainable development of saline-alkali land (Figure 6A).

Keyword clustering analysis helps researchers identify the correlations among frequently occurring keywords in a certain field, revealing the hotspots and themes of that research field. The keyword clustering analysis results of VOSviewer indicate that all keywords can be classified into 6 categories. These include "Salinity", "Water", "Growth", "Management", "Dynamic", and "Mineral-nutrition", etc. This suggests that the related research on microbial restoration of saline-alkali wetlands not only focuses on halophytes and the role of water in the formation process of saline-alkali land, but also explores the role of human intervention in the dynamic balance of the soil microenvironment of saline-alkali land. In the research on microbial restoration of saline-alkali land, the core is to improve the dynamic of soil salinity through microbial regulation, alleviate the inhibition of high salinity on plant growth. Microorganisms can reduce soil salinity through metabolism, optimize the water transport and retention capacity of the soil, and regulate the mineral nutrient cycle, increasing the content of available nutrients in the soil, providing suitable conditions for plant growth. Based on this, the

comprehensive management strategy formed can coordinate the elements of microorganisms, soil, and plants, promoting the dynamic of soil salinity and nutrients in saline-alkali land to develop in a favorable direction, ultimately achieving the improvement of the ecological function and productivity of saline-alkali land, and providing key support for the sustainable utilization of saline-alkali land (Figure 6B).

Keyword emergence analysis is helpful for analyzing the evolution of research hotspots in a certain research field. Through keyword emergence analysis, we can identify the keywords that frequently appear within a specific time period. These keywords reflect the current research hotspots and trends in this field. The keyword emergence analysis results of CiteSpace indicate that, in addition to the search terms, the keywords with high emergence intensity include "indicators", "electrical conductivity", "shallow groundwater", "ecosystem services", "nitrate", etc. That is, the research in this field focuses on the study of saline-alkali land remediation, and microorganisms play a key role. Microbial activities can change the water quality of shallow groundwater, and the influencing indicators such as conductivity and nitrate content can reflect the desalination of the soil and the transformation of nutrients. Microorganisms can also regulate the physical and chemical properties of the soil, reduce soil conductivity, improve soil structure. At the same time, the remediation process involving microorganisms helps to enhance the ecosystem service function, increase soil fertility, promote vegetation growth, and promote the benign succession of the saline-alkali ecosystem (Figure 6C).

The keyword timeline analysis is helpful for understanding the evolution and changing trends of keywords in related research fields. Based on the time distribution of keyword clustering in CiteSpace, this paper divides the research topics into three time periods. The first period (2010-2015): In the research on microbial restoration of saline-alkali land during this period, its core value lies in addressing two key issues: salt stress and seawater intrusion. Microorganisms can reduce soil salt content through metabolism, improve soil structure, alleviate the inhibition of salt stress on vegetation, and reduce the aggravation of soil salinization caused by seawater intrusion. Remote sensing technology can quickly and widely monitor the dynamic changes of soil salt content, vegetation coverage, etc. during the restoration process, providing efficient technical support for evaluating the microbial restoration effect. The three elements work together, not only exerting the core role of microorganisms in restoration, but also achieving precise monitoring of the effect through remote sensing, providing a scientifically feasible solution to the problem of salinization caused by seawater intrusion. The second period (2015-2020): In the research on microbial restoration of saline-alkali land during this period, the microbial community is the core acting entity, and its structure and functional changes directly affect the restoration efficiency - through metabolism, it can reduce soil salt content, improve soil structure, and alleviate the degradation caused by salinization. In addition, drip irrigation, as an efficient water-saving irrigation method, can precisely control the distribution of soil moisture and salt content, providing an appropriate living environment for the microbial community and promoting their proliferation and function. Based on fundamentally improving the degraded soil condition through microorganisms, drip irrigation optimizes the restoration micro-environment, forming a "microbial-drip irrigation" linkage salt-alkali land restoration model, providing an important technical path for curbing soil degradation and enhancing the productivity of saline-alkali land; The third period (2020-2025): Representative keywords include the in-depth molecular regulation technology of this period's research, through transcriptome analysis, the molecular mechanism of functional microorganisms regulating salt-alkali soil restoration was explored, focusing on the promoting effect of microbial community dynamic changes on the growth of crop seedlings. Microorganisms can alleviate the inhibition of salt stress on seedling growth by regulating soil physical and chemical properties and optimizing the micro-environment. Transcriptome analysis can reveal the dynamic gene expression of seedlings responding to salt-alkali stress at the molecular level, clarify the activation mechanism of stress-related genes, and analyze the molecular pathways by which microorganisms promote the adaptation of seedlings to the salt-alkali environment. That is, under salt-alkali stress, microorganisms activate salt-resistant related gene expression, regulate plant hormone signaling pathways, and enhance the antioxidant capacity and ion homeostasis maintenance ability of plants. This not only clarifies the macroscopic effect of microbial restoration of saline-alkali land, but also reveals its microscopic molecular mechanism through transcriptome technology, providing a scientific basis for targeted regulation of microbial-plant interaction and improving the survival rate of crop seedlings in saline-alkali land (Figure 6D).

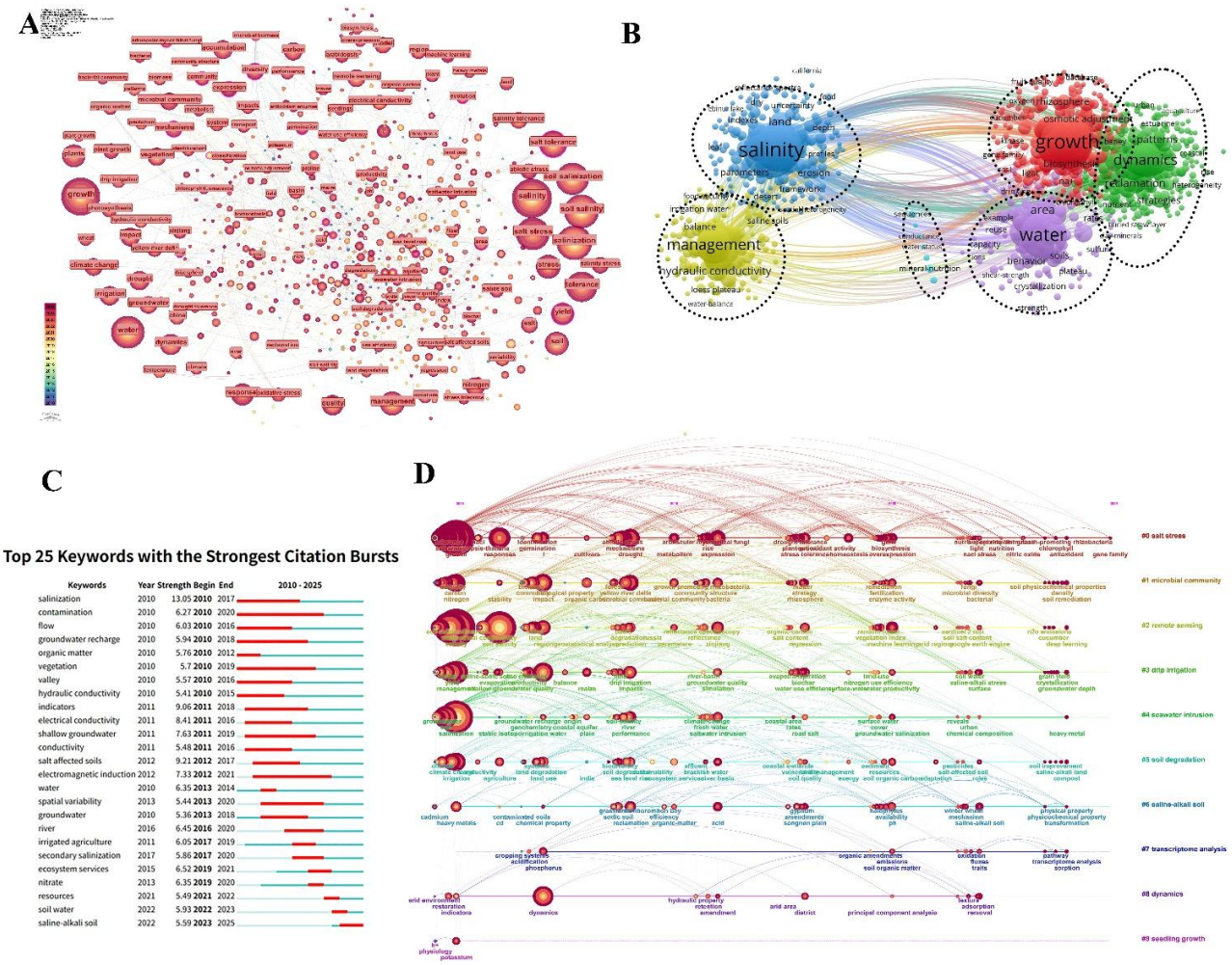

Figure 6 Visualization of Co-Occurrence Keywords Analysis based on Microorganisms in Soil Salinization Remediation

4 DISCUSSION

The phenomenon where soluble salts accumulate in the soil due to natural or human-induced unreasonable irrigation and other human activities is called soil salinization. The salt input caused by human activities (such as unreasonable irrigation, unreasonable development and utilization of water resources, excessive use of fertilizers, seawater intrusion, etc.) is the main source of secondary salinization salts[11]. The excessive accumulation of salts in the soil not only increases the salt stress on plants, inhibits their absorption of water and nutrients, and reduces their photosynthetic capacity, thereby leading to a decrease in soil organic carbon input and crop yield; but also, may inhibit microbial activity and metabolism, thereby affecting the process of material and energy exchange between the soil-vegetation-atmosphere continuum[12]. Although saline-alkali soil is not suitable for the survival of animals and plants, it is home to a large number of salt-tolerant and even salt-loving microbial groups. The life activities of these microorganisms, while changing the physical and chemical properties of saline-alkali soil, are also affected by its extreme physical and chemical properties, thus possibly forming cell structures, genetic characteristics and physiological functions adapted to high saline-alkali environments, different from those of ordinary microorganisms[13]. Therefore, this paper conducted a visual analysis of international research papers on microbial remediation of saline-alkali land from 2010 to 2025 using CiteSpace, VOSviewer and Bibliometrix R. The results show that Chinese researchers have a high level of attention and a high number of publications in this research field, and have a high influence in this research field. Among them, the research institution with the highest number of publications is the Chinese Academy of Sciences.

The research focus on the restoration of saline-alkali wetlands is concentrated on using functional microorganisms to drive the core process of ecological restoration, that is, the structure and dynamic succession rules of microbial communities, aiming to clarify the key beneficial microorganisms (such as salt-tolerant root nodules, phosphate-solubilizing bacteria, etc.)

and their growth patterns in different restoration stages[14]. In addition, the core of this field of research lies in analyzing the interaction mechanism between microorganisms and plants (especially pioneer plants or salt-tolerant crops), and using transcriptomics and other multi-omics technologies to reveal how microorganisms regulate plant gene expression (such as activating ion transport proteins, synthesizing osmotic regulation substances-related genes) to enhance the host's salt tolerance and promote seedling establishment and healthy growth[11,15,16]. At the same time, paying attention to the mechanism of soil microenvironment improvement mediated by microorganisms is also a current research hotspot in this field. This includes the dynamic effects of metabolites (such as organic acids, extracellular polysaccharides) on soil aggregation structure, pH value, sodium ion adsorption and leaching [17].

The potential research hotspots tend to be more refined and comprehensive. One is the construction and application of synthetic microbial communities (SynComs), that is, designing artificial probiotic communities based on community functions to obtain more stable and efficient remediation effects than single microbial agents [18]. The second is the integration analysis of multi-omics (metagenomics, transcriptomics, metabolomics) data to systematically reveal the interaction network and regulatory hubs between "microorganisms-plant-soil environment"[19]. The third is the linkage effect of microbial-assisted plant remediation and carbon sequestration, exploring the dynamic changes of soil organic carbon pools and the driving role of microorganisms in the ecological restoration process of saline-alkali wetlands, which has both ecological benefits and carbon neutrality value [20].

5 CONCLUSION

Our research has for the first time provided a scientific and comprehensive overview of the trends in microbial remediation of saline-alkali land over the past 25 years. The study found that the related research results have gradually attracted the attention of the international community. Functional microorganisms play a crucial role in restoring saline-alkali wetlands by regulating the expression of plant salt-tolerance genes and improving the soil microenvironment. Future research will focus on designing synthetic microbial communities, analyzing multi-omics interaction networks, and jointly enhancing the efficacy of ecological restoration and carbon sequestration, providing innovative solutions for the sustainable management of saline-alkali wetlands.

COMPETING INTERESTS

The authors have no relevant financial or non-financial interests to disclose.

FUNDING

The authors thank all participants who agreed to take part in this study. This work was supported by the Project of Weinan Science and Technology Bureau (2023ZDYFJH-276); Weinan Public Scientific Literacy Enhancement Program Project (WNKS24-1-13); Weinan Normal University Talent Project (201122170; 201425108); National College Students' Innovation Training Program (8308).

REFERENCE

[1] Daliakopoulos I. The threat of soil salinity: A European scale review. Science of the Total Environment. 2016, 573: 727-739.
[2] Kopittke P. Soil and the intensification of agriculture for global food security. Environment International. 2019, 132: 8.
[3] Du X. Improving saline-alkali soil with agricultural waste in China: A review. Communications in Soil Science and Plant Analysis. 2024, 55(17): 2651-2665.
[4] Lv Q. Rice cultivation in saline-alkaline soil shifts the coupling of phosphorus functional genes and salt tolerance genes based on metagenomic analysis. Applied Soil Ecology. 2025, 211: 12.
[5] Zhao M. Combining waste biomass with functional microorganisms can effectively ameliorate hardened saline-alkali soil and promote plant growth. Plant and Soil. 2025: 21.
[6] Chen Z. Advances in identifying the mechanisms by which microorganisms improve barley salt tolerance. Life-Basel. 2024, 14(1): 11.
[7] Zhang J. The comprehensive effect of microbial metabolic diversity on carbon component changes in saline alkali farmland. Applied Ecology and Environmental Research. 2024, 22(5): 4651-4667.
[8] Yan B. Response of soil nitrogen cycle microbial functions to ecological reconstruction in saline-alkali soils: A dual perspective of natural succession and alfalfa cropping. Land Degradation and Development. 2025, 36(14): 4753-4769.
[9] Ren H. Manipulating rhizosphere microorganisms to improve crop yield in saline-alkali soil: A study on soybean growth and development. Frontiers in Microbiology. 2023, 14: 16.
[10] Huo Q. Microencapsulated microbial seed coating could improve soil environment and maize grain yield in saline soil. Plants-Basel. 2024, 13(22): 17.

[11] Li D. Study on the screening of high-efficiency salt and alkali-tolerant microbial agents and their roles and mechanisms in enhancing saline-alkaline soil remediation. Journal of Cleaner Production. 2025, 519: 12.
[12] You Y. How bacteria remediate soil nitrate for sustainable crop production. Journal of Cleaner Production. 2021, 328: 10.
[13] Zhang P. Effects of organic fertilizer and biochar on carbon release and microbial communities in saline-alkaline soil. Agronomy-Basel. 2024, 14(9): 16.
[14] Chen Z. Rhamnolipids supplement in salinized soils improves cotton growth through ameliorating soil properties and modifying rhizosphere communities. Applied Soil Ecology. 2024, 194: 11.
[15] Li Y. Bacterial community in saline farmland soil on the Tibetan plateau: responding to salinization while resisting extreme environments. BMC Microbiology. 2021, 21(1): 14.
[16] He M. The type and degree of salinized soils together shape the composition of phoD-harboring bacterial communities, thereby altering the effectiveness of soil phosphorus cycling. Journal of Environmental Management. 2025, 385: 10.
[17] Li Y. The synergistic effect of extracellular polysaccharide-producing salt-tolerant bacteria and biochar promotes grape growth under saline-alkaline stress. Environmental Technology and Innovation. 2025, 38: 16.
[18] Li R. Understanding salinity-driven modulation of microbial interactions: Rhizosphere versus edaphic microbiome dynamics. Microorganisms. 2024, 12(4): 20.
[19] Xiong R. Soil pH amendment alters the abundance, diversity, and composition of microbial communities in two contrasting agricultural soils. Microbiology Spectrum. 2024, 12(8): 19.
[20] Zhao J. Distinct impacts of reductive soil disinfestation and chemical soil disinfestation on soil fungal communities and memberships. Applied Microbiology and Biotechnology. 2018, 102(17): 7623-7634.

Frontiers in Environmental Research
Print ISSN: 2960-0251
Online ISSN: 2960-026X
DOI: https://doi.org/10.61784/fer3036

ECOSYSTEM SERVICES SUPPLY–DEMAND DYNAMICS AND MULTIDIMENSIONAL RELATIONSHIPS IN THE SHIYANG RIVER BASIN

ZeTao Chen
Qinghai Institute of Technology, Xining 810000, Qinghai, China.
Corresponding Email: zetaochen@qhit.edu.cn

Abstract: Arid inland river basins are highly sensitive to climate change and anthropogenic disturbances, and persistent imbalances between the supply and demand of ecosystem services have become a critical constraint on regional sustainable development. Taking the Shiyang River Basin, a typical arid inland river basin in northwestern China, as the study area, this research selected four categories of ecosystem services—food provision, water yield, carbon storage, and windbreak and sand fixation. Using a parameter-calibrated InVEST model and GIS-based spatial analysis, we quantified ecosystem services supply and demand from 2000 to 2020, and evaluated supply–demand relationships across three dimensions: quantity matching, spatial matching, and trade-off/synergy assessment. The results show that: (1) From 2000 to 2020, the average supply of food provision and water yield exhibited an increasing trend, whereas carbon storage and windbreak and sand fixation showed fluctuating changes. High food supply was mainly concentrated in oasis areas, while the supply of water yield, carbon storage, and windbreak and sand fixation decreased from the southwest to the northeast; (2) During 2000−2020, the average demand for food provision and carbon storage continued to increase, while the average demand for water yield and windbreak and sand fixation gradually declined. High-demand areas for food provision, water yield, and carbon storage were primarily located in the main urban areas of the oasis, whereas demand for windbreak and sand fixation was mainly distributed in oasis−desert transition zones and desert regions; (3) In terms of quantity matching, food provision and carbon storage were predominantly surplus-oriented, water yield exhibited comparable proportions of surplus and deficit areas, and windbreak and sand fixation were dominated by deficit conditions. For all ecosystem services, low-low spatial matching and synergistic relationships were dominant, with synergy zones accounting for more than 50% of the basin.
Keywords: Ecosystem services; Multidimensional supply–demand relationships; Spatiotemporal differentiation; Shiyang River Basin

1 INTRODUCTION

Global climate change, land degradation, and water scarcity are continuously weakening the functions of ecosystem services (ESs) [1,2]. Northwest China has long faced severe ecological and environmental problems, including vegetation degradation, intensified wind erosion, oasis shrinkage, and excessive exploitation of water resources. Against this background, identifying resource–environment constraints from the perspective of ESs has become an important entry point for ecological management and high-quality development in arid inland river basins.

Research on ES supply–demand relationships in arid basins has primarily focused on evaluating supply patterns, characterizing demand intensity, and identifying supply–demand balance or gaps [3,4]. Although existing studies have made progress in the quantitative characterization of ES supply–demand patterns and spatial heterogeneity, most of them remain at the level of a "static comparison between supply and demand." Comprehensive analyses integrating quantity matching, spatial matching, and trade-off/synergy relationships are still relatively insufficient [4,5].

The SRB, a typical arid inland river basin in northwestern China, is characterized by a distinct "mountain–oasis–desert" gradient, fragile ecological environment, and pronounced conflicts between water-resource supply and demand [6,7]. Under this complex socio-ecological context, focusing solely on ES supply or on a single spatial pattern is insufficient to support refined ecological management at the basin scale. Therefore, it is essential to analyze the supply–demand relationships of multiple ecosystem services in the SRB from the ecological context of the region, and to systematically examine these relationships across the quantity, spatial, and trade-off/synergy dimensions, so as to identify key conflict areas and priority zones for management interventions.

In this study, four major ESs—food production, water yield, carbon storage, and wind−sand fixation—were evaluated using the InVEST model and multi-source spatial datasets. We constructed a comprehensive evaluation framework that integrates supply – demand quantity, spatial matching patterns, and trade-off/synergy relationships. The specific objectives of this research are to: (1) reveal the spatiotemporal evolution of major ES supply−demand patterns in the SRB from 2000 to 2020; and (2) systematically characterize ES supply–demand relationships in terms of quantity matching, spatial distributions, and trade-off/synergy mechanisms, thereby providing scientific evidence for ecological conservation, water-use regulation, and land-use optimization in typical arid inland river basins.

2 MATERIALS AND METHODS

2.1 Study Area Overview

The Shiyang River Basin (SRB) is located in the arid inland region of northwestern China, in the eastern part of the Hexi Corridor, Gansu Province. It is bordered by the Badain Jaran Desert and the Tengger Desert to the north, and by the Qilian Mountains to the south (36°29′N–39°27′N, 101°22′E–104°16′E) (Fig1). The basin covers a total area of 4.16 × 10^4 km² and administratively encompasses three prefecture-level cities (Jinchang, Wuwei, and Zhangye) and seven county-level units (Jinchuan District, Yongchang County, Liangzhou District, Minqin County, Gulang County, and parts of Tianzhu and Subei Counties). The total population is approximately 2.27 million, with an average population density of 55 persons/km².The region experiences a typical temperate continental climate, with a mean annual precipitation of around 200 mm, a mean annual temperature of 7.75 °C, and an annual potential evaporation exceeding 1000 mm. Topographically, the SRB slopes from southwest to northeast, with elevation gradually decreasing from south to north. Three major geomorphological units are distributed from upstream to downstream: mountains, oasis, and desert. The southern mountainous area has a cold semi-humid climate, abundant precipitation, relatively good vegetation cover, and functions as the primary water-yield area. The central oasis zone is dominated by irrigated agriculture and has experienced rapid development; however, intensive water consumption has resulted in severe water scarcity and prominent supply–demand conflicts. The northern desert area is characterized by limited water availability, widespread desertification and soil salinization, and high ecological vulnerability.

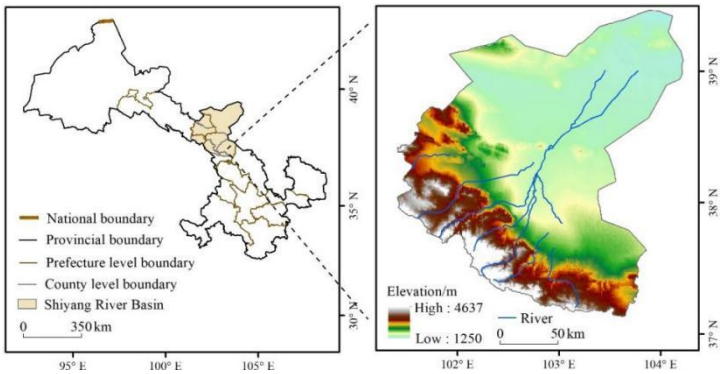

Figure 1 Location of the Study Area
Source: https://www.ngcc.cn

2.2 Data Sources

The data used in this study are listed in Table 1. All datasets were processed with spatial correction, reprojecting, and resampling. A Gauss-Krüger projection was applied, with a central meridian of 102°E, and the spatial resolution was set to 1000m.

Table 1 Data Sources and Descriptions

Data	Source	Resolution
Land Use Data		30m
DEM Data	http://www.resdc.cn	30m
Population Density Data		1km
NDVI	USGS	250m
Precipitation and Evapotranspiration Data	http://www.geodata.cn	1km
Wind Speed and Precipitation Station Data	http://data.cma.cn/	1km
Snow Cover Factor Data	http://www.ncdc.ac.cn/portal/	1km
Soil Data	World Soil Database (HWSD), China Soil Data Set (V1.2)	1km
Socio-Economic Statistical Data	"China Statistical Yearbook," "Gansu Development Yearbook," "Gansu Rural Yearbook," "Gansu Water Resources Bulletin," and various municipal statistical yearbooks	—
Basic Geographical Data	https://www.ngcc.cn	—

2.3 Ecosystem Service Supply and Demand Assessment

2.3.1 Food provision

(1) Supply: Food supply plays a crucial role in sustaining human life and supporting regional sustainable development. Studies have shown a significant linear relationship between crop and livestock yields and the Normalized Difference Vegetation Index (NDVI) [8]. By spatially modeling agricultural and pastoral output using land use data and NDVI, the food supply potential of a region can be more accurately assessed. Specifically, agricultural output is distributed based on the ratio of raster NDVI values to the total NDVI value of cultivated land, pastoral output is allocated using the ratio of raster NDVI values to the total NDVI value of grassland, and aquatic product output is distributed according to the ratio of raster NDVI values to the total NDVI value of water bodies. This method enables a more detailed characterization of food supply capacity at the grid level, thereby quantifying the actual food supply provided in the Shiyang River Basin. The calculation formula is as follows:

$$F_i = F_{sum} \times \frac{NDVI_i}{NDVI_{sum}} \quad (1)$$

In the formula, F_i represents the unit yield of agricultural and pastoral products assigned to grid i; F_{sum} is the total yield of agricultural and pastoral products in the Shiyang River Basin; $NDVI_i$ is the NDVI value for grid$i$; $NDVI_{sum}$ is the sum of the NDVI values of cultivated land, grassland, and water bodies in the Shiyang River Basin.

(2) Demand: The calculation of food demand is based on the per capita food demand standards for Gansu Province published by the National Bureau of Statistics of China. The food demand is estimated by multiplying per capita food demand by population density [9]. The calculation formula is as follows:

$$F_i = F_{per} \times P_{ipop} \quad (2)$$

In the formula, F_i represents the food demand for grid i, F_{per} is the per capita food demand, and P_{ipop} is the population density of grid i.

2.3.2 Water yield

(1) Supply: Water yield supply refers to the ability of ecosystems to regulate the distribution of water resources by intercepting and storing precipitation, which helps mitigate surface runoff, improve regional water cycling, and maintain ecological balance. In the Shiyang River Basin, due to its arid and water-scarce nature, evaluating the supply capacity of water yield supply is crucial for ensuring the sustainable use of regional water resources and the health of ecosystems. Quantifying this service provides scientific support for water resource management, land use planning, and ecological restoration. The InVEST model is the most effective method for quantifying the supply of water yield supply in the Shiyang River Basin [10]. The calculation formula is as follows:

$$W_{xj} = \left(1 - \frac{AET_{xj}}{P_x}\right) \times P_x \quad (3)$$

In the formula, W_{xj} represents the water supply (mm) for grid x of the j land use type, AET_{xj} is the average annual evapotranspiration (mm) for grid x of the j land use type, and P_x is the average annual precipitation (mm) for grid x.

(2) Demand: Water yield demand refers is calculated based on the total water consumption. Water usage for industrial, agricultural, residential, and ecological purposes is distributed across various land use types, including built-up areas, cultivated land, urban land, rural residential areas, forests, and grasslands. This distribution enables the calculation of water yield demand for each grid cell [11].

$$D_Y = D_{agricultural} + D_{industrial} + D_{domestic} + D_{ecological} \quad (4)$$

In the formula, ： D_Y represents the total water yield demand, while $D_{agricultural}$、$D_{industrial}$、$D_{domestic}$、$D_{ecological}$ correspond to agricultural water use, industrial water use, domestic water use, and ecological water use (m^3), respectively.

2.3.3 Carbon storage

(1) Supply: Carbon storage supply refers to the ability of ecosystems to absorb and store carbon, thereby reducing atmospheric carbon dioxide concentrations and mitigating global warming [12]. The InVEST model can accurately estimate the supply for carbon storage. The calculation formula is as follows:

$$S_{cs} = C_{above} + C_{below} + C_{soil} + C_{dead} \quad (5)$$

In the formula, S_{cs} represents the total Carbon storage supply (t/hm²), with C_{above}、C_{below}、C_{soil} and C_{dead} referring to aboveground biomass carbon (t/hm²), belowground biomass carbon (t/hm²), soil organic carbon (t/hm²), and dead organic matter (t/hm²), respectively.

(2) Demand: Based on the carbon emission conversion factor (0.68) published by the Chinese government, the standard coal consumption in the Shiyang River Basin is converted into carbon emissions, which is then divided by the population of the basin to obtain the per capita carbon emissions. Finally, by combining the population density of the Shiyang River Basin, the carbon storage demand in the basin is calculated.

$$D_{cs} = D_{pcfc} \times D_{pop} \quad (6)$$

In the formula, D_{cs} represents the carbon storage demand (t), D_{pcfc} is the per capita carbon emissions (t), and D_{pop} is the raster population density (people/km²).

2.3.4 Windbreak and sand fixation

(1) Supply: The suppression and stabilization of wind and sand by ecosystems is referred to as wind-sand fixation service. By comparing the difference in soil erosion flux between bare land and vegetated areas, the windbreak and sand fixation supply in the Shiyang River region can be quantified. The Revised Wind Erosion Equation (RWEQ) is an effective method for assessing the supply of windbreak and sand fixation in the region [13]. The calculation formula is as follows:

$$F_S = SL_p - SL_r \quad (7)$$

$$SL_p = \frac{2Z}{sp^2} \times Q_p \times e^{-(z/sp)^2} \quad (8)$$

$$Q_p = 109.8 \times (\mathrm{WF} \times \mathrm{EF} \times \mathrm{SCF} \times K') \quad (9)$$

$$sp = 150.71 \times (WF \times EF \times SCF \times K')^{-0.3711} \quad (10)$$

$$SL_r = \frac{2Z}{sr^2} \times Q_r \times e^{-(z/sr)^2} \quad (11)$$

$$Q_r = 109.8 \times (WF \times EF \times SCF \times K' \times C) \quad (12)$$

$$sr = 150.71 \times (WF \times EF \times SCF \times K' \times C)^{-0.3711} \quad (13)$$

In the formula, F_S represents the supply of windbreak and sand fixation (kg/m²), SL_p is the potential wind erosion amount (kg/m²), SL_r is the actual wind erosion amount (kg/m²), Q_p is the maximum sand transport capacity of potential wind force (kg/m), sp is the actual length of key areas (m), Q_r is the maximum sand transport capacity of actual wind force (kg/m), sr is the length of potential key areas (m), Z represents the downwind distance (taken as 50m), WF is the climate factor (kg/m); EF and SCF are the soil erodibility and soil crusting factors, respectively; K′ and C represent surface roughness and vegetation factors.

(2) Demand: Ecosystem service demand refers to the services or products that humans expect or can obtain, without causing negative impacts or harm. Therefore, in this study, the actual wind erosion amount is used as the demand for windbreak and sand fixation. The calculation formula is as follows:

$$F_D = \frac{2Z}{sr^2} \times Q_r \times e^{-(z/sr)^2} \quad (14)$$

In the formula, F_D represents the demand for windbreak and sand fixation (kg/m²), with the other parameters being the same as those used in the equation.

2.4 Multidimensional Analysis of Ecosystem Services Supply-demand Relationships

2.4.1 Quantity matching analysis

In this study, the Ecosystem Service Supply-Demand Ratio (ESDR) is used to compare the actual supply of ecosystem services with human demand, thereby quantitatively analyzing the degree of matching between the two. The ESDR index provides an effective tool for assessing the balance between ecosystem supply capacity and human demand. By calculating the ratio between supply and demand, it is possible to identify regions or services where supply is insufficient or excessive. This method offers a quantitative basis for further developing ecological management measures, optimizing resource allocation, and enhancing regional sustainable development capacity [1]. The specific calculation formula is as follows:

$$ESDR = \frac{ESS - \mathrm{ESD}}{(ESS_{max} + ESD_{max})/2} \quad (15)$$

In the formula, ESDR represents the ecosystem supply-demand ratio, ESS and ESD represent the actual supply and demand of ecosystem services, respectively, while ESS_{max} and ESD_{max} represent the maximum values of ecosystem service supply and demand. ESDR > 0 indicates that the supply of ecosystem services exceeds the demand, defined as a surplus state; ESDR < 0 indicates that the supply is lower than the demand, defined as a deficit state.

2.4.2 Spatial matching analysis

This study employs the four-quadrant model to explore the supply and demand patterns of different ecosystem services, aiming to identify the spatial discrepancies and potential mismatches between supply and demand within a region. The Z-score standardization method is applied to the supply and demand data of ecosystem services, allowing for a comparative analysis of different service types on a unified scale [14]. The standardized supply is placed on the X-axis, and the demand on the Y-axis, creating a two-dimensional coordinate system. Using the four-quadrant model, ecosystem services in the region are categorized into four matching patterns: high-high spatial matching (areas with both high supply and demand), low-low spatial matching (areas with both low supply and demand), low-high spatial mismatching (areas with low supply but high demand), and high-low spatial mismatching (areas with high supply but low demand). This approach not only reveals the spatial distribution of ecosystem services but also provides a basis for optimizing the allocation of services within the region. Spatial visualization further helps to clearly illustrate the supply and demand relationships between different regions and service types, offering data support for ecological protection, resource management, and sustainable development decision-making.

2.4.3 Trade-offs and synergies in ecosystem services supply–demand

We employed the root mean square deviation (RMSD) to quantify the interaction between ecosystem services supply and demand, thereby characterizing their spatial trade-off relationships [15]. The calculation formulas are as follows:

$$ESS_s = (ESS_i - ESS_{min})/(ESS_{max} - ESS_{min}) \quad (16)$$

$$ESD_d = (ESD_d - ESD_{min})/(ESD_{max} - ESD_{min}) \quad (17)$$

$$\mathrm{TF} = \sqrt{(ESS_s - \overline{ESS_s})^2 + (ESD_d - \overline{ESD_d})^2} \quad (18)$$

$$\mathrm{SY} = 1 - \mathrm{TF} \quad (19)$$

where ESS_s denotes the normalized ecosystem services supply, ESS_i is the actual supply value, and ESS_{max} and ESS_{min} represent the maximum and minimum supply values, respectively. $\overline{ESS_s}$ denotes the expected supply value. ESD_d denotes the normalized ecosystem services demand, ESD_i is the actual demand value, and ESD_{max} and ESD_{min}represent the maximum and minimum demand values, respectively. $\overline{ESD_d}$ denotes the expected demand value.

TF represents the degree of trade-off between ecosystem services supply and demand, whereas SY represents the degree of synergy.

3 RESEARCH RESULTS

3.1 Ecosystem Services Supply and Demand Assessment

3.1.1 Spatiotemporal changes in ecosystem services supply

From 2000 to 2020, the supply of different ecosystem services in the study area changed markedly. Among them, food provision exhibited a pronounced increasing trend, water yield showed a slight overall increase, carbon storage fluctuated within a relatively narrow range, windbreak and sand fixation initially decreased and subsequently increased, with rates of change of –8.66% and 19.97%, respectively (Table 2). Spatially, ecosystem services displayed pronounced regional heterogeneity. High-supply zones of food supply were mainly concentrated in the central oasis regions, and the spatial extent of these high-value areas expanded progressively over time, indicating a substantial overall increase in food production across the basin (Fig 2a1–a4). Water yield supply exhibited a general decreasing gradient from southwest to northeast, accompanied by marked local changes. In particular, the southern Qilian Mountains and parts of the oasis showed notable increases and clear spatial clustering of water yield, whereas water supply declined in most desert areas (Fig 2b1–b4). Carbon storage supply followed a similar southwest–northeast decreasing pattern, with substantial changes in some sectors of the basin. Large areas experienced reductions in carbon sequestration, and only scattered small patches showed increases (Fig 2c1–c4). The supply of windbreak and sand fixation exhibited a spatially decreasing trend from southeast to northwest. Significant increases were observed in the Qilian Mountains, oasis zones, and portions of the desert margins, while only limited areas showed decreases, suggesting that wind erosion control measures have produced positive effects (Fig 2d1–d4). Overall, the different ecosystem services presented distinct magnitudes of change and temporal trajectories. The Qilian Mountains and oasis regions functioned as core areas for the enhancement of ecosystem services supply, whereas the desert regions generally maintained low supply levels, with some services still exhibiting declining trends. This pattern indicates a pronounced regional imbalance in the improvement of ecosystem services supply within the basin.

Table 2 Mean Values and Changes in Ecosystem Services Supply–demand from 2000 to 20**20**

Type	Food supply (t/km^2)		Water yield (×10^5 m^3/km^2)		Carbon sequestration (t/hm^2)		windbreak and sand fixation (kg/m^2)	
	Supply	Demand	Supply	Demand	Supply	Demand	Supply	Demand
2000	50.59	18.42	9.22	0.11	2.09	0.03	2.09	28.69
2010	146.7	19.59	9.82	0.09	1.91	0.04	0.9	26.37
2020	196.32	21.87	9.92	0.08	2.29	0.1	2.29	23.50

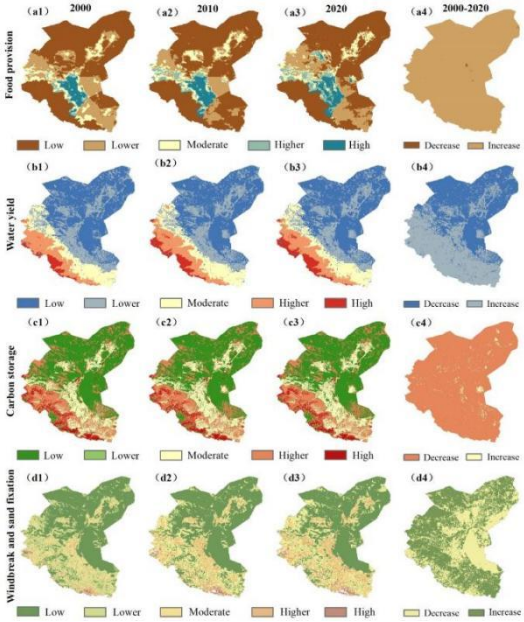

Figure 2 Spatial Distribution and Changes in Ecosystem Services Supply
Source: https://www.ngcc.cn

3.1.2 Spatiotemporal changes in ecosystem services demand

From 2000 to 2020, ecosystem services demand exhibited clear temporal divergence. Average demand increased consistently for food provision and carbon storage, whereas water yield and windbreak and sand fixation showed gradual declines (Table 2). These contrasting trajectories indicate structural shifts in resource use intensity and

environmental regulation needs within the basin. Spatial patterns revealed marked heterogeneity in ecosystem service demand. Food provision demand mirrored the spatial structure of population density and underwent continuous outward expansion, reflecting intensified consumption pressure associated with urban growth and land-use concentration (Fig 3a1–a4). Water yield demand was primarily concentrated in industrial, agricultural, and residential clusters, with high-demand zones expanding mainly within oasis regions and contracting in peripheral areas, suggesting spatial redistribution of water-use pressure (Fig 3b1–b4). Carbon storage demand formed distinct high-value clusters in highly urbanized zones, while remaining low across most other areas; increases were most evident in oasis belts, indicating a growing dependence on local carbon sinks under continued economic expansion (Fig 3c1–c4). In contrast, windbreak and sand fixation demand was concentrated along desert transition zones, with notable increases in eastern Minqin and other desert–gobi sectors, where sparse vegetation and high wind erosion potential maintain persistent regulatory demand (Fig 3d1–d4). Overall, high-demand patterns for food provision, carbon storage, and water yield were tightly associated with population aggregation, industrial activities, and intensive land use within oasis regions, highlighting a strong anthropogenic control on ecosystem service demand. Conversely, windbreak and sand fixation demand was predominantly shaped by biophysical constraints—especially vegetation scarcity, soil exposure, and wind-driven erosion—indicating that ecological vulnerability remains the principal driver in desert–oasis ecotones.

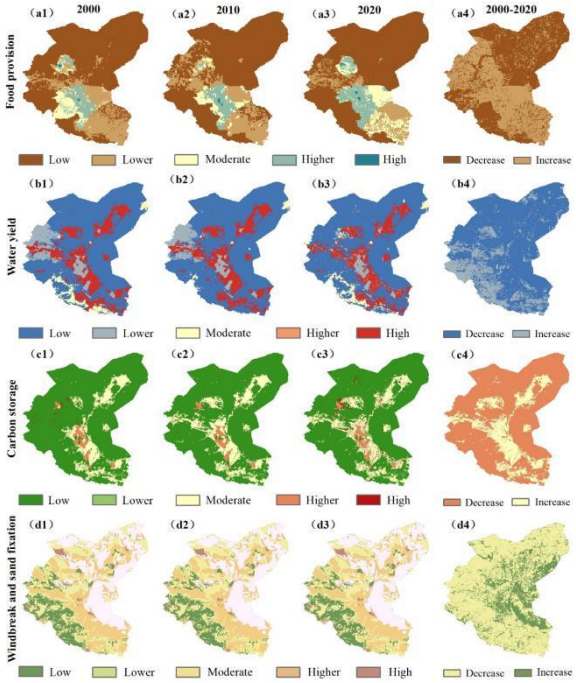

Figure 3 Spatial Distribution and Changes in Ecosystem Services Demand
Source: https://www.ngcc.cn

3.2 Multidimensional Analysis of Ecosystem Services Supply–demand Relationships

3.2.1 Quantity matching analysis

For food provision, surplus conditions overwhelmingly dominated, covering more than 95% of the basin and clustering in oasis regions. Localized deficits within oasis areas progressively transitioned to surplus (Fig. 4a1–a3), suggesting that optimized agricultural input structures and improved water allocation have reduced supply–demand conflicts. This pattern indicates a sustained enhancement of regional food security under continued cropland expansion. The quantity matching of water yield demonstrated a distinct mountain–oasis–desert gradient. Surplus conditions occurred primarily in the Qilian Mountains and adjacent foothill zones, accounting for over 50% of the basin, where high-surplus areas formed a continuous belt along the mountain front. Deficit conditions were concentrated in desert regions (Fig. 4b1–b3). High water yield capacity in the Qilian Mountains reflects extensive forest–grassland cover and favorable runoff generation, whereas oasis regions experience intensified demand derived from concentrated agricultural and residential water use. In desert zones, limited precipitation and fragile ecological conditions constrain supply, resulting in chronic deficits. For carbon storage, surplus conditions dominated across the entire basin, with the Qilian Mountains consistently acting as high-surplus cores (Fig. 4c1–c3). Ecological restoration projects—including widespread afforestation under Grain-for-Green—have enhanced vegetation structure and carbon accumulation. Concurrently, although economic expansion has increased carbon emissions, energy-saving policies and industrial restructuring have moderated emission growth, maintaining a basin-wide surplus in carbon storage. In contrast, windbreak and sand fixation remained dominated by deficit conditions, exceeding 95% of the basin area, with only scattered surplus patches (Fig. 4d1–d3). Persistent deficits reflect low vegetation cover, extensive desert–gobi surfaces, and high wind erosion potential, which maintain strong regulation demand. Nonetheless, long-term ecological engineering—such as shelterbelt

construction, desertification control projects, and high-standard farmland development—has incrementally reduced wind erosion intensity, suggesting gradual mitigation of structural regulatory deficits rather than full supply restoration.

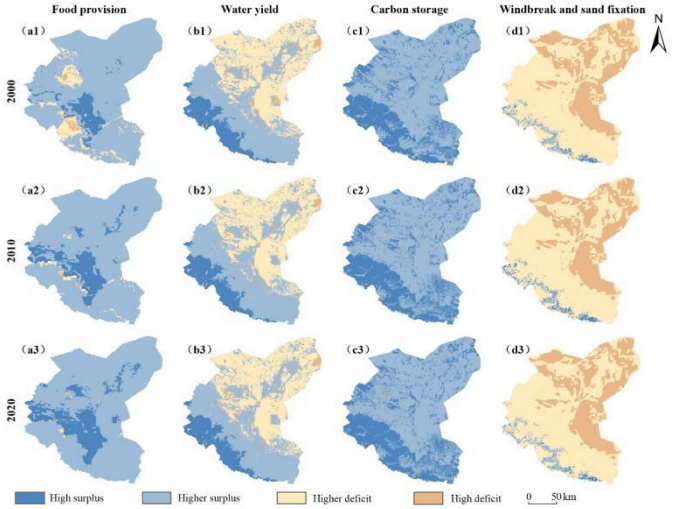

Figure 4 Spatial Distribution of Quantity Matching Relationships in Ecosystem Services Supply–demand
Source: https://www.ngcc.cn

3.2.2 Spatial matching analysis

From 2000 to 2020, spatial matching for food provision was consistently dominated by low–low matching areas (Fig. 5a1–a3). High–high clusters were restricted to oasis cores, whereas high–low mismatches occurred in localized central oasis sectors (e.g., Minqin). Low–high mismatches appeared sporadically in Gulang and Yongchang, comprising a minor share of the basin. The concentration of low–low matching (56%) across the northwestern desert–gobi belt reflects structurally weak agricultural production potential constrained by environmental limitations rather than temporary demand shocks. Spatial matching of water yield exhibited a clear mountain–oasis–desert gradient, with low–low matching (51%) dominating desert regions and high–low mismatching (27%) concentrated along the Qilian Mountain front (Fig. 5b1–b3). High–high matching and low–high mismatching zones were comparatively small and occurred mainly in oasis and transitional foothill areas. This pattern indicates that topographically driven runoff generation in mountain areas is insufficient to offset demand intensification in densely populated oasis belts, generating persistent supply–demand decoupling toward desert margins. For carbon storage, spatial matching was overwhelmingly dominated by low–low and high–low types (95%) distributed across the Qilian Mountains and desert regions (Fig. 5c1–c3). High–high patches were confined to central oasis zones and contracted over time, consistent with vegetation aging effects and limits on additional carbon accumulation under stabilized land use. The rarity of low–high mismatching suggests that carbon demand seldom exceeds supply outside intensive urbanization clusters, reinforcing the role of restoration programs as the primary supply-side control. Spatial matching for windbreak and sand fixation was governed by low–low and high–low patterns (69%), distributed mainly in mountainous and oasis regions (Fig. 5d1–d3). High–high matching occurred only as small, isolated patches, while low–high mismatches (29%) clustered along the Minqin Oasis margin and lower Shiyang River desert transition zones. This configuration indicates that wind erosion regulation remains structurally supply-limited due to sparse vegetation and high aeolian energy, with ecological engineering (e.g., shelterbelts, desertification control, farmland protection) delivering incremental mitigation rather than systemic balancing.

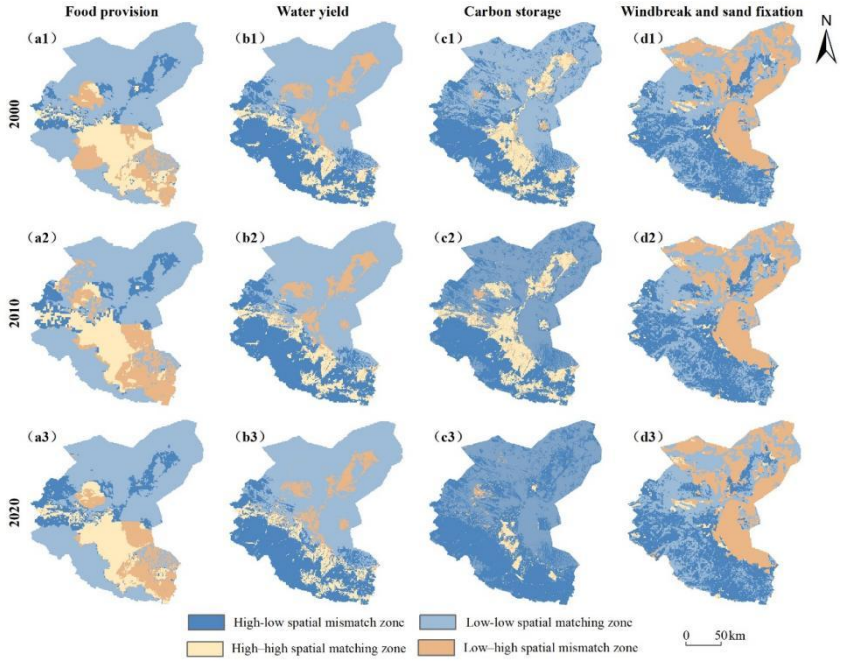

Figure 5 Spatial Distribution of Spatial Matching Relationships in Ecosystem Services Supply–demand
Source: https://www.ngcc.cn

3.2.3 Trade-off and synergy analysis

Spatial patterns of trade-offs and synergies among ecosystem service supply and demand exhibited pronounced geographic differentiation. For food provision, synergy relationships dominated (>70%), primarily distributed across desert sectors and the eastern Qilian Mountains. Notably, the spatial extent of strong synergy progressively contracted over time, indicating a weakening co-benefit structure under intensified agricultural production. Trade-off areas were limited and concentrated in oasis cores (e.g., Minqin and Liangzhou), and remained comparatively stable in spatial extent (Fig. 6a1–a3). For water yield, synergy relationships also prevailed (>70%), with strong synergy concentrated in desert regions and weak synergy forming along mountain–oasis transition belts (Fig. 6b1–b3). Trade-off zones represented a small proportion of the basin and were primarily located in the Qilian Mountains and oasis districts. Over time, strong trade-off areas systematically transitioned toward weak trade-off patterns, reflecting gradual improvements in water-use efficiency and reduced conflict between natural supply and anthropogenic demand. Carbon storage displayed synergy dominance (>60%), concentrated in oasis and desert zones, with weak synergy prevalent in oases and strong synergy in desert regions (Fig. 6c1–c3). Trade-off areas were limited in extent and primarily restricted to the Qilian Mountains, occurring elsewhere only sporadically at small scales. This indicates that ecological restoration and land management policies effectively stabilized carbon supply–demand relations outside high-elevation energy-intensive zones. For windbreak and sand fixation, synergy relationships accounted for ~50%, mainly located in oasis districts and selected desert margins (Fig. 6d1–d3). Trade-off zones were comparatively minor and distributed in the Qilian Mountains and portions of the desert fringe, with weak trade-off dominating mountainous sectors and strong trade-off localized within high aeolian energy environments. Overall, spatial configurations of trade-offs and synergies remained relatively stable with limited temporal variability, demonstrating structural persistence governed by vegetation cover, wind-energy gradients, and long-term ecological engineering interventions.

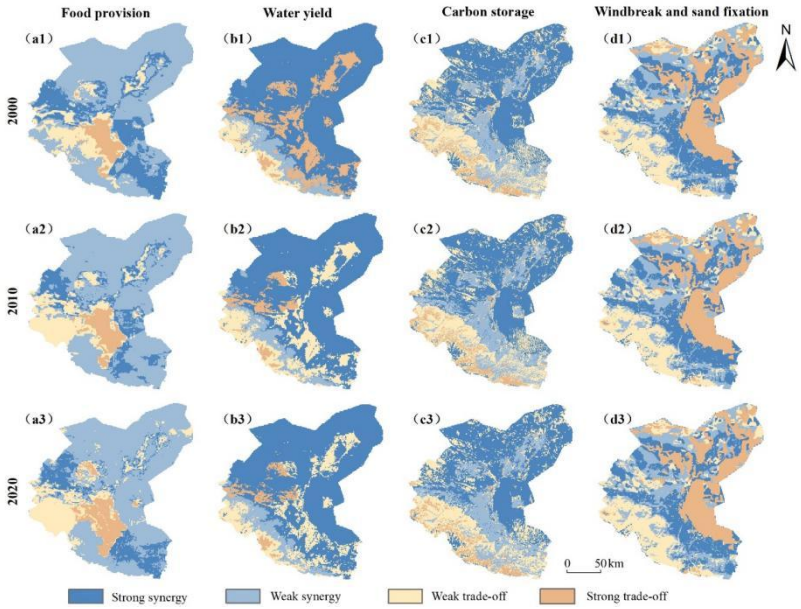

Figure 6 Spatial Distribution of Trade-offs and Synergies in Ecosystem Services Supply–demand Relationships
Source: https://www.ngcc.cn

4 DISCUSSION

This study developed a comprehensive evaluation framework that integrates supply–demand quantity, spatial quadrant matching, and synergy–trade-off analysis, aimed at characterizing ecosystem services supply–demand relationships and their temporal evolution in an arid inland river basin. The framework specifically addresses the dual impacts of natural processes and human activities, and the distinct spatial heterogeneity associated with supply–demand imbalances in such regions. Traditional valuation approaches, such as value-equivalent coefficients and supply–demand evaluation matrices, offer operational simplicity but have limited capacity for spatially explicit identification of supply–demand patterns. These shortcomings are particularly evident in landscape systems with strong geomorphological contrasts between oasis, desert, and mountain environments, where such methods are unable to pinpoint specific imbalance zones or uncover underlying drivers [16-18]. In contrast, the grid-based quantitative assessment adopted in this study directly couples supply capacity with actual demand, enabling identification of overall "surplus supply" or "unmet demand" states from the quantitative dimension. The spatial quadrant model identifies specific hotspots of spatial mismatch and delineates supply–demand discontinuities, while the synergy–trade-off analysis reveals inter-service constraints and potential ecological costs [19]. The results demonstrate that this three-dimensional framework not only identifies concentrated zones of "high supply–low demand," supply–demand discontinuities, and synergy–trade-off hotspots at the basin scale, but also uncovers dominant controlling factors and evolutionary mechanisms, thereby confirming the applicability and explanatory power of quantity–space–synergy integrated analysis in arid inland river basins.

In evaluating ESs in arid inland river basins, the regional adaptability of the modeling approach is often more critical than the choice of the model itself. The default parameter system of the InVEST model was primarily developed for humid or semi-humid regions. Direct application in arid environments typically overestimates vegetation contributions, underestimates wind erosion intensity, and fails to capture the aggregation effects of oasis agriculture [20-22]. Instead of using default settings, this study performed targeted modifications to individual ES modules based on the "mountain recharge–oasis cultivation–desert dissipation" structure of hydrology and vegetation in the Shiyang River Basin. For food production, the combination of "county-level statistics–NDVI weighted spatial allocation" minimized scale-induced bias associated with generalized yield coefficients in oasis agricultural systems. The water yield module incorporated multi-factor constraints including precipitation, evapotranspiration, soil texture, and land use, thereby avoiding the "vegetation increase necessarily enhances water yield" assumption commonly applied in humid regions, and better reflecting the climate threshold-controlled hydrological processes of arid environments. Carbon storage parameters were modified according to precipitation–temperature gradients to prevent systematic overestimation of carbon density in areas with sparse vegetation, aligning with previous findings that carbon sequestration capacity in the Qilian Mountains and the Hexi Corridor is strongly water-limited [19]. For wind–sand fixation, the revised wind erosion mechanism (RWEQ) model explicitly incorporated wind speed, soil particle composition, and surface roughness, thus providing stronger process representation than using NDVI as a single proxy. These adjustments go beyond simple parameter replacements: they significantly enhanced the spatial interpretability of model outputs, with high supply–demand values forming contiguous patterns in oasis regions, stable "supply–demand discontinuities" emerging along mountain recharge zones and desert margins, and temporal trajectories displaying consistent trends of "delayed vegetation recovery followed by progressive enhancement of wind–sand fixation." This evidence indicates that contextual calibration improves the model's ability to capture spatial heterogeneity and process-dominant mechanisms of ESs in arid regions.

This study primarily focused on typical ecosystem services in arid regions and did not explicitly incorporate non-material demands such as landscape aesthetics, cultural recreation, and ecological perception. Consequently, the representation of human well-being structures and the dynamic responses of ecosystem services remains insufficient. Future research could employ emerging perception-based approaches, including public participatory GIS (PPGIS), geo-tagged social media data, and mobile big data, and integrate them with process-based models (e.g., SWAT, RWEQ, and surface evapotranspiration models) to improve the spatial identification of cultural services and enhance the temporal accuracy of ecosystem service assessments in arid regions. Moreover, combining long-term monitoring networks with scenario-based simulations may strengthen the robustness of supply–demand mechanism interpretation and enhance the transferability of cross-basin comparisons.

5 CONCLUSIONS

This study quantified the supply and demand of four ecosystem services using a calibrated InVEST model and GIS–based spatial analysis, and evaluated their multidimensional supply–demand relationships. The main results are as follows:

5.1 Temporal Dynamics of Supply

From 2000 to 2020, the average supply of food provision and water yield increased, whereas the supply of carbon storage and windbreak and sand fixation exhibited marked interannual fluctuations. High supply of food provision was concentrated in the central oasis belt and progressively expanded, while water yield, carbon storage, and windbreak and sand fixation showed a consistent southwest–to–northeast attenuation pattern. These spatial gradients reflect the combined effects of orographic precipitation, land-use intensification in oasis systems, and degraded vegetation structure in desert margins.

5.2 Temporal Dynamics of Demand

Over the same period, demand for food provision and carbon storage continuously rose, whereas demand for water yield and windbreak and sand fixation declined. Spatially, high demand for food provision, water yield, and carbon storage was concentrated in urbanized core areas of the oasis, indicating intensified anthropogenic pressure associated with population aggregation and industrial expansion. In contrast, windbreak and sand fixation demand remained highest in oasis–desert ecotones and desert hinterlands, driven by persistent wind erosion exposure and low vegetation cover.

5.3 Multidimensional Supply–demand Matching

Quantity matching revealed clear divergence among services. Food provision and carbon storage were dominated by surplus conditions (>95% of the basin), water yield exhibited comparable proportions of surplus and deficit zones, and windbreak and sand fixation remained persistently deficit-driven (>95% deficit area). Spatial quadrant analysis indicated that low–low matching types were dominant for all services, particularly in desert basins and oasis fringes, implying structurally low supply–low demand equilibria in environmental resource–limited landscapes. Trade-off/synergy analysis further demonstrated that synergistic interactions prevailed (>50% of the basin), with distinct regional partitioning: synergy dominated in desert matrices, while trade-offs were concentrated in the Qilian Mountain foothills and selected oasis clusters, consistent with competing biophysical controls on water allocation, vegetation recovery, and disturbance regulation.

Overall, the results reveal that ecosystem service enhancement in the Shiyang River Basin remains highly spatially uneven, strongly constrained by topographic gradients, vegetation conditions, and anthropogenic water–energy–land demands, highlighting the necessity of region-specific management rather than uniform basin-wide interventions.

COMPETING INTERESTS

The authors have no relevant financial or non-financial interests to disclose.

REFERENCES

[1] Wei Y, Lu H, Wang J. Dual influence of climate change and anthropogenic activities on the spatiotemporal vegetation dynamics over the Qinghai-Tibetan plateau from 1981 to 2015. Earth's Future, 2022, 10(5): 135-138.

[2] R Costanza, R de Groot, P Sutton, et al. Turner Changes in the global value of ecosystem services Glob. Environ. Chang, 2014, 26, 152-158.

[3] Zhai T, Zhang D, Zhao C. How to optimize ecological compensation to alleviate environmental injustice in different cities in the Yellow River Basin? A case of integrating ecosystem service supply, demand and flow. Sustainable Cities and Society, 2021, 75, 101-106.

[4] Teng Y, Chen G, Su M. Ecological management zoning based on static and dynamic matching characteristics of ecosystem services supply and demand in the Guangdong–Hong Kong–Macao Greater Bay Area. Journal of Cleaner Production, 2024, 448, 141-145.
[5] Zhao Q, Chen Y, Cuan Y. Application of ecosystem service bundles and tour experience in land use management: A case study of Xiaohuangshan Mountain (China). Remote Sensing, 2021, 13(2): 242-243.
[6] Men D, Pan J. Integrating key species distribution and ecosystem service flows to build directed ecological network: Evidence from the Shiyang River Basin, China. Journal of Environmental Management, 2025, 381, 125-127.
[7] Wang Y, Pan J. Landscape-based ecological resilience and impact evaluation in arid inland river basin: A case study of Shiyang River Basin. Applied Geography, 2024, 167, 103-109.
[8] Chen T, Feng Z, Zhao H, et al. Identification of ecosystem service bundles and driving factors in Beijing and its surrounding areas. Science of the Total Environment, 2020, 711, 101-106.
[9] Tang H J, Li Z M. Study on per capita grain demand based on Chinese reasonable dietary pattern. Scientia Agricultura Sinica. 2012, 45(11): 2315-2327.
[10] Wang H, Wang L, Fu X, et al. Spatial-temporal pattern of ecosystem service supply-demand and coordination in the Ulansuhai Basin, China. Ecological Indicators. 2022, 143, 109-112.
[11] Chen J, Jiang B, Bai Y, et al. Quantifying ecosystem services supply and demand shortfalls and mismatches for management optimisation. Science of the Total Environment. 2019, 650, 143-149.
[12] Liu L, Wu J. Ecosystem services-human wellbeing relationships vary with spatial scales and indicators: The case of China. Resources, Conservation and Recycling. 2021, 172, 105-112.
[13] Gong J, Shi J, Zhu C, et al. Accounting for land use in an analysis of the spatial and temporal characteristics of ecosystem services supply and demand in a desert steppe of Inner Mongolia, China. Ecological Indicators. 2022, 144, 109-116.
[14] Yin D, Yu H, Shi Y, et al. Matching supply and demand for ecosystem services in the Yellow River Basin, China: A perspective of the water-energy-food nexus. Journal of Cleaner Production. 2023, 384, 135-142.
[15] Bradford J B, D'Amato A W. Recognizing trade-offs in multi-objective land management. Frontiers in Ecology and the Environment, 2012, 10(4): 210-216.
[16] Wei W, Nan S, Xie B, et al. The spatial-temporal changes of supply-demand of ecosystem services and ecological compensation: A case study of Hexi Corridor, Northwest China. Ecological Engineering. 2023, 187, 106-112.
[17] Zhou L, Zhang H, Bi G, et al. Multiscale perspective research on the evolution characteristics of the ecosystem services supply-demand relationship in the chongqing section of the three gorges reservoir area. Ecological Indicators. 2022, 142, 109-227.
[18] Sitch S, Smith B, Prentice I C, et al. Evaluation of ecosystem dynamics, plant geography and terrestrial carbon cycling in the LPJ dynamic global vegetation model. Global change biology. 2003, 9(2): 161-185.
[19] Zhang X, Li X, Wang Z, et al. A study on matching supply and demand of ecosystem services in the Hexi region of China based on multi-source data. Scientific Reports, 2024, 14(1): 13-32.
[20] González-García A, Palomo I, González J A, et al. Quantifying spatial supply-demand mismatches in ecosystem services provides insights for land-use planning. Land use policy. 2020, 94, 104-109.
[21] Cui F, Tang H, Zhang Q, et al. Integrating ecosystem services supply and demand into optimized management at different scales: A case study in Hulunbuir, China. Ecosystem Services. 2019, 39, 100-112.
[22] Wang H, Wang L, Fu X. Spatial-temporal pattern of ecosystem service supply-demand and coordination in the Ulansuhai Basin, China. Ecological Indicators, 2022, 143, 109-121.

Frontiers in Environmental Research
Print ISSN: 2960-0251
Online ISSN: 2960-026X
DOI: https://doi.org/10.61784/fer3037

COMPARATIVE STUDY OF DIFFERENT WAVELET TRANSFORM METHODS FOR GNSS COORDINATE TIME SERIES ON THE QINGHAI–TIBET PLATEAU

Wei Wu*, JiWei Ma
School of Engineering, Qinghai Institute of Technology, Xining 810016, Qinghai, China.
Corresponding Author: Wei Wu, Email: 1500744258@qq.com

Abstract: This study analyzes 1,611 days of GNSS data from the LHAZ IGS station on the Qinghai–Tibet Plateau (2018–2022). Daily coordinate time series were derived using GAMIT, followed by outlier removal and spline interpolation. Multi-resolution denoising was performed with DWT, CWT, and MODWT. Results show westward X displacement, minor Y fluctuations, and ~3 mm/year Z uplift with periodic variations. MODWT achieved the best denoising, outperforming DWT and CWT. MODWT is recommended for full 3D time series, while DWT suffices for horizontal-only applications. This study provides robust technical support for GNSS time series analysis on the Qinghai–Tibet Plateau.
Keywords: Wavelet transform; CORS station; GNSS processing; Coordinate time series; Noise analysis

1 INTRODUCTION

Global Navigation Satellite Systems (GNSS), when supported by a well- distributed network of continuously operating reference stations (CORS), can deliver centimeter-level positioning precision and uninterrupted positioning services. This capability has enabled GNSS/CORS systems to play an essential role across a wide range of domains, including surveying and mapping, land-use investigations, traffic management, disaster prevention and mitigation, and other geospatial applications.

The CORS infrastructure — composed of multiple high-precision, continuously operating GNSS reference stations — constitutes a foundational geodetic framework. It provides stable and continuous high-accuracy coordinate services that support engineering construction, large-scale surveying, and precision positioning needs. With the rapid development of GNSS, including multi-constellation systems, and the intensifying demand for high-precision positioning and monitoring, many countries and regions — including high-altitude and tectonically active areas — have accelerated the deployment and enhancement of CORS networks.

Specifically, in regions such as the Qinghai–Tibet Plateau, the establishment and densification of CORS stations enable robust geodetic and geophysical applications. Long-term GNSS observations from CORS networks combined with other geodetic techniques (e.g. InSAR) have become indispensable for accurate monitoring of crustal deformation, tectonic motion, and seismic hazard assessment in plateau regions.

An accurate characterization of temporal variations in CORS station coordinates — especially the vertical (uplift/subsidence) and horizontal displacement — is crucial. Such characterization not only underpins regional crustal deformation studies and seismic risk assessments, but also supports maintenance and densification of GNSS reference frameworks, and improves the reliability of high-precision navigation and surveying applications. Meanwhile, effective denoising and analysis of coordinate time-series data is technically significant for enhancing the quality and trustworthiness of GNSS-derived positioning results, especially in challenging environments like high-altitude plateaus

Therefore, it is imperative to conduct in-depth analysis of coordinate time series from CORS stations in the Qinghai–Tibet Plateau region. By designing a systematic methodological framework and investigating advanced noise-removal techniques, this study aims to reveal long-term coordinate variation patterns and assess the effectiveness of different denoising approaches. The outcomes will not only contribute to geodetic and geophysical understanding of plateau deformation, but also provide practical guidance for high-precision GNSS applications and reference network maintenance in high-altitude, tectonically active regions.

2 DATA SOURCES AND PREPROCESSING

2.1 Study Site and Dataset

The LHAZ station, a long-term IGS GNSS site in southeastern Qinghai–Tibet Plateau, was selected for this study due to its stable geological conditions and low environmental noise. From 2018 to 2022, the station recorded 1,611 days of continuous multi-system GNSS observations (GPS, BDS, GLONASS) with over 98% completeness. The high-performance receiver and multi-frequency antenna ensure better stability than ordinary regional CORS stations, providing representative data for regional crustal deformation analysis.

2.2 Auxiliary Data

Precise ephemeris and clock products from IGS were used, along with broadcast ephemeris for initial processing. Tropospheric delays were modeled using GPT/GPT3, and tidal effects were corrected with IERS2010 for solid Earth tides and GAMIT defaults for ocean and load tides. All auxiliary data were format-checked and stored uniformly to ensure reproducibility..

2.3 Baseline Processing with GAMIT/GLOBK

GAMIT/GLOBK was used to process the LHAZ data. Double-differenced observations eliminated satellite and receiver clock errors. Tropospheric delay was estimated every 2 hours and corrected using mapping functions. IGS precise orbit and clock products ensured high-precision long-baseline solutions. Double-difference ambiguities were fixed with LAMBDA, and stable reference stations established an ITRF-constrained framework. Daily 3D coordinate solutions (X, Y, Z) with covariance were generated, forming a high-quality time series for further analysis.

2.4 Time Series Construction

Cubic spline interpolation was applied to fill occasional missing data, producing a continuous XYZ time series of 1,611 days. The method preserves smoothness, avoids sharp bends, and minimizes oscillations, providing a reliable basis for trend analysis and wavelet-based denoising.
By applying outlier removal and cubic spline interpolation to the raw data, the time series of the LHAZ reference station was obtained. This study focuses on the XYZ coordinate time series of the IGS station in Tibet, as shown in Figure 1.

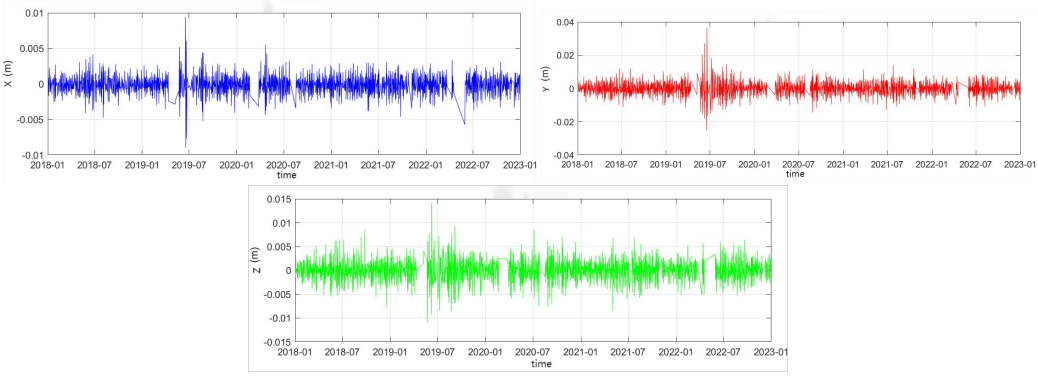

Figure 1 Coordinate Time Series Analysis Diagram of the XYZ Components of the LHAZ Station

As illustrated, the station coordinates vary over the period from January 2018 to January 2023. The X component exhibits a stable negative displacement trend, indicating that the station is continuously moving westward. The Y component shows small high-frequency fluctuations (±0.02 m) without a significant long-term trend. The Z component displays a clear upward trend, averaging approximately 3 mm per year, superimposed with periodic oscillations, reflecting ongoing vertical uplift of the station.

3 COMPARATIVE ANALYSIS OF COORDINATE TIME SERIES USING DIFFERENT WAVELET TRANSFORM METHODS

3.1 Wavelet Transform

Wavelet analysis adjusts time–frequency resolution by modifying the window function and achieves multi-scale decomposition through scaling and translation operations. This allows the method to capture low-frequency/high-time, high-frequency/low-time characteristics. Due to its multi-scale nature, wavelet analysis is often referred to as a "mathematical microscope" . The wavelet transform process can be described as follows:
Let the Fourier transform of the original signal ε(u) be ϕ(u). If ϕ(u) satisfies the condition:

$$C_\delta = \int_R \frac{|\varphi(t)|^2}{|t|} dt < \infty \tag{1}$$

then ε(u) is called a mother wavelet. By translating and scaling ε(u) along the time dimension, multiple target wavelet functions are obtained:

$$\delta_{a,b}(t) = a^{-\frac{1}{2}} \varphi\left(\frac{t-b}{a}\right) \tag{2}$$

where b is the scale parameter and c is the translation parameter. $c(u)$ is called the continuous wavelet generated from ε(u), the wavelet basis function. When u=0, in order for the integrand to have a nonzero value, it is required that ε(0)=0:

$$\delta(0) = \int_{-\infty}^{+\infty} \delta(t) dt = 0 \tag{3}$$

Equation indicates that ε(u) has oscillatory characteristics. To ensure ε(u) decays rapidly to zero over a finite time interval, a decay condition is required:$|\varepsilon(u)| \leq (1+|u|)1+\varepsilon$,where d is a positive constant (d>0). As u→±∞, d|ε(u)| decays

faster than|u|. Because the "wave" is localized and small under decay, it is called a "wavelet" . The wavelet transform of an arbitrary time series function g(u) is then defined as:

$$W_f(a,b) = \int_R f(t)\bar{\delta}_{a,b}(t)dt = \frac{1}{\sqrt{a}}\int_R f(t)\bar{\delta}(\frac{t-b}{a})dt \quad (4)$$

In practice, to avoid losing information from the original signal, the parameters b and c are usually discretized. Expanding b and c allows the original time series signal to be analyzed at arbitrary time and scale, yielding its spectrum. In the frequency domain, wavelet transforms at different scales are equivalent to a set of band-pass filters applied to the signal. The reconstruction formula is:

$$f(t) = \frac{1}{a^2 C_\delta}\int_0^{+\infty}\left[\int_{-\infty}^{+\infty} W_f(a,b)\delta_{a,b}(t)db\right]da \quad (5)$$

Wavelet transform is an extension of Fourier transform and is closely related to it. The construction of the core wavelet basis and the existence proofs of the wavelet transform rely on Fourier transform. Due to the non-uniqueness of wavelet basis functions compared to a single basis function, using different wavelet bases for the same application may lead to significant differences. Therefore, selecting an appropriate wavelet function is a key and challenging aspect in wavelet analysis.

Although wavelet analysis can separate low-frequency components and coarsely partition high-frequency components, its frequency band division is still limited and cannot achieve fully adaptive segmentation. In principle, wavelet analysis does not completely overcome the limitations of Fourier transform, as it has no intrinsic connection to the signal itself, which significantly constrains its applicability.

3.2 Discrete Wavelet Transform (DWT)

The discrete wavelet transform decomposes a signal using a set of orthogonal wavelet basis functions. Let the original signal be x(t); its DWT can be expressed as:

$$W_\psi x(j,k) = \int_{-\infty}^{\infty} x(t)\psi_{j,k}^*(t)dt \quad (6)$$

Here, j and k are the scale and translation parameters of the wavelet, and ψ* (t) denotes the complex conjugate of the wavelet function. The signal is decomposed into approximation coefficients and detail coefficients, corresponding to the low- and high-frequency components, respectively.

The DWT can be used to separate trend and noise components in GNSS coordinate time series. For example, a 5-level decomposition using the Daubechies wavelet (db4) was applied to the coordinate series of CMONOC I, producing detail coefficients at each level and approximation coefficients. The trend component is extracted by reconstructing the low-frequency approximation coefficients, while the high-frequency detail coefficients are used to analyze noise characteristics.

3.3 Continuous Wavelet Transform (CWT)

The continuous wavelet transform analyzes a signal by continuously varying the scale and translation parameters. It is defined as:

$$W_\psi x(a,b) = \frac{1}{\sqrt{a}}\int_{-\infty}^{\infty} x(t)\psi^*\left(\frac{t-b}{a}\right)dt \quad (7)$$

Here, a is the scale parameter, b is the translation parameter, and ψ(t) is the mother wavelet function. The time–frequency resolution of CWT varies with scale, allowing it to flexibly capture local features of the signal.

CWT is suitable for analyzing transient and non-stationary periodic signals in GNSS coordinate time series. For example, a CWT analysis using the Morlet wavelet was applied to the coordinate series of the SCIGN network. Significant annual and semi-annual signals were detected via the Wavelet Power Spectrum (WPS), and amplitude modulation over time was observed.

3.4 The Maximal Overlap Discrete Wavelet Transform (MODWT)

MODWT overcomes the limitations of DWT regarding data length and translation sensitivity by retaining all possible shift information through a non-decimated approach. Its coefficients are computed as:

$$\widetilde{W}_{j,t} = \frac{1}{2^{j/2}}\sum_{l=0}^{L-1}\widetilde{\psi}_l x_{t-l \bmod N} \quad (8)$$

MODWT has been widely used in GNSS data analysis. For noise separation, it decomposes time series into multi-scale components, allowing high-frequency noise to be removed via thresholding while preserving low-frequency signals. MODWT supports data of arbitrary length and exhibits translation invariance, reducing information loss. For example, combining MODWT with the Median Absolute Deviation (MAD) method for outlier detection significantly improves the identification of anomalies in CMONOC II data.

3.5 Comparative

Analysis of GNSS coordinate time series is an important research topic in geodesy, and data denoising is a key step to improve analysis accuracy. Due to its excellent time–frequency localization properties, wavelet transform has become an effective tool for denoising GNSS time series.

This study conducts a comprehensive comparison of the performance of three mainstream wavelet transform methods — DWT, CWT, and MODWT — for denoising IGS station coordinate time series, as summarized in Table 1.

Table 1 Performance Comparison of DWT, CWT and MODWT

Feature	DWT	MODWT	CWT
Sampling	Downsampling (decimation)	No downsampling	No downsampling (continuous scale and translation)
Translation Invariance	No	Yes	Yes
Reconstruction	Fully orthogonal reconstruction	Reconstructable (redundant)	Requires analytic conditions; reconstruction is relatively complex
Computational / Storage Cost	Low (O(N))	Moderate to high (redundancy factor ≈ $\log_2 N$)	High (continuous scales generate a large number of coefficients)
Typical Applications	Data compression, fast denoising, feature extraction	Denoising, edge detection, signal alignment	Time–frequency analysis, transient detection, fine signal feature localization

In summary, DWT is suitable for quickly extracting coarse and fine signal components at multiple resolutions; MODWT eliminates translation dependence inherent in DWT, making it more suitable for aligned analysis and denoising; CWT provides the most detailed time–frequency distribution information, suitable for detecting transient features but with high computational cost.

4 COMPARATIVE ANALYSIS OF DIFFERENT WAVELET TRANSFORM METHODS

After preprocessing the data and setting parameters, the three wavelet transforms were applied in MATLAB for decomposition, noise removal, and signal reconstruction. Performance metrics such as signal-to-noise ratio (SNR) were calculated. By comparing the original and reconstructed signals, analyzing SNR values, residual distributions, and MB/RMSE errors, the performance of each method was comprehensively evaluated.

From the MB comparison plot(Figure 2), it can be seen that all three methods yield MB values on the order of 10^{-6}m for the X, Y, and Z components. MODWT performs best overall, with MB values closest to zero and minimal fluctuations (X ≈ 0.5×10^{-6}, Y ≈ 1×10^{-6}, Z ≈ 2×10^{-6}), indicating the smallest systematic bias after denoising. DWT performs moderately, showing good results for X and Y (≈1×10^{-6}) but slightly larger bias in Z (≈3×10^{-6}). CWT exhibits a significant negative bias in the Z component (≈-1×10^{-6}), suggesting potential systematic errors in vertical denoising. Notably, all three methods show higher MB values in the Z component compared to horizontal components, likely because vertical data inherently contain more noise or are more sensitive to wavelet denoising.

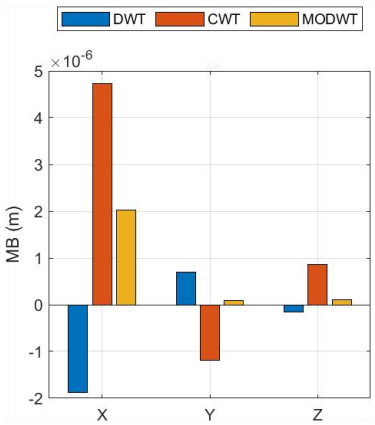

Figure 2 Comparison Chart of Mean Deviation (MB)

From the RMSE comparison plot, it can be seen that the RMSE values of all methods range from 10^{-4} to 10^{-3} m. MODWT performs best overall, maintaining the lowest RMSE values across all components (approximately 10^{-4} m), indicating the highest denoising accuracy and stability. DWT performs moderately, with RMSE values slightly higher than MODWT but still at a relatively low level. CWT shows relatively higher RMSE values (close to 10^{-3} m), with the largest errors in the Z component, indicating relatively poor denoising performance.

It is noteworthy that for all three methods, RMSE values in the Z component are significantly higher than those in the X and Y components. This is consistent with the MB analysis results and further confirms that denoising vertical data is more challenging, possibly due to the more complex noise structure or different signal characteristics in the Z component. As shown in Figure 3:

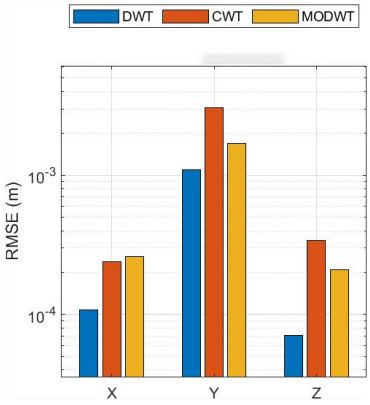

Figure 3 Comparison Chart of Root Mean Square Error (RMSE)

Analysis of the residual distribution plots shows that the X-component residuals are on the order of 10^{-3} m, significantly smaller than those of the Y-component (maximum ~0.025 m) and Z-component. For the X-component, DWT exhibits the most concentrated residual distribution, with the smallest box height and fewest outliers, indicating the highest denoising stability. In the Y-component, MODWT has a median residual closest to zero (~0.002 m) and an interquartile range (IQR) better than CWT, while CWT produces more positively shifted outliers.

For the Z-component, the residual range is significantly larger for all three methods, with CWT showing numerous extreme values (maximum exceeding that of Y-component by an order of magnitude). MODWT, while maintaining a median near zero, reduces the number of extreme values by approximately 60% compared to CWT. Overall, the analysis indicates:

(1)Denoising accuracy in the horizontal components (X/Y) is generally higher than in the vertical component (Z);

(2)DWT is suitable for scenarios requiring stability, whereas MODWT performs best in balancing accuracy and anti-noise capability;

(3)CWT may amplify noise in the vertical data due to its sensitivity in time–frequency analysis, suggesting that Z-component processing should adopt MODWT with elevation-specific parameter optimization.

In summary, MODWT demonstrates the most balanced performance in terms of accuracy, stability, and adaptability, making it the recommended method for global denoising. DWT can serve as a lightweight alternative for processing purely horizontal data.

5 RESULTS AND CONCLUSION

This study analyzed GNSS coordinate time series from the LHAZ station on the Qinghai–Tibet Plateau, comparing three wavelet transform methods — DWT, CWT, and MODWT — for denoising multi-dimensional GNSS data. The main findings are:

(1)The XYZ coordinate series (2018–2023) show westward X displacement, small high-frequency Y fluctuations, and upward Z movement (~3 mm/year) with periodic oscillations.

(2)MODWT outperforms other methods, achieving the lowest MB and RMSE values, highest SNR, and reduced extreme residuals, especially in the vertical component.

(3)DWT is effective for horizontal components with low computational cost but shows larger vertical bias. CWT provides detailed time–frequency information but performs poorly for continuous coordinate denoising.

(4)Horizontal denoising is generally more accurate than vertical due to the complexity of Z-component noise.

In summary, MODWT is recommended for global denoising of multi-dimensional GNSS time series, while DWT can be used for horizontal-only applications. Wavelet-based denoising enhances GNSS data quality, supporting precise geodetic monitoring and crustal deformation studies in high-altitude regions.

COMPETING INTERESTS

The authors declare that they have no known competing financial interests or personal relationships that could have appeared to influence the work reported in this paper.

FUNDING

This research was supported by Integrated Space–Air–Ground Monitoring and Forecasting of Deformation in Hydraulic Infrastructure in Cold-Region Environments.

REFERENCES

[1] Liu Hui, Zou Rong, Wang Yu'e. Global Navigation Satellite System: Technology Innovation and Application. Scirp, 2023, 7(1): 1-10. DOI: 10.4236/xyz.2023.7.1.

[2] Wang Wei, Dang Yamin, Zhang Chuanyin, et al. CORS Network and GNSS Technology in Ground Deformation Monitoring: A Case Study in Southeastern Zhejiang. Journal of Geological Hazards and Prevention, 2021, 32(2): 45-52. DOI: 10.12265/j.gnss.2021.02.10.

[3] Zhou Xiaohong, Feng Zhen, Li Jian. A Novel Method for Analyzing the Spatiotemporal Characteristics of GNSS Time Series: A Case Study in Sichuan Province, China. Applied Sciences, 2024, 14(1): 432. DOI: 10.3390/app14010432.

[4] Lu Zhong, Wang Qiang, Liu Hong. Three-dimensional interseismic crustal deformation in the northeastern margin of the Tibetan Plateau using GNSS and InSAR. Journal of Asian Earth Sciences, 2024, 276: 106328. DOI: 10.1016/j.jseaes.2024.106328.

[5] Gu Rui, Xu Shuang'an, Wang Jianhong. GNSS Vertical Coordinate Time Series Noise Model in Southeastern Tibet Plateau Based on Environmental Loading. Journal of Wuhan University (Geography & Information Science), 2024, 49(4): 115-125. DOI: 10.13203/j.whugis20240098.

[6] Zhou Xiang, Li Fang, Zhang Lei. Time-Series Analysis of GNSS Crustal Deformation Network in China: Effects of Polynomial Deterministic Terms. Geodesy and Geodynamics, 2025, 16(4): 378-386. DOI: 10.1016/j.geog.2024.12.002.

[7] Li Shuying, Gao Yong, Jin Hongli. Upper Crustal Deformation Characteristics in the Northeastern Tibetan Plateau and Its Adjacent Areas Revealed by GNSS and Anisotropy Data. Earthquake Science, 2023, 36(4): 297-308. DOI: 10.1016/j.eqs.2023.05.003.

[8] Zhang Guohua, Qu Cheng, Shan Xinyu, et al. Present-Day Crustal Deformation of the Northwestern Tibetan Plateau Based on InSAR Measurements. Remote Sensing, 2023, 15(21): 5195. DOI: 10.3390/rs15215195

[9] Yin Taotao, Wang Qianxin. A Method to Weaken the Non-Linear Changes in the Coordinate Time Series of Regional CORS Stations. Journal of Geodesy and Geodynamics ,2021, 41(07): 695-699 . DOI:10.14075/j.jgg.2021.07.007.

Frontiers in Environmental Research
Print ISSN: 2960-0251
Online ISSN: 2960-026X
DOI: https://doi.org/10.61784/fer3038

SPATIO TEMPORAL EVOLUTION AND INFLUENCING FACTORS OF WATER RESOURCE USE EFFICIENCY IN THE BEIJING−TIANJIN−HEBEI REGION: EVIDENCE FROM A SUPER EFFICIENCY SBM AND TOBIT MODEL

YuYang Liu
Beijing Technology and Business University, Beijing 100048, China.
Corresponding Email: 13103189963@163.com

Abstract: This study investigates the efficiency of water resource utilization in the Beijing–Tianjin–Hebei (BTH) region from 2013 to 2023. By employing a super-efficiency Slacks-Based Measure (SBM) model incorporating undesirable outputs, this research evaluated the spatial-temporal evolution of efficiency. Subsequently, a Tobit regression model was applied to analyze 13 determinants across natural, economic, social, and environmental dimensions. The results reveal that the region's efficiency followed a fluctuating trajectory characterized by phases of stability, growth, decline, and leveling off, with a mean value of 0.870. Significant spatial heterogeneity was observed, with Beijing and Tianjin exhibiting higher efficiency levels than Hebei. The Tobit analysis identified positive correlations with per-capita water resources, annual precipitation, per-capita GDP, the share of the tertiary industry, and water intensity, reflecting the influence of resource endowment, economic structure, and management capacity. Conversely, factors such as per-capita water use, the share of the primary industry, and insufficient scientific and technological investment exerted negative impacts, suggesting constraints related to redundant consumption and structural imbalances. Based on these findings, we recommend implementing differentiated regional management strategies, establishing a market-oriented agricultural water rights trading system, and creating an integrated BTH platform for the collaborative innovation and diffusion of water-saving technologies. These measures aim to foster sustainable resource utilization and high-quality regional development.
Keywords: Beijing–Tianjin–Hebei region; Water resource utilization efficiency; Super-SBM model; Tobit regression model; Influencing factors

1 INTRODUCTION

Water is a fundamental natural resource and a strategic economic asset vital to the national economy and public welfare. It also serves as a critical constraint on the ecological environment [1]. According to the 2024 "China Water Resources Bulletin", the national total water consumption has reached 5.928×10^{11} m^3, but the per capita comprehensive water consumption is only 421 m^3, highlighting a severe imbalance between water supply and demand. In terms of regional disparity, the Beijing – Tianjin – Hebei (BTH) region and other northern areas face significantly greater water scarcity than water-rich southern economic hubs like the Yangtze River Delta and the Pearl River Delta. Given that the BTH region is currently undergoing critical economic restructuring and a transition toward high-quality development, achieving efficient, scientific, and sustainable water utilization is urgent. Therefore, investigating the spatiotemporal evolution and determinants of water resource efficiency in the BTH region holds significant practical value for promoting resource conservation and meeting high-quality development goals.

Domestic and international literature on water resource efficiency has established a systematic framework encompassing methodological evolution, scale-specific empirical studies, and driver identification. Measurement approaches have progressed from simple single-factor ratios to total-factor evaluation models. While early single-factor methods were intuitive, they failed to capture the complexity of multi-input, multi-output systems. Consequently, Data Envelopment Analysis (DEA) has been widely adopted. Notably, the super-efficiency Slacks-Based Measure (SBM) distinguishes between efficient decision-making units (DMUs) and incorporates undesirable outputs, yielding more precise estimates [2]. Regional studies have deepened across spatial scales: Zheng et al. combines the Meta-frontier Super-SBM model and the Tobit model to analyze efficiency and factors influencing regional urban water resources utilization efficiency disparities across different technological frontiers [3]; Zhao et al. used the Super-SBM model to estimate water environmental governance efficiency for 283 prefecture-level cities in China over 2013–2022 and observed a shift from a dispersed spatial distribution to a multi-center agglomeration [4]. Analyses of determinants support policy design using tools such as the Theil index to measure regional disparity [5], the Malmquist index to decompose efficiency change [6], and Tobit regression to disentangle the complex drivers of performance [7].

In summary, existing studies provide a solid theoretical foundation but also leave gaps. Prior research often focuses either on efficiency measurement or on individual drivers, but rarely examines the coordinated multi-dimensional interplay of supply, structure, technology, and management needed to reveal the coexistence of promoting and inhibiting mechanisms. To address this gap, this study employs a slack-based measure (SBM) model that accounts for undesirable

outputs to quantify BTH water-use efficiency, and uses Tobit regression to probe its determinants, aiming to inform policy for sustainable regional water management.

2 STUDY AREA, METHODOLOGY AND DATA SOURCES

2.1 Study Area

Located in the northern part of China's North China Plain, the BTH region spans approximately 216,000 km^2. Its topography exhibits distinct west-high-east-low characteristics, with mountains in the west and north and plains in the east. The region has a temperate monsoon climate, featuring major rivers such as the Haihe, Luanhe, and Yongding flowing along the terrain, and forming key water sources including Miyun Reservoir, Panjiakou Reservoir, and Baiyangdian Lake. However, the region has poor natural water endowment with low and uneven annual precipitation, mostly concentrated in the flood season [8]. According to 2023 data (from *China Statistical Yearbook 2024*), the total water resources in BTH amount to 3.0×10^{10} m^3, accounting for only 1.2% of the national total, with a per capita water resource of 274.4 m^3, less than one-sixth of the national per capita level. One of the core challenges facing the region is the long-term imbalance between development patterns and resource endowments, making water scarcity and irrational water use structure prominent bottlenecks restricting high-quality development, and revealing the complex coupling characteristics of water-economy-ecosystem [9]. Given its typicality and strategic importance, this study selects Beijing, Tianjin, and Hebei Province as research objects.

2.2 Methodology

2.2.1 SBM model incorporating undesirable outputs

The traditional DEA models, notably the CCR and BCC models, are radial and angular in nature and therefore fail to account for the effects of slack variables on water-use efficiency, often leading to efficiency overestimation for decision-making units (DMUs).Tone extended the SBM in 2003 to include undesirable outputs by placing slacks directly in the objective function [10]. This formulation resolves slackness issues and accommodates undesirable outputs, has been widely applied in ecological and environmental efficiency assessments, and substantially improves the accuracy of water-use efficiency estimation. The model is constructed as follows.

Assuming: x ∈ R^q， ∈ R^{u1}, y^b ∈ R^{u2}, define the matrices X、Y^g、Y^b， as follows:

$$\begin{aligned} X &= [x_1 \quad ,\cdots, \quad x_n] \in R^{q\times n} > 0 \\ Y^g &= \left[y_1^g,\cdots, \quad y_n^g\right] \in R^{u_1\times n} > 0 \\ Y^b &= \left[y_1^p,\cdots, \quad y_n^g\right] \in R^{u_2\times n} > 0 \end{aligned} \tag{1}$$

A production possibility set P incorporating undesirable (non-desired) outputs can be constructed.

$$\begin{gathered} P = \{(x, y^g, y^b) | x \geqslant X\lambda, y^g \leqslant Y^g\lambda, y^b \geqslant \lambda, i \geqslant 0\} \\ \bar{x} \geqslant \sum_{i=1,\neq 0}^{n} \lambda_i x_i, \bar{y}^g \leqslant \sum_{i=1,\neq 0}^{n} \lambda_i y_i^g \\ \bar{y}^b \geqslant \sum_{i=1,\neq 0}^{n} \lambda_i y_i^b, \bar{x} \geqslant x_0, \bar{y}^g \leqslant y_0^g, \bar{y}^b \geqslant y_0^b \\ \bar{y}^g \geqslant 0, \lambda \geqslant 0 \\ \rho = min \frac{\frac{1}{q}\sum_{i=1}^{q} \frac{\bar{x}_i}{x_{i0}}}{\frac{1}{u_1+u_2}\left(\sum_{r=1}^{u_1} \frac{\bar{y}_r^g}{y_{r0}^g} + \sum_{i=1}^{u_2} \frac{\bar{y}_1^b}{y_{10}^b}\right)} \end{gathered} \tag{2}$$

In the equations, x, y^g and y^b denote a decision-making unit's inputs, desirable (good) outputs, and undesirable (bad) outputs, respectively; s$^-$, s^g, and s^b are the slack vectors for inputs, desirable outputs, and undesirable outputs; λ is the weight vector; the subscript 0 refers to the unit under evaluation; and ρ (the objective value) is the efficiency score.

Although the SBM model with undesirable outputs improves efficiency assessment, it cannot further discriminate among multiple DMUs that attain an efficiency score of 1. To address this, the super-efficiency SBM (super-SBM) model applies additional treatment (e.g., excluding the evaluated DMU from the reference set) to rank the relative efficiency of previously efficient DMUs. Therefore, this study employs the super-efficiency SBM model to measure water-use efficiency; the model is constructed as follows.

Assume that in period t there are n decision-making units DMU_i. For each DMU_i, let x_i be the input vector, y_i^g the desirable (good) output vector, and y_i^b the undesirable (bad) output vector. Define matrices X = [x_1， x_2， …， x_n], Y_i^g= [y_1^g， y_2^g， …， y_n^g], and Y_i^b= [y_1^b， y_2^b， …， y_n^b]. Assuming x_i,y_i^g and y_i^b are strictly positive, the functional form of the super-efficiency SBM model with undesirable outputs is given as follows:

$$\rho = min\frac{1+\frac{1}{m}\sum_{i=1}^{m}\frac{s_i^-}{x_{ik}}}{1-\frac{1}{n_g+n_b}\left(\sum_{i=1}^{n_g}\frac{s_i^g}{y_{ik}^g}+\sum_{i=1}^{n_b}\frac{s_i^b}{y_{ik}^b}\right)}$$
$$s.t.\begin{cases} s_i^- \geqslant \sum_{j=1,\neq k}^{n} x_j\lambda_j + x_{ik}, i=1,2,\cdots,m \\ s_i^g \leqslant \sum_{j=1,\neq k}^{n} y_j^g\lambda_j - y_{ik}^g, i=1,2,\cdots,n_g \\ s_i^b \geqslant \sum_{j=1,\neq k}^{n} y_j^b\lambda_j - y_{ik}^b, i=1,2,\cdots,n_b \\ \sum_{j=1,\neq 0}^{n}\lambda_j = 1, \lambda\geqslant 0, y^g\geqslant 0, y^b\geqslant 0 \\ s_i^-\geqslant x_k, s_i^g\leqslant y_k^g, s_i^b\geqslant y_k^b \end{cases} \quad (3)$$

Here, ρ is the efficiency score estimated by the model for each DMU; s_i^-, s_i^g and s_i^b are the slack variables for DMU i's inputs, desirable outputs, and undesirable outputs, respectively; and λ is the weight vector.

2.2.2 The tobit model

Using DMU efficiency scores as the dependent variable and estimating them with standard OLS produces severely biased and inconsistent parameter estimates. The Tobit model, designed for limited/censored dependent variables, can effectively address this problem.

The Tobit model, proposed by Tobin [11], is a limited-dependent-variable model used for censored or truncated outcomes. By introducing a latent variable it converts the censored regression into a linear model, allowing consistent parameter estimation and avoiding the biases that ordinary least squares can produce. Given that water-use efficiency is nonnegative, the standard Tobit specification is:

$$y_i^* = \beta x_i + \mu_i$$
$$\mu_i \sim N(0,\sigma^2) \quad (4)$$
$$y_i = \begin{cases} y_i^*, y_i \geqslant 0 \\ 0, y_i < 0 \end{cases}$$

Here, y_i^* denotes the latent (original) dependent variable; y_i the truncated (observed) dependent variable; x_i the vector of independent variables; β the vector of regression coefficients; and μ_i an independent, normally distributed error term.

2.3 Construction of the Indicator Framework and Data Sources

2.3.1 Input–output indicators

A scientifically grounded input–output indicator system is fundamental for accurately measuring urban water-resource efficiency. Drawing on the economic theory of production factors, the concept of water-resource efficiency, and previous studies, this paper classifies inputs into three categories—resources, labor, and capital—and explicitly accounts for industrial undesirable outputs to construct an evaluation framework tailored to the BTH region.

For input indicators, following Yin [12], resource input is measured by annual total water use. To analyze water-use structure, this is further decomposed into industrial, agricultural, domestic, and ecological water consumption. Labor input follows Deng et al [13], and is proxied by employment counts in the primary, secondary, and tertiary sectors. Capital input is proxied by total fixed-asset investment in the period, capturing the flow of physical capital in regional economic development [14].

For outputs, the desirable output is measured by regional GDP to capture positive economic benefits, while the undesirable output is proxied by chemical oxygen demand (COD) emissions. Detailed definitions of the indicators are presented in Table 1.

Table 1 Input–Output Indicator System

Indicator type	Criterion	Definition / Unit	Reference
Input indicators	Resource input	Industrial water use (100 million m^3)	[12]
		Agricultural water use (100 million m^3)	
		Domestic water use (100 million m^3)	
		Ecological water use (100 million m^3)	
	Productivity input	Employment by three	[13]

Indicator type	Criterion	Definition / Unit	Reference
		sectors (10,000 persons)	
	Human capital input	Total fixed-asset investment (100 million CNY)	
Output indicators	Desirable outputs	Regional GDP (100 million CNY)	[14]
	Undesirable outputs	COD emissions (10,000 tonnes)	

2.3.2 Determinants

The spatiotemporal variation in water-use efficiency arises from the interplay of natural background, economic development, social structure, and environmental policy. To systematically analyze the key drivers and constraints in the BTH region, and based on a review of relevant studies, we adopt a systems approach that classifies determinants into three dimensions—natural, economic and social—and construct an indicator framework (Table 2) to comprehensively reveal their internal pathways and mechanisms.

(1) Natural dimension: resource endowment is the foundational condition. Natural factors constitute the physical basis of water supply and demand. This study selects per-capita water resources, annual precipitation, and per-capita water use as core indicators of resource endowment. Generally, richer natural water endowments are often associated with lower water-use efficiency—the "resource curse" can shape production and consumption patterns and water-management attitudes [15].

(2) Economic dimension: development pattern and structure as core drivers. Economic development level and industrial structure directly determine water-consumption intensity and utilization patterns. We use GDP per capita to measure regional economic development and, drawing on the environmental Kuznets curve theory, examine possible nonlinear relationships between efficiency and growth. We also include the GDP shares of the primary, secondary, and tertiary sectors to capture the optimizing effect of industrial upgrading on water-use efficiency [16].

(3) Social dimension: population agglomeration and intellectual support as long-term foundations. Social factors—population distribution, human capital, and technological innovation—profoundly shape water-management capacity and use patterns. We use water consumption per RMB10,000 of GDP, urbanization rate, and population density to capture spatial agglomeration; urbanization may generate scale effects that improve supply efficiency but can also intensify local water stress. The shares of education expenditure and of science & technology investment measure societal commitment to human capital and innovation, which directly affect the development, diffusion, and application of water-saving technologies and thus provide intrinsic drivers for improving water-use efficiency [17].

(4) Environmental dimension: governance investment and pollution control as constraint boundaries. The environmental dimension reflects societal responses and governance efforts addressing water environment issues. This study selects the proportion of environmental protection investment in GDP to characterize the government's emphasis and financial support for environmental governance, which directly affects the construction and operation effectiveness of pollution treatment facilities [18].

Table 2 Indicator System of Influencing Factors

Indicator layer	Criterion layer	Measurement layer (unit)	Reference
Natural	Water resource endowment	Per-capita water resources (m^3/person) Annual precipitation (m^3) Per-capita water use (m^3//person))	[15]
Economic	Economic development level	Per-capita GDP (10,000 CNY/person)	[16]
	Industrial structure	Primary industry GDP share (%) Secondary industry GDP share (%) Tertiary industry GDP share (%)	
Social	Water intensity	Water use per 10,000 CNY GDP (m^3/10k CNY)	[17]
	Degree of spatial agglomeration	Population density (persons/km^2)	
	Urbanization level	Urban population share of total population (%)	
	Education investment level	Education expenditure as share of total expenditure (%)	
	Science & technology investment level	Science & technology expenditure as share of total expenditure (%)	
Environment	Environmental protection investment level	Environmental protection expenditure as share of total expenditure (%)	[18]

2.4 Data Sources

All data in this study, including input indicators, output indicators, and influencing factor indicators, are sourced from the *China Statistical Yearbook*, *Hebei Statistical Yearbook*, *Beijing Statistical Yearbook*, *Tianjin Statistical Yearbook* (2014–2024), *Water Resources Bulletins* (2013–2023), and other relevant literature. For statistical issues, missing data

for specific regions/periods were supplemented using linear interpolation.

3 MEASUREMENT OF WATER-RESOURCE EFFICIENCY AND ANALYSIS OF ITS SPATIO-TEMPORAL EVOLUTION

The study divides the research area into three units: Beijing, Tianjin, and Hebei, to measure and analyze water use efficiency separately. Using the non-radial, non-oriented super-efficiency SBM model on the DEArun software platform, we evaluated the water use efficiency of the BTH region from 2013 to 2023, and visualized its spatiotemporal evolution characteristics with the help of ArcGIS tools.

Table 3 Water-Resource Utilization Efficiency by Province and Municipality in the BTH Region, 2013-2023

Province	2013	2014	2015	2016	2017	2018	2019	2020	2021	2022	2023	Mean
Beijing	1.023	1.004	1.008	1.009	1.055	1.015	1.017	1.019	1.009	1.122	1.030	1.028
Tianjin	1.249	1.013	1.008	1.055	1.020	1.021	1.077	1.032	1.013	1.015	1.038	1.049
Hebei	1.009	0.790	1.026	1.023	0.749	0.249	0.224	0.195	0.191	0.197	0.196	0.532
Mean	1.093	0.935	1.014	1.029	0.941	0.762	0.773	0.748	0.738	0.778	0.755	0.870

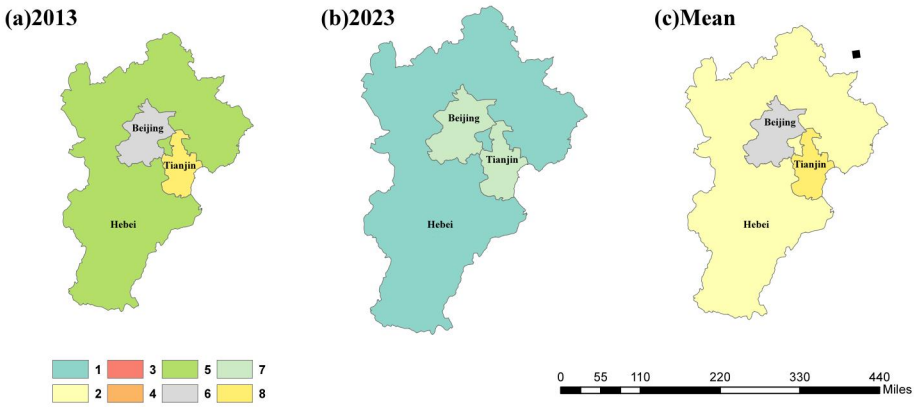

Figure 1 Comparison of Water-Resource Efficiency in the BTH Region for 2013, 2023, and the 2013–2023 Mean (Efficiency Increased from 1 to 8)

Table 3 and Figure 1 indicate that from 2013 to 2023 the BTH region's water-use efficiency exhibited an overall pattern of "stable → rise → decline → eventual low-level stabilization." The mean efficiency was 0.870, well below the effective level, indicating overall inefficiency and that water resources have not yet been used intensively and efficiently in production. Over time, aggregate efficiency fell from 1.094 in 2013 to 0.755 in 2023, with an average annual contraction rate of 3.39%, reflecting a fluctuating downward trajectory. This trend suggests that, despite ongoing industrial upgrading, capacity elimination, increased technological investment, and talent attraction, these measures have not yet produced substantive improvements in water-use efficiency; considerable scope for improvement remains [19].

By stage, efficiency was highest in 2013; it rose rapidly from 2014 to 2016, peaking at 1.029 in 2016; then fell sharply in 2018 and remained at a low level of about 0.759 from 2018 to 2023. This trajectory reflects the combined effects of national policies, industrial restructuring, and natural-condition variability. Specifically, the 2013 peak benefited from the cumulative effects of the 2011 national decision to accelerate water-conserving reforms, structural optimization in the region (e.g., a higher services share in Beijing and tighter controls on high-consumption projects in Tianjin Binhai New Area), and above-average precipitation. The 2014–2016 rise and 2016 peak were driven by implementation of the Outline of the BTH Coordinated Development Plan, the establishment of cross-regional unified water-resource management, water supply from the Middle Route of the South-to-North Water Diversion Project, and policy measures such as stepped water pricing and water-use quotas from water-saving pilots. The slight downturn in 2017 was associated with a surge in infrastructure water use during the initial construction of Xiong'an New Area and below-average rainfall [20]. The 2018 collapse mainly reflected reduced industrial water efficiency during Hebei's capacity-reduction campaign, lower emergency water-use efficiency after closure of self-supplied wells during groundwater remediation, and urban demand peaks from extreme summer weather. The prolonged weakness from 2019–2023 is linked to uneven cross-regional policy implementation, increased demand from major events (e.g., snowmaking for the Winter Olympics), and routine ecological water replenishment competing with production use.

The analysis indicates that policy and regulatory guidance, natural-condition variability, and short-term pressures associated with economic structural transformation jointly shaped the fluctuating trajectory of water-use efficiency in the BTH region.

4 ANALYSIS OF INFLUENCING FACTORS

To further elucidate the drivers of the estimated water-use efficiency in the BTH region, this study performed panel Tobit regression analysis in Stata 18.0; the results are reported in Table 4.

Table 4 Tobit Regression Results for Key Determinants of Water-Resource Efficiency in the BTH Region

Criterion	Explanatory variable	Coefficient	Standard error	*z value*	*P value*
Water resource endowment	Per-capita water resources	1.104×10^{-4}	3.850×10^{-4}	0.290	0.774
	Annual precipitation	-9.952×10^{-4}	3.645×10^{-3}	-0.270	0.785
	Per-capita water use	1.604×10^{-4}	2.876×10^{-4}	0.560	0.577
Economic development level	Per-capita GDP	3.210×10^{-6}	1.860×10^{-6}	1.720	0.085
Industrial structure	Primary industry GDP share	-17.384**	8.278	-2.100	0.036
	Secondary industry GDP share	0.390	1.006	0.390	0.698
	Tertiary industry GDP share	0.000	0.000	0.000	0.000
Water intensity	Water use per 10,000 CNY GDP	0.048***	0.014	3.300	0.001
Degree of spatial agglomeration	Population density	1.332	2.633	0.510	0.613
Urbanization level	Urban population share of total populatio	-2.420	8.133	-0.300	0.766
Education investment level	Education expenditure as share of total expenditure	1.983	4.140	0.480	0.632
Science & technology investment level	Science & technology expenditure as share of total expenditur	-3.850×10^{-5}	4.650×10^{-5}	-0.830	0.408
Environmental protection investment level	Environmental protection expenditure as share of total expenditure	-0.296	2.196	-0.130	0.893
	Constant	-1.706	3.669	-0.460	0.642

Note: ***, ** denote significance at the 1% and 5% levels, respectively.

Based on the regression results for the primary determinants reported in Table 4, the detailed analysis is as follows.

The Tobit results indicate that some factors promote water-use efficiency in the BTH region. Water use per 10,000 CNY of GDP is negative and statistically significant at the 1% level, confirming that reductions in this core water-intensity indicator are a key manifestation of improved water-use efficiency. Other variables (e.g., annual precipitation, per-capita GDP) have positive coefficients but are not statistically significant; their effects remain inconclusive, possibly due to limited sample size, endogeneity, or regional heterogeneity. Overall, lowering water use per 10,000 CNY GDP is the most direct and statistically robust pathway to raise regional water-use efficiency, achievable through technological upgrades and strengthened water-management practices to foster efficiency-driven intensive development.

Among the inhibitory factors, the share of the primary industry is significantly negative (coefficient = -17.384, $p < 0.05$), indicating a robust adverse relationship with water-use efficiency and reflecting agriculture's still-large share of water consumption that structurally constrains overall efficiency. Other variables (e.g., per-capita water use, R&D/technology investment) have negative coefficients but are not statistically significant, so their suppressive effects remain inconclusive. Hence, an excessively high primary-industry share is the key shortcoming hindering efficiency improvements; advancing agricultural water-saving modernization and optimizing the three-sector structure should be priority responses.

5 DISCUSSION

This study makes two key contributions: methodologically, it integrates a super-efficiency SBM model with undesirable outputs and Tobit regression to provide a holistic evaluation of water resource utilization efficiency, addressing the limitations of conventional DEA models by distinguishing efficient decision-making units and accounting for environmental costs. Substantively, it pioneers a four-dimensional analytical framework (natural, economic, social, and environmental) to dissect the determinants of water efficiency, revealing a "double-edged mechanism" where factors like per capita GDP and tertiary industry share synergistically promote efficiency, while primary industry share and insufficient R&D investment impose structural constraints. A primary limitation is the omission of intra-regional variations: the provincial-level analysis masks disparities within sub-region, which could be addressed by incorporating prefecture-level data to capture localized efficiency dynamics.

6 CONCLUSIONS AND RECOMMENDATIONS

This study employs a super-efficiency SBM model to measure water resource efficiency in the BTH region from 2013 to 2023. The results indicate an overall trend of "initial stability, followed by an increase, subsequent decrease, and final stabilization at a low level." The average water resource utilization efficiency is 0.870, significantly below the effective level, indicating an overall non-effective state. The water resource utilization efficiency of Beijing and Tianjin is generally higher than that of Hebei Province, suggesting that there is still room for improvement in the overall water

resource utilization efficiency of the BTH region. In-depth analysis of efficiency causes is conducted by applying Tobit regression to analyze 13 refined factor indicators across four dimensions: natural, economic, social, and environmental. The results show that per capita water resources, annual precipitation, per capita GDP, the proportion of the secondary industry, the proportion of the tertiary industry, water consumption per 10,000 yuan of GDP, education investment level, and urbanization degree can significantly promote the improvement of water resource utilization efficiency in the BTH region. In contrast, per capita water consumption, the proportion of the primary industry, scientific and technological investment level, population density, and environmental protection investment level have an inhibitory effect on water resource utilization efficiency in the region. Based on the above research conclusions, in order to improve the water resource utilization efficiency of the BTH region and achieve high-quality regional economic development, the following suggestions are put forward.

(1) Establish a differentiated assessment system and implement regionally targeted management. This study confirms that reducing water use per 10,000 CNY GDP is the most direct and significant pathway to improve regional water-use efficiency. Therefore, it is recommended to include its reduction rate as a key mandatory indicator in the BTH coordinated development assessment. Based on the industrial bases and water-use structures of the three regions, differentiated target management should be implemented: Beijing and Tianjin should focus on improving water-saving efficiency in high-tech industries and modern services; Hebei should prioritize assessing the reduction in water intensity after upgrading traditional industries such as steel and chemicals, thereby decomposing macro-efficiency goals into quantifiable micro-management actions.

(2) Establish a market-based agricultural water-rights trading mechanism to drive structural optimization via economic incentives. Tobit results show an excessively high primary-sector share is a key structural constraint on water-use efficiency. Pilot a “conservation-to-rights” conversion in major agricultural water users (e.g., Hebei): finance agricultural water-saving upgrades, certify saved water as tradable entitlements, and permit paid transfers to industrial or ecological users in Beijing and Tianjin. This both internalizes incentives for agricultural water saving and, through market allocation, shifts water from low-productivity to higher-productivity uses, fundamentally optimizing regional water-use structure.

(3) Establish an integrated BTH collaborative platform for water-saving technology innovation and promotion. Ultimately, improvements in water-use efficiency depend on technological progress and widespread application. It is recommended that the governments of the three regions jointly take the lead in regularly releasing a catalog of water-saving technologies for key industries in BTH, and recommend the implementation of mature and reliable water-saving technologies in the catalog for new construction and renovation projects. At the same time, a regional collaborative innovation fund should be established to support the formation of a "Water-Saving Technology Alliance" composed of scientific research institutions in Beijing and Tianjin and industrial parks in Hebei, to carry out joint research on common high water-consuming links, and ensure that advanced water-saving technologies can be implemented and transformed to produce practical results.

COMPETING INTERESTS

The authors have no relevant financial or non-financial interests to disclose.

REFERENCES

[1] Ren Y, Su X, He Y, et al. Urban water resource utilization efficiency and its influencing factors in different eco-geographical regions of China. Acta Ecologica Sinica, 2020, 40(18): 6459-6471.

[2] Wu J, Feng Z, Kong X, et al. Multi-Scenario Analysis of Brackish Water Irrigation Efficiency Based on the SBM Model. Water, 2025, 17(19): 2860.

[3] Zheng H, Wang H, He H, et al. Quantifying the heterogeneity of urban water resources utilization efficiency through meta-frontier super SBM model: Application in the yellow river Basin. Journal of Cleaner Production, 2024, 485: 144410.

[4] Zhao X, Yang D. Research on Regional Disparities, Dynamic Evolution, and Influencing Factors of Water Environment Governance Efficiency in China. Water (20734441), 2025, 17(4).

[5] Wang Y, Long A, Deng X, et al. Spatiotemporal changes and influencing factors of the intensity of the agricultural water footprint in Xinjiang, China. International Journal of Agricultural and Biological Engineering, 2023, 16(3): 262-272.

[6] Yang L, Li X, Wang B, et al. Measurement and Spatio-Temporal Evolution Analysis of Green Water Efficiency in Shaanxi Province Based on the SBM-Malmquist Model. Water, 2025, 17(17): 2603.

[7] Liu H, Liu H, Geng L. Analysis of industrial water use efficiency based on SFA–Tobit panel model in China. Sustainability, 2024, 16(19): 8708.

[8] Li J, Xie H. Green Water Resources Utilization Efficiency, Spatio-Temporal Difference and Driving Factors in Beijing-Tianjin-Hebei Region. Journal of Water Resources and Water Engineering, 2021, 32(06): 10-18.

[9] Wang F, Ying Z, Lü S, et al. Evaluation on Characteristics of Coordinated Development of Water-Economy-Ecology Coupling in Beijing-Tianjin-Hebei Region. Water Resources Protection, 2022, 38(05): 80-86.

[10] Tone K. Dealing with undesirable outputs in DEA: A slacks-based measure (SBM) approach. GRIPS Discussion Papers, 2015, 1.
[11] Tobin J. Estimation of relationships for limited dependent variables. Econometrica: journal of the Econometric Society, 1958: 24-36.
[12] Yin Y. Research on the Change of Water Resource Utilization Efficiency in Anhui Province Based on SBM-Malmquist. Polish Journal of Environmental Studies, 2025, 34(3).
[13] Deng G, Li L, Song Y. Provincial water use efficiency measurement and factor analysis in China: based on SBM-DEA model. Ecological Indicators, 2016, 69: 12-18.
[14] Wang M, Sun C, Wang X. Analysis of the water-energy coupling efficiency in China: Based on the three-stage SBM-DEA model with undesirable outputs. Water, 2019, 11(4): 632.
[15] Mu Y, Cheng Y, Wang J. Calculation and Influencing Factors of Water Resources Utilization Efficiency in Receiving Area of Bailong River Water Diversion Project. Journal of Hohai University (Natural Sciences), 2025, 53(04): 38-46+134.
[16] Xiao Y, Ci X, Yang B, et al. Green Efficiency Measurement and Influencing Factors of Water Resources in Urban Agglomeration in the Middle Reaches of Yangtze River. Journal of Yangtze River Scientific Research Institute, 2023, 40(09): 8-16.
[17] Sun Z, Lu S, Liu B. Research on the Evaluation and Improvement Path of Provincial Regional Ecological Efficiency: Based on Super-Efficiency SBM Model and Tobit Regression. Ecological Economy, 2021, 37(01): 124-129.
[18] Li G, Liu J, Li T. Regional Differences of Manufacturing Energy Eco-Efficiency Considering Undesirable Outputs: A Two-Stage Analysis Based on SBM and Tobit Model. Chinese Journal of Management Science, 2019, 27(11): 76-87.
[19] Liu H. Study on the Green Economic Efficiency Measurement and Influencing Factors in Beijing-Tianjin-Hebei Region: Based on the Analysis of Super-Efficiency SBM and Tobit Model. Ecological Economy, 2023, 39(04): 67-73.
[20] Liu T, Tian X. Coordinated Development of Beijing-Tianjin-Hebei Region: Progress, Effect and Prospect. China Business and Market, 2019, 33(11): 116-128.

Frontiers in Environmental Research
Print ISSN: 2960-0251
Online ISSN: 2960-026X
DOI: https://doi.org/10.61784/fer3040

ENVIRONMENTAL RISKS AND ECOTOXICOLOGY OF ANTIBIOTIC POLLUTION IN WATER ENVIRONMENTS AND COMPREHENSIVE PREVENTION AND CONTROL STRATEGIES

ZhiJiang Nan
Qinghai Institute of Technology, Xining 810016, Qinghai, China.
Corresponding Author Email: zjnan@qhit.edu.cn

Abstract: The widespread detection of antibiotics in aquatic environments has become a global environmental issue, posing huge potential threats to ecosystems and human health. This paper systematically reviews research progress on antibiotic pollution in aquatic environments, focusing on its environmental behavior, ecotoxicological effects, and comprehensive prevention and control strategies. Firstly, an overview of the global and Chinese pollution status, major sources, and occurrence characteristics of antibiotics in aquatic environments is provided. Secondly, the migration and transformation laws, environmental fate, and ecological risk assessment methods of antibiotics in aquatic environments are explored in depth. Then, the ecotoxicological effects of antibiotics on aquatic organisms are elaborated in detail, including impacts on microbial community structures, the generation and spread of antibiotic resistance genes (ARGs), toxic effects on aquatic animals and plants, and potential risks to human health. Finally, comprehensive prevention and control strategies are proposed from four levels: source control, process interception, end-of-pipe treatment, and system management. Future research directions are also outlined to provide a scientific basis for the risk management of antibiotic pollution in aquatic environments.
Keywords: Antibiotic pollution; Aquatic environment; Environmental risk; Ecotoxicology; Antibiotic resistance genes (ARGs); Comprehensive prevention and control

1 INTRODUCTION

The discovery and application of antibiotics is a milestone in the history of human medicine, having drastically reduced the mortality rates of infectious diseases. However, with the widespread application of antibiotics in medical, livestock breeding, and aquaculture fields, large quantities of antibiotics and their metabolites have entered aquatic environments through various pathways, forming a new class of pollutants[1-2]. These substances are ubiquitous in the environment; even at extremely low concentrations (ng/L–μg/L), they may exert adverse effects on aquatic ecosystems and induce the generation and spread of resistant bacteria and antibiotic resistance genes (ARGs), thereby threatening human health[3-4].

Over the past two decades, with advancements in analytical techniques—particularly the popularization of high-sensitivity detection methods such as High-Performance Liquid Chromatography-Tandem Mass Spectrometry (HPLC-MS/MS)—the detection frequency and concentration ranges of antibiotics in aquatic environments have continuously expanded[5]. Research indicates that antibiotics have been detected in global surface water, groundwater, drinking water, and even polar environments. As a major producer and consumer of antibiotics, China faces particularly prominent problems regarding antibiotic pollution in aquatic environments, which has attracted widespread attention from the government, academia, and the public. This paper aims to systematically review the research progress on environmental risks and ecotoxicology of antibiotic pollution in aquatic environments. Based on the systematic thinking of "source-process-end", it proposes comprehensive prevention and control strategies to provide a reference for the scientific management and control of antibiotic pollution in aquatic environments[6-7].

2 POLLUTION STATUS AND SOURCES OF ANTIBIOTICS IN AQUATIC ENVIRONMENTS

2.1 Pollution Levels and Distribution Characteristics in Global and Chinese Aquatic Environments

According to existing literature reports, antibiotic pollution in aquatic environments globally presents obvious spatiotemporal differences and species specificity[5].

Global Overview: In developed regions such as Europe and North America, due to strict regulations and perfect sewage treatment facilities, antibiotic concentrations in surface water are usually at the ng/L level. However, in developing countries in Asia, Africa, and Latin America, due to relatively lax regulations and low sewage treatment rates, surface water antibiotic concentrations can reach the μg/L level. High concentrations of fluoroquinolones and macrolides are frequently detected in rivers in India, Pakistan, and other countries[7].

Current Status in China: China is the world's largest producer and consumer of antibiotics, with an annual usage of tens of thousands of tons. Consequently, the problem of antibiotic pollution in China's aquatic environment is particularly prominent. The main characteristics are as follows:

Uneven Spatial Distribution: Pollution levels show a trend of being higher in the eastern coastal and densely populated

areas than in the western regions. The Pearl River Delta, Yangtze River Delta, and Beijing-Tianjin-Hebei regions are hotspots for antibiotic pollution. Studies indicate that the concentration of sulfamethoxazole in the Guangzhou section of the Pearl River can reach hundreds of ng/L, and quinolone antibiotic concentrations in the Tianjin section of the Haihe River are also at a relatively high level[8].

Diverse Species: A wide variety of antibiotic species are detected in China's aquatic environments, mainly including Sulfonamides (SAs), Quinolones (FQs), Macrolides (MLs), Tetracyclines (TCs), and β-Lactams. Among them, fluoroquinolones (e.g., norfloxacin, ciprofloxacin) and sulfonamides (e.g., sulfamethoxazole) are the two classes with the highest detection frequency and most prominent concentrations[9-11].

Differences in Water Body Types:

Surface Water:* Rivers, lakes, and reservoirs are generally polluted by antibiotics. River sections receiving sewage treatment plant effluent, aquaculture wastewater, and runoff pollution have the highest antibiotic concentrations[10].

Groundwater:* Affected by soil leaching and septic tank leakage, antibiotics are also detected in groundwater in some areas, but concentrations are usually lower than in surface water[12].

Drinking Water:* Conventional water treatment processes struggle to completely remove antibiotics. Trace amounts have been detected in drinking water in some areas. Although far below therapeutic doses, the health risks of long-term low-dose exposure cannot be ignored[12-14].

Coastal Seawater:* Estuaries and coastal waters are increasingly affected by antibiotic pollution due to terrestrial inputs[12].

2.2 Major Sources and Input Pathways of Antibiotic Pollution

The pathways for antibiotics to enter aquatic environments are complex and diverse, mainly including point sources and non-point sources.

2.2.1 Point source pollution

Domestic Sewage: About 30–90% of antibiotics consumed by humans are excreted in urine and feces in their original form or as metabolites, entering sewage treatment plants (STPs) through sanitary systems. However, the removal efficiency of traditional activated sludge processes for many antibiotics is limited (ranging from 0 to 90%), resulting in large quantities of antibiotics being discharged into receiving waters with the effluent[7,13,15-17].

Medical Wastewater: Hospitals are the places where antibiotics are most intensively used. Their wastewater is characterized by complex composition, high concentration, and strong biological toxicity. Although some large hospitals have sewage treatment facilities, treatment effects vary, making them important point sources[16].

Pharmaceutical Industrial Wastewater: High-concentration process wastewater generated during antibiotic production. Although enterprises are required to perform pretreatment, accidental incidents or lax supervision may lead to the direct discharge of high-concentration antibiotics[18-20].

Aquaculture Wastewater: The livestock and aquaculture industries use large amounts of antibiotics to prevent diseases and promote growth. Animal feces and aquaculture pond water contain high concentrations of antibiotics and their metabolites. Without effective treatment, they are discharged or applied as fertilizer, eventually entering water bodies through runoff[19].

2.2.2 Non-point source pollution

Agricultural Runoff: Farmland applied with animal manure containing antibiotics can see antibiotics enter nearby water bodies through runoff during rainfall or irrigation[21].

Urban Runoff: Urban surface runoff containing pet feces, landfill leachate, etc., may also carry antibiotics into urban drainage systems or directly into water bodies[18].

Diffusion from Aquaculture Areas: In modes such as cage farming, antibiotics are applied directly to open waters, easily causing widespread pollution in surrounding waters[22-24].

2.3 Physicochemical Properties and Environmental Persistence of Typical Antibiotics

The environmental behavior and ecological risks of antibiotics are closely related to their physicochemical properties, with key parameters including the octanol-water partition coefficient (log Kow), acid dissociation constant (pKa), water solubility, and photolysis and biodegradation half-lives[25].

Sulfonamides: Strong polarity, high water solubility, and low log Kow (usually <1). They migrate easily in the water phase and do not easily accumulate in sediments, but their photolysis rate is relatively slow[26].

Quinolones: Mostly amphoteric ions with multiple pKa values, taking different forms in water environments with different pH levels. Water solubility varies significantly. They can form complexes with metal ions and easily adsorb onto sediments and suspended particles; photolysis is an important natural attenuation pathway[27].

Macrolides: Relatively strong hydrophobicity, easy to adsorb onto solid particles, but relatively stable in water[26-28].

Tetracyclines: Prone to forming stable complexes with divalent and trivalent cations (e.g., Ca^{2+}, Mg^{2+}, Fe^{3+}). They strongly adsorb onto soil and sediments. Concentrations in the water phase are usually not high, but they may remain in sediments for a long time.

Most antibiotics belong to "pseudo-persistent pollutants" in the environment. Although they can be partially degraded, continuous input leads to their long-term presence in the environment[25,29-31].

3 ENVIRONMENTAL BEHAVIOR AND FATE OF ANTIBIOTICS IN AQUATIC ENVIRONMENTS

After entering the aquatic environment, antibiotics undergo a series of complex migration and transformation processes, including adsorption/desorption, hydrolysis, photolysis, and biodegradation. These processes jointly determine their environmental fate, persistence, and ultimate destination.

3.1 Migration and Transformation Processes

3.1.1 Adsorption and desorption

Adsorption is a key process affecting the distribution of antibiotics between the solid and liquid phases, controlling their distribution in water and sediments/soil. Adsorption mechanisms mainly include:

Electrostatic Interaction: Depends on the charge form of the antibiotic and the charge properties of the solid surface[31].

Hydrophobic Partitioning: For antibiotics with higher log Kow (e.g., some macrolides, fluoroquinolones), hydrophobic interaction is the main adsorption mechanism.

Coordination Complexation: Antibiotics such as tetracyclines and quinolones can form complexes with metal ions or metal oxide surfaces through functional groups like carboxyl and keto groups[32].

Hydrogen Bonding and π-π Interaction: Aromatic antibiotics can interact with aromatic-rich organic matter (e.g., black carbon) through π-π electron donor-acceptor interactions.

Environmental factors such as the organic matter content of sediments, clay mineral types, pH, and ionic strength significantly affect adsorption behavior. Although adsorption can temporarily reduce the aqueous concentration, sediments may become a “sink” and a “secondary source” for antibiotics, releasing them again when conditions change[33].

3.1.2 Hydrolysis

Hydrolysis is a chemical reaction between antibiotic molecules and water. Its rate is affected by pH, temperature, and ionic strength. The β-lactam ring of β-lactam antibiotics (e.g., penicillin) is unstable and prone to hydrolysis, which is one of their main degradation pathways. In contrast, the hydrolysis rates of sulfonamides and quinolones are usually slow[34].

3.1.3 Photolysis

Photolysis is an important attenuation pathway for many antibiotics in the surface water layer, including direct photolysis (antibiotics absorb light energy and react) and indirect photolysis (oxidized by photoactive substances such as hydroxyl radicals and singlet oxygen). Quinolones, tetracyclines, and sulfonamides, which contain chromophores, are sensitive to photolysis. Photolysis rates are influenced by light intensity, wavelength, water depth, dissolved organic matter (DOM, which can both sensitize and quench photochemical reactions), pH, and nitrate/nitrite concentrations. Photolysis products may still retain biological activity or toxicity, and their ecological risks deserve attention[34-35].

3.1.4 Biodegradation

Biodegradation is an important transformation process for antibiotics in deep water bodies and sediments. However, since many antibiotics were designed to resist microbial degradation, their biodegradability is generally poor.

Aerobic Degradation: Occurs in aerobic units of sewage treatment plants and oxygen-rich surface water layers, but rates are often limited[32].

Anaerobic Degradation: In sediments and oxygen-deficient water bodies, certain antibiotics (e.g., metronidazole) can be reductively degraded by anaerobic microorganisms, but overall, research on degradation efficiency under anaerobic conditions is insufficient.

Co-metabolism: Many antibiotics cannot serve as the sole carbon and energy source for microorganisms but can be partially transformed through co-metabolism in the presence of other easily degradable organic matter[36].

Microbial community structure, antibiotic concentration, temperature, and nutritional conditions affect biodegradation efficiency. Notably, low concentrations of antibiotics may screen for and enrich microorganisms with degradation potential, but long-term exposure may also inhibit the activity of degrading bacteria[37].

3.2 Environmental Fate Models and Multi-Media Simulation

To predict the distribution and persistence of antibiotics in complex environments, researchers have developed various fate models, ranging from simple mass balance models to complex multi-media fugacity models. These models integrate the physicochemical properties of antibiotics, environmental parameters (temperature, pH, hydrological conditions, etc.), and rate constants for various migration and transformation processes. They can be used to simulate the dynamic distribution of antibiotics among water, sediments, and biota; assess long-term exposure concentrations; identify key source and sink areas; and provide decision support for environmental risk management[38].

3.3 Ecological Risk Assessment Methods for Antibiotics

Accurately assessing the environmental risks of antibiotics is a prerequisite for formulating control standards. Currently, the Risk Quotient (RQ) method is widely used for preliminary assessment:

Risk Quotient (RQ) = Predicted No Effect Concentration (PNEC) in the environment / Predicted Environmental Concentration (PEC) in the environment

Acquisition of PEC: Can be obtained through actual monitoring (MEC) or estimation based on usage, emission factors, and dilution models[39].

Derivation of PNEC: Usually based on chronic or No Observed Effect Concentrations (NOEC) obtained from

laboratory toxicity tests, divided by an assessment factor (usually 10–1000, depending on data quality). Due to the specificity of antibiotic action, it is necessary to consider effects on the most sensitive species (e.g., specific algae, bacteria) and conduct special assessments for microbial resistance risks[35].

Studies show that in hotspots such as sewage treatment plant outlets and downstream of aquaculture areas, the RQ values for multiple antibiotics (e.g., sulfamethoxazole, erythromycin, ciprofloxacin) are greater than 1, indicating medium to high ecological risks. However, the Risk Quotient method has limitations, such as not considering the mixture effects of antibiotics, the chronic effects of long-term low-dose exposure, and the development of resistance. Therefore, higher-level ecological risk assessments need to combine methods such as field community surveys, mesocosm experiments, and effect-directed analysis[33].

4 ADVANCES IN ECOTOXICOLOGICAL RESEARCH ON ANTIBIOTIC POLLUTION

Antibiotics are a special class of pollutants with biological activity. Their ecotoxicological effects are reflected not only in traditional acute/chronic toxicity but, more prominently, in the interference with microbial communities and the selection pressure for resistance.

4.1 Impact on Aquatic Microbial Communities

Microorganisms are the cornerstone of aquatic ecosystems, driving the biogeochemical cycling of elements such as carbon, nitrogen, and phosphorus. The effects of antibiotics on microorganisms are the most direct and significant.

4.1.1 Community structure and diversity

Long-term exposure to sub-inhibitory concentrations of antibiotics can significantly alter the composition and diversity of microbial communities in water and sediments. This usually manifests as a decrease in the abundance of sensitive flora (e.g., certain nitrifying bacteria, phosphorus-accumulating bacteria) and an increase in the abundance of tolerant flora or flora with degradation capabilities. Such structural changes may further affect ecologically driven functions, such as organic matter degradation and nitrification/denitrification processes. Research indicates that even at the ng/L level, sulfonamide antibiotics can alter the bacterial community structure in sediments[40].

4.1.2 Functional genes and metabolic pathways

Metagenomic studies show that under antibiotic stress, the metabolic pathway profiles of microbial communities change. Genes related to stress response, efflux pumps, cell membrane repair, and antibiotic resistance are upregulated, while some genes involved in basic metabolism (e.g., amino acid synthesis, energy metabolism) may be downregulated. This disturbance at the functional level may undermine the stability of microbial ecological services41.

4.2 Emergence, Enrichment, and Spread of Antibiotic Resistance Genes (ARGs)

This is one of the most concerning consequences of antibiotic pollution. The aquatic environment is a key site for the generation and spread of ARGs.

4.2.1 Selection pressure and enrichment of ARGs

The presence of antibiotics exerts strong selection pressure on bacterial communities. Bacteria carrying resistance genes (e.g., genes encoding inactivating enzymes, target site modification, enhanced efflux pumps) have a survival advantage and can reproduce in large numbers, leading to an increase in the abundance and diversity of ARGs in environmental microbial populations. Studies show that in sewage treatment plants, downstream of farms, and in polluted rivers, the abundance of ARGs such as sulfonamides, tetracyclines, and β-lactams is significantly higher than background values[42].

4.2.2 Horizontal Gene Transfer (HGT)

HGT is the primary mechanism for the diffusion of ARGs among environmental bacteria, mainly including conjugation (via plasmids), transformation (uptake of free DNA), and transduction (via phages). Many factors in the aquatic environment can promote HGT:

Antibiotics themselves: Sub-inhibitory concentrations of certain antibiotics (e.g., fluoroquinolones) can act as inducers, stimulating the bacterial SOS response and increasing mutation rates and gene transfer frequencies[43].

Co-selection: Other pollutants such as heavy metals (e.g., Cu, Zn) and disinfection by-products may exert co-selection pressure with antibiotics, promoting the spread of plasmids or integrons carrying multiple resistance genes[44].

Mobile Genetic Elements (MGEs): Plasmids, transposons, and integrons are “vehicles” for ARGs. They are widely present in environmental microorganisms and can transfer ARGs between different species or even different bacterial phyla.

4.2.3 Environmental resistome and human health risks

Environmental ARGs and antibiotic-resistant bacteria (ARB) may spread to humans directly or indirectly through drinking water, recreational water, and consumption of contaminated aquatic products. Even more concerning is that environmental bacteria can serve as a “reservoir” and “incubator” for ARGs, where novel resistance genes may evolve and subsequently transfer to human pathogens. Therefore, controlling antibiotic pollution and the spread of ARGs in the environment is a crucial link in addressing the global public health crisis of antibiotic resistance[45].

4.3 Toxic Effects on Aquatic Animals and Plants

4.3.1 Aquatic animals

Acute and Chronic Toxicity: High concentrations of antibiotics can cause acute toxicity to fish, crustaceans, shellfish, etc., affecting survival. More common are chronic toxicity effects caused by long-term low-dose exposure, including:
Growth Inhibition: Affecting feeding, digestion, and energy metabolism.
Reproductive and Developmental Toxicity: Interfering with the endocrine system, affecting gonad development, gametogenesis, reproductive capacity, and offspring survival rates. For example, certain antibiotics have estrogenic or anti-androgenic activity.
Oxidative Stress and Tissue Damage: Inducing the production of reactive oxygen species (ROS), leading to lipid peroxidation and DNA damage, causing pathological changes in organs such as the liver, gills, and kidneys[46].
Immunotoxicity: Inhibiting immune cell function and reducing disease resistance.
Behavioral Changes: Affecting swimming ability, foraging behavior, and social interaction.
Species Sensitivity Differences: Sensitivity to the same antibiotic varies significantly among different species and life stages. Usually, juvenile stages are more sensitive.

4.3.2 Aquatic plants and algae

Algae (especially cyanobacteria and green algae) are sensitive groups to antibiotics. Antibiotics can inhibit algae growth by inhibiting chlorophyll synthesis, interfering with the photosynthetic system, and destroying cell division, thereby altering the algae community structure (e.g., causing a decrease in sensitive algae species and making resistant or tolerant species dominant). This may destroy the primary productivity of aquatic ecosystems and produce cascading effects through the food web. Macrophytes (e.g., submerged plants) may also suffer from growth inhibition and physiological interference[47].

4.4 Potential Risks to Human Health

The general public is exposed to trace amounts of antibiotics and their ARGs/ARB in the environment over long periods through drinking water and consuming aquatic products. The health risks are not yet fully clear, but potential threats include:
Direct Toxicity: The concentration of antibiotics in drinking water is extremely low, so the risk of direct toxicity alone is very small, but the “cocktail effect” of long-term co-exposure to multiple antibiotics and other pollutants needs attention[48].
Allergy and Hypersensitivity: A very small number of sensitive individuals may have allergic reactions to trace amounts of antibiotics (e.g., penicillin).
Gut Microbiota Disturbance: Antibiotics in drinking water may affect the balance of human gut microorganisms.
Increased Risk of Resistant Bacterial Infection: This is the most significant risk. Environmental ARB or ARGs may enter the human body through various pathways, colonize the gut or skin, or, if pathogens acquire these ARGs, lead to refractory infections.

5 COMPREHENSIVE PREVENTION AND CONTROL STRATEGIES FOR ANTIBIOTIC POLLUTION

Addressing the complex problem of antibiotic pollution in aquatic environments requires comprehensive strategies combining “source reduction, process control, end-of-pipe treatment, and system management” to build a whole-process prevention and control system covering production, consumption, and discharge[49].

5.1 Source Control Strategies

Source control is the most fundamental and economical way to solve pollution problems.

5.1.1 Regulating and reducing antibiotic use

Medical Field: Strengthen the management of clinical antibiotic application, implement prescription review, hierarchical management, and usage monitoring, and reduce unnecessary prophylactic and therapeutic use. Strengthen public education to put an end to self-purchasing and abuse.
Livestock Breeding Industry:
Strictly enforce the “antibiotic ban”, prohibiting the addition of antibiotics for growth promotion to feed.
Therapeutic antibiotics must be used with a veterinary prescription and comply with withdrawal period regulations.
Promote “antibiotic-free farming” and “antibiotic-reduction farming” modes, improve breeding environments, and enhance animal immunity.
Research and apply antibiotic alternatives, such as probiotics, prebiotics, antimicrobial peptides, plant extracts, and phages.
Aquaculture Industry: Optimize farming modes (e.g., ecological integrated farming) to reduce disease occurrence; promote vaccine immunization and green fishery drugs.
Pharmaceutical Industry: Encourage the development and production of new, environmentally friendly (easily degradable, low ecotoxicity) antibiotics and improve production processes to reduce the loss of raw materials.

5.1.2 Improving laws, regulations, and standard systems

Include more high-risk antibiotics in the list of priority controlled pollutants. Research and timely formulate environmental quality standards for antibiotics and their ARGs in aquatic environments. Increase indicators related to antibiotics in the discharge standards for wastewater from industries such as pharmaceuticals and farming.

5.2 Process Blockade and End-of-Pipe Treatment Technologies

For wastewater containing antibiotics that has already been generated or is unavoidable, efficient treatment is required.

5.2.1 Strengthening traditional sewage treatment processes

Optimizing Operating Parameters: Extending the sludge retention time (SRT) helps enrich slow-growing microorganisms and may improve the biodegradation efficiency of certain antibiotics.

Combined Processes: Processes such as A^2/O and MBR have better removal effects on some antibiotics than the traditional activated sludge process. Combining biochemical treatment with advanced treatment units (e.g., ozone, activated carbon adsorption) can enhance overall removal efficiency.

5.2.2 Advanced Oxidation Processes (AOPs)

AOPs can effectively degrade or even mineralize refractory antibiotics by generating strongly oxidizing hydroxyl radicals (·OH), etc., making them a promising depth treatment technology.

Ozone Oxidation: Effective in removing antibiotics containing unsaturated bonds or aromatic rings (e.g., sulfonamides, fluoroquinolones), often used in combination with H_2O_2 (O_3/H_2O_2) to enhance ·OH yield.

Fenton and Fenton-like Technologies: Using the Fe^{2+}/H_2O_2 system to generate ·OH has low costs but requires a narrow pH range (~3). Heterogeneous Fenton, photo-Fenton, and electro-Fenton technologies have improvements in broadening the pH application range and reducing iron sludge.

Photocatalytic Oxidation: Semiconductor catalysts represented by TiO_2 generate electron-hole pairs under ultraviolet irradiation, subsequently generating oxidizing species. Developing visible-light responsive catalysts (e.g., doped modified TiO_2, g-C_3N_4) is a current hotspot.

Persulfate Advanced Oxidation: Oxidation technology based on $SO_4^{\cdot -}$ has advantages such as high oxidation potential, long half-life, and wide pH adaptation range, showing excellent degradation effects on some antibiotics.

AOPs need to address energy consumption, cost, by-product toxicity, and the quenching effect of actual water matrices (e.g., DOM, carbonate).

5.2.3 Adsorption technology

Adsorbent materials such as activated carbon, biochar, carbon nanotubes, graphene, and metal-organic frameworks (MOFs) can be used to remove antibiotics from water. Biochar has attracted much attention due to its wide source of raw materials, low cost, and environmental friendliness. Its adsorption capacity and selectivity can be enhanced through physical and chemical modification. Adsorption is the concentration and transfer of pollutants; saturated adsorbents need to be properly handled to avoid secondary pollution.

5.2.4 Membrane separation technology

Nanofiltration (NF) and Reverse Osmosis (RO) membranes can effectively intercept antibiotics with larger molecular weights and produce good water quality, but problems such as concentrate treatment, membrane fouling, and high operating costs exist[37].

5.2.5 Natural and ecological treatment systems

Ecological engineering measures such as constructed wetlands, stabilization ponds, and riparian filtration zones remove antibiotics through synergistic effects of plant absorption, substrate adsorption, and microbial degradation. They have the advantages of low cost and good landscape and ecological benefits, making them suitable for the deep purification of tail water from sewage treatment plants or the interception of non-point source pollution. However, they require large land areas, and treatment efficiency is affected by seasons and climate.

5.2.6 Removal and control of antibiotic resistance genes

Controlling the spread of ARGs is a deeper challenge. Some AOPs (e.g., UV, ozone, advanced oxidation) can destroy cell structures and free DNA, effectively reducing the abundance of ARB and ARGs. Disinfection processes (chlorine, UV) have a certain inactivating effect on ARB, but it is necessary to be alert to the possibility of inducing bacterial stress responses and gene transfer. Research shows that Membrane Bioreactors (MBR) have better removal effects on certain ARGs than traditional activated sludge processes[37-43].

5.3 System Management and Policy Recommendations

5.3.1 Establishing lifecycle management and multi-department collaborative mechanisms

Establish a management system covering the entire lifecycle of antibiotics "R&D-production-circulation-use-disposal-emission". Strengthen communication and collaboration among environmental protection, health, agriculture, drug administration, and science and technology departments to form regulatory synergy, achieve information sharing, and conduct joint law enforcement.

5.3.2 Improving environmental monitoring networks and risk assessment systems

Incorporate antibiotics and representative ARGs into national and local water environment monitoring or special survey plans to grasp their spatiotemporal distribution and trends. Develop rapid, sensitive, high-throughput on-site monitoring and screening technologies. Develop more refined ecological and health risk assessment models that incorporate mixture effects, long-term chronic effects, and resistance risks[48].

5.3.3 Promoting green pharmaceutical manufacturing and circular economy

Encourage the pharmaceutical industry to adopt green synthesis routes to reduce the use and generation of toxic and hazardous substances from the source. Explore reduction technologies for antibiotics and ARGs in aquaculture waste (feces, litter) and, based on safety assessment, achieve resource utilization (e.g., composting after harmless treatment for

field application).

5.3.4 Strengthening public participation and international cooperation

Raise public awareness of the harm and environmental consequences of antibiotic abuse, advocating for green consumption and healthy lifestyles. Antibiotic pollution and resistance are global challenges; we should actively participate in international conventions and cooperative projects, sharing data, technologies, and experiences to respond together[38].

6 FUTURE RESEARCH PROSPECTS

Despite a large amount of research, there are still many scientific gaps and challenges regarding antibiotic pollution in aquatic environments that urgently need to be addressed:

Identification and Risk of New Antibiotics and Transformation Products: With the development and market launch of new antibiotics, their behavior and risks in the environment are unknown. At the same time, the identification, toxicity, and resistance development potential of complex transformation pathways and products of antibiotics in the environment need to be strengthened.

Ecological Effects of Long-Term Low-Dose Combined Exposure: Real environments often involve the coexistence of multiple antibiotics and other pollutants (e.g., heavy metals, nanomaterials, microplastics). Research on the joint effects and mechanisms of this type of long-term, low-dose, multi-component combined exposure on aquatic ecosystems (from molecular to community levels) is at the forefront of ecotoxicology.

Transmission Mechanisms and Control of Resistance Genes in the Environment: There is a need to reveal the transmission dynamics, key driving factors, and barriers of ARGs in different environmental media more deeply, and to develop specific control technologies targeting MGEs and HGT processes.

Research and Development of High-Efficiency, Low-Carbon Treatment Technologies and Integration: Develop new removal technologies (e.g., novel catalysts, functional materials) with low cost, high efficiency, low energy consumption, and few by-products, and optimize combined processes of different technologies to deal with complex and variable actual wastewater[38-41].

Risk-Based Precise Control and Standard Formulation: Accumulate more comprehensive toxicity data for native species and environmental exposure data, develop risk assessment methods suitable for China’s national conditions, and provide a basis for scientifically formulating environmental quality standards, discharge standards, and ecological restoration goals.

Systematic Research under the “One Health” Framework: Conduct interdisciplinary and cross-media comprehensive research under the integrated health framework of “Human-Animal-Environment”, tracing the complete chain of antibiotics and ARGs from the source to the human body, to provide a scientific basis for formulating systematic solutions[42-45].

7 CONCLUSION

Antibiotic pollution in aquatic environments is a complex environmental problem accompanying the development of modern society. Its environmental risks are reflected not only in the direct toxicity to aquatic organisms but, more profoundly, in the disturbance of microbial ecological functions and the accelerated spread of antibiotic resistance, posing long-term threats to ecosystem security and public health. This paper systematically reviews research progress in this field, revealing the widespread existence and locally severe pollution status of antibiotics in global and Chinese aquatic environments, and elucidating their complex migration and transformation behaviors and multiple ecotoxicological effects, especially the driving role in the development of resistance. Facing this challenge, single technologies or management measures are unlikely to be effective; comprehensive governance strategies must be adopted. This requires us to not only regulate source use and strengthen process and end-of-pipe treatment but also focus on building long-term prevention and control mechanisms from multiple dimensions, including laws and regulations, standard systems, monitoring and assessment, technological innovation, and public education. Future research should pay more attention to deep-seated scientific issues such as combined pollution effects, transformation product risks, and resistance gene transmission control, and commit to developing efficient and practical pollution control technologies. Only through continuous scientific research, strict regulation, and the joint efforts of the whole society can we effectively curb antibiotic pollution in aquatic environments and its cascading risks, protecting aquatic ecological security and human health to achieve sustainable development.

COMPETING INTERESTS

The authors have no relevant financial or non-financial interests to disclose.

REFERENCES

[1] Xie X, Liu W, Zhang J, et al. Enhanced adsorption and photocatalytic degradation performance of lomefloxacin by C60/CNTs composite under LED light irradiation. Journal of Materials Science: Materials in Electronics, 2025, 37 (1): 30-30. DOI:10.1007/S10854-025-16443-X.

[2] Böckmann M, Axtmann K, Bierbaum G, et al. Pulsed antibiotic release into the environment may foster the spread of antimicrobial resistance. FEMS microbiology ecology, 2025. DOI:10.1093/FEMSEC/FIAF128.
[3] Celano R M, Pinho D V J, Azevedo E O D F M S, et al. Environmentally relevant concentrations of the antibiotic azithromycin enhance the toxicity of the cyanobacterium Microcystis aeruginosa on the water flea Daphnia similis. Harmful Algae, 2026, 152: 103040-103040. DOI: 10.1016/J.HAL.2025.103040.
[4] Chen P, Huang F, Kou X, et al. Portable hierarchical MXene-graphene hybrid sensor for ultrasensitive multiplex antibiotic detection in aquatic environments. Chemical Engineering Journal, 2026, 527: 171523-171523. DOI: 10.1016/J.CEJ.2025.171523.
[5] Yalcin S, Cebeci T. Prevalence, antibiotic resistance, and heavy metal resistance genes of Raoultella species in marine fish from coastal districts in Türkiye: Potential health risk and environmental implications. Regional Studies in Marine Science, 2026, 93: 104712-104712. DOI: 10.1016/J.RSMA.2025.104712.
[6] Oluwakoya M O, Okoh I A. Antibiotic resistance profile of Campylobacter species recovered from some freshwater milieu in the Eastern Cape Province, South Africa.. BMC microbiology, 2025. DOI: 10.1186/S12866-025-04557-5.
[7] Li X, Han M, Shen S, et al. Exposure to Evironmentally Relevant Concentrations of Antibiotics Increases N2O Emissions and Delays Nitrate Removal: New Insights into Bacteriostatic Antibiotics at the Cellular Level. Environmental science & technology, 2025. DOI: 10.1021/ACS.EST.5C09865.
[8] Zhang M, Feng M, Zhou M, et al. Environmental Drivers and Source Apportionment of Antibiotic Pollution in Shichuan River Basin, China. Water, Air, & Soil Pollution, 2025, 237(4): 232-232. DOI: 10.1007/S11270-025-08902-2.
[9] Meireles N A, Sandahl M, Turner C, et al. Environmental fingerprinting of recent strategies for detection of macrolides and fluoroquinolones in environmental and food matrices based on green analytical chemistry indexes. Green Analytical Chemistry, 2026, 16: 100313-100313. DOI: 10.1016/J.GREEAC.2025.100313.
[10] Group I C C, Nofal R M, Rwamatwara A, et al. Strengthening surgical antibiotic stewardship in low-resource settings: a multicentre, prospective, quality improvement study.. The British journal of surgery, 2025, 112 (Supplement_15): xv65-xv67. DOI: 10.1093/BJS/ZNAF241.
[11] Choi U, Son E J, Han G, et al. Identification of Genetic and Environmental Factors Suppressing the Lethality and Antibiotic Susceptibility Mediated by Depletion of LptD, a Lipopolysaccharide Transport Protein. Journal of microbiology and biotechnology, 2025, 35: e2509011. DOI: 10.4014/JMB.2509.09011.
[12] Dilxat D, Zhang W, Wang J L, et al. Click chemistry-empowered multi-channel biosensing for highly-efficient detection of antibiotic resistance genes in aquatic environments. Water research, 2025, 290: 125121. DOI: 10.1016/J.WATRES.2025.125121.
[13] Liu X, Liu Y, Wo Y, et al. Synergistic application of photocatalysis and biocatalysis in antibiotic degradation: emerging strategies for sustainable environmental remediation. Chemical Papers, 2025(prepublish): 1-14. DOI: 10.1007/S11696-025-04541-3.
[14] Gong Z, Yu M, Jiang Y, et al. Emerging Transition Metal Sulfides for Sensing of Antibiotics in Environmental, Food and Biological Samples. Journal of Analysis and Testing, 2025(prepublish): 1-22. DOI: 10.1007/S41664-025-00414-6.
[15] Huang H, Wei L, Li L, et al. Microbial interactions as the key to understanding and controlling environmental spread of antibiotic resistance genes. npj Antimicrobials and Resistance, 2025, 3(1): 97-97. DOI: 10.1038/S44259-025-00174-4.
[16] Kumari H, Singh M, Chakrawarti K M, et al. Distribution and antibiotic resistance patterns of airborne staphylococci in urban environments of Delhi, India. Scientific Reports, 2025, 15(1): 43026-43026. DOI: 10.1038/S41598-025-95462-4.
[17] Lai J, Su J, Li Z, et al. Impact of extracellular polymeric substances from Skeletonema costatum on the combined toxicity of microplastics and antibiotics in estuarine environment.. Marine pollution bulletin, 2025, 223: 119077. DOI: 10.1016/J.MARPOLBUL.2025.119077.
[18] Shi C, Yang J, Yang L, et al. Micro and macro interaction behaviors analysis between microplastics and antibiotics in complex hydrodynamic environment. Journal of Environmental Chemical Engineering, 2025, 13(6): 120341-120341. DOI: 10.1016/J.JECE.2025.120341.
[19] Sundar S, Jayaprakash N, Govindaraj D. Carbon-based nanomaterials in the remediation of antibiotics from aquatic environments: Advances, mechanisms, and future perspectives. Environmental Pollution and Management, 2026, 3: 99-116. DOI: 10.1016/J.EPM.2025.11.002.
[20] Pizzol D L J, Lubschinski L T, Mohr B T E, et al. Future Trends in Antibiotic Concentrations and Risk Assessment of Selection Pressure Based on Reported Antibiotic Concentrations in Brazil's Aquatic Environments.. Integrated environmental assessment and management, 2025. DOI:10.1093/INTEAM/VJAF177.
[21] Tateno B K, Ricchizzi E, Latour K, et al. Infections and antibiotic treatment in long-term care facilities: results from 1-year cross sectional study in three Polish settings.. Antimicrobial resistance and infection control, 2025, 14 (1): 142. DOI: 10.1186/S13756-025-01659-7.
[22] Chen W, Li L, Dai X, et al. Health risk and benefit assessment methods for antibiotic resistance bacteria/genes in the environment: A critical review. Journal of environmental management, 2025, 396: 128071. DOI: 10.1016/J.JENVMAN.2025.128071.

[23] Borah P, Roy S, Ahmaruzzaman M. Environmental fate of complex antibiotics in aquatic systems and its degradation by electrochemical advanced oxidation process: A holistic review of process variables, mechanistic insights, and implications. Journal of Environmental Chemical Engineering, 2025, 13(6): 120267-120267. DOI: 10.1016/J.JECE.2025.120267.

[24] Wang J, Tao Y. Effects of Antibiotics at Environmental Concentrations on Cyanobacteria and its Mechanisms: A Review Focusing on Hormesis. Current Pollution Reports, 2025, 11(1): 61-61. DOI: 10.1007/S40726-025-00390-6.

[25] Yi X, Cai H, Liu H, et al. Environmental exposure augments the abundance and transferability of antibiotic resistance genes in the respiratory tract. Cell reports, 2025: 116517. DOI: 10.1016/J.CELREP.2025.116517.

[26] Diabil J M H G, Jalali A, Komijani M. Metagenomic analysis of antibiotic resistance and pathogens in landfill leachates: Environmental implications.. Journal of hazardous materials, 2025, 500: 140365. DOI: 10.1016/J.JHAZMAT.2025.140365.

[27] Hamdi S, Issaoui M, González M A, et al. Agro-waste materials: A low-cost approach to ionophore antibiotics mitigation in aquatic environment. Bioresource Technology Reports, 2025, 32: 102412-102412. DOI: 10.1016/J.BITEB.2025.102412.

[28] Wang H, Guo J, Chen X. Comparative Profiling of Antibiotic Resistance Genes and Microbial Communities in Pig and Cow Dung from Rural China: Insights into Environmental Dissemination and Public Health Risks. Biology, 2025, 14(11): 1623-1623. DOI: 10.3390/BIOLOGY14111623.

[29] Hao W, Zhang H, Wang K, et al. Determination of quinolone antibiotic residues in surface water environments by THB-Salen-COFs combined with UPLC−MS/MS. Microchemical Journal, 2025, 219: 116059-116059. DOI: 10.1016/J.MICROC.2025.116059.

[30] Sun J, Xu C, Wang D, et al. Comprehensive Review on the Distribution, Environmental Fate, and Risks of Antibiotic Resistance Genes in Rivers and Lakes of China. Water, 2025, 17(22): 3228-3228. DOI: 10.3390/W17223228.

[31] Jiménez G M D, Matias F M, Paiva I, et al. Antibiotic–Cyclodextrin Interactions: An Effective Strategy for the Encapsulation of Environmental Contaminants. Molecules, 2025, 30(22): 4359-4359. DOI: 10.3390/MOLECULES30224359.

[32] Li B, Gao H, Li R, et al. Characteristics of regionalized distribution of antibiotics and ARGs in Daliao River-Liaodong Bay waters and their environmental impact factors. Journal of Environmental Sciences, 2026, 160: 722-731. DOI: 10.1016/J.JES.2025.04.060.

[33] Wäfler N, Knüsli J, Lhopitallier L, et al. Screening for antibiotics residues among adults with respiratory infections in primary care in Switzerland: evaluating over-the-counter use and environmental exposure. Clinical microbiology and infection: the official publication of the European Society of Clinical Microbiology and Infectious Diseases, 2025. DOI: 10.1016/J.CMI.2025.10.024.

[34] Malik S S, Sadaiappan B, Hassan A A, et al. Environmental Footprint of Antibiotics: A Multi-Source Investigation of Wastewater Systems in UAE. Antibiotics, 2025, 14(11): 1105-1105. DOI: 10.3390/ANTIBIOTICS14111105.

[35] Shu Q, Sun J, Li H, et al. Environmental safety evaluation of organic fertilizer produced from spiramycin fermentation residue via thermally activated persulfate integrated with aerobic composting: Effects on antibiotic resistance genes, microbial communities, and soil quality. Environmental Technology & Innovation, 2025, 40: 104596-104596. DOI: 10.1016/J.ETI.2025.104596.

[36] Wen L, Dai J, Ma J, et al. Comprehensive Profiling of Quinolone Antibiotics in the Bohai Sea: Occurrence, Source Apportionment, and Environmental Risks.. Environmental pollution (Barking, Essex : 1987), 2025, 387: 127338. DOI: 10.1016/J.ENVPOL.2025.127338.

[37] Nian Q, Zhang H, Wang K, et al. MOF-801 and polydopamine dual-modified PAN nanofiber membranes for simultaneous removal of multiple antibiotic classes from environmental water. Journal of Environmental Management, 2025, 395: 127706-127706. DOI: 10.1016/J.JENVMAN.2025.127706.

[38] Manzoor I, Vijayaraghavan R. Ag-Capped Zinc Peroxide (Ag–ZnO_2) Nanocomposite: An Efficient Heterostructure Photocatalyst for the Environmental Remediation of Organic Dyes and Pharmaceuticals Antibiotics Under UV and Sunlight Irradiation. International Journal of Environmental Research, 2025, 19(6): 272-272. DOI: 10.1007/S41742-025-00952-Y.

[39] Chi T, Liu Z, Zhang B, et al. Risk assessment of the spread of antibiotic resistance genes from hospitals to the receiving environment via wastewater treatment plants. Ecotoxicology and environmental safety, 2025, 306: 119264. DOI: 10.1016/J.ECOENV.2025.119264.

[40] Pandey K N, Simon M, Vishwakarma K R, et al. Exploring Microbial Diversity, Antibiotic Resistance, and their Environmental Drivers in Urban and Peri-Urban Riverbed Sediments of Sub-tropical River Basins.. Environmental research, 2025, 288 (P1): 123174. DOI: 10.1016/J.ENVRES.2025.123174.

[41] Wang Y, Wu H, Lou X, et al. Sustainable and microwave-assisted extraction of tetracycline antibiotics from environmental water via magnetic pH-responsive block copolymer.. Talanta, 2025, 298(PB): 129034. DOI: 10.1016/J.TALANTA.2025.129034.

[42] Zhang J, Chang X, Ma Y, et al. Environmentally relevant concentrations of representative aquatic compounds promote the conjugative transfer of antibiotic resistance genes. Journal of Water Process Engineering, 2025, 79: 108936-108936. DOI: 10.1016/J.JWPE.2025.108936.

[43] Zhang X, Liu J, Zhan T, et al. Environmental concentrations of benzalkonium chloride promote the horizontal transfer of extracellular antibiotic resistance genes via natural transformation. Process Safety and Environmental Protection, 2025, 203 (PB): 108003-108003. DOI: 10.1016/J.PSEP.2025.108003.

[44] Hammerton G J C, Hooton P S, Sands K, et al. Sublethal concentrations of antibiotics enhance transmission of antibiotic resistance genes in environmental Escherichia coli. Frontiers in Microbiology, 2025, 16: 1675089-1675089. DOI: 10.3389/FMICB.2025.1675089.

[45] Guo Y, Zhang Z, Wang J, et al. Microplastic-mediated interactions with antibiotics and antibiotic resistance genes in sludge: combined effects and environmental implications.. Environmental geochemistry and health, 2025, 47 (11): 506. DOI: 10.1007/S10653-025-02811-3.

[46] Wang W, Duan L, Sun Y, et al. Occurrence forms and transformation mechanisms of typical antibiotics in the aquatic environment of the Zaohe-Weihe River estuary. Environmental geochemistry and health, 2025, 47(11): 502. DOI: 10.1007/S10653-025-02816-Y.

Frontiers in Environmental Research
Print ISSN: 2960-0251
Online ISSN: 2960-026X
DOI: https://doi.org/10.61784/fer3041

SPATIOTEMPORAL EVOLUTION OF CULTIVATED LAND PATTERN AND MULTIDIMENSIONAL DRIVING FORCE MECHANISM IN HEILONGJIANG PROVINCE

YiHui Chen[1*], BoRui Li[2], XuSheng Zhao[1], BingYu Sun[2]
[1]*College of Science, Jiamusi University, Jiamusi 154004, Heilongjiang, China.*
[2]*School of Humanities, Jiamusi University, Jiamusi 154004, Heilongjiang, China.*
Corresponding Author: YiHui Chen, Email: 18745493112@163.com

Abstract: To deeply explore the dynamics of cultivated land use and its driving mechanism in Heilongjiang Province, a major grain-producing area in China, this study systematically reveals the spatiotemporal evolution characteristics of the cultivated land pattern in the study area over the past 20 years based on three phases of remote sensing of land use monitoring data (2000, 2010, and 2020) using methods such as land use transfer matrix and spatial analysis. On this basis, a driving force index system including natural factors (elevation, slope, precipitation, farmland production potential) and socioeconomic factors (population density, night-time light) was constructed. The Geographical Detector model was used to quantitatively examine explanatory capacity and interactive effects of each driving driver affecting the spatial heterogeneity of cultivated land changes in two time cross-sections (2000 and 2020). The research aims to clarify the evolution path of the cultivated land utilization pattern and its multidimensional driving force mechanism in Heilongjiang Province, providing a scientific basis for cultivated land protection, regional territorial space optimization, and the implementation of the national food security strategy.
Keywords: Cultivated land pattern; Land use transfer; Driving forces; Geographical detector; Heilongjiang province

1 INTRODUCTION

Land Use/Cover Change (LUCC) is a significant manifestation of human activities affecting the ecological environment and a key research agenda in global environmental change research [1,2]. Cultivated land is an important foundation for food production and a key resource for ensuring national food security and maintaining ecological balance. Against the backdrop of global climate change, continuous population growth, and increasingly severe resource and environmental constraints, how to achieve stable quantity and improved arable land quality has become one of the core issues of global sustainable development. For China, a country with a huge population, ensuring the stability and improvement of food production capacity is an important pillar of national security and social stability. Systematically identifying changes in cultivated land and their driving mechanisms not only helps optimize territorial spatial layout and improve land use efficiency but also has important strategic value for building a national food security guarantee system. As one among the world's principal black soil zones, Heilongjiang Province possesses unique cultivated land resources and high soil fertility, making it China's most important major grain-producing area and commodity grain base. Its grain output has ranked first in the country for many consecutive years, accounting for more than a quarter of the national total output. The commodity grain and grain transfer volumes account for about one-third and 40% of the national total, respectively, serving as a core underpinning for protecting national food security and boosting sustainable agricultural progress. However, amid the rapid advancement of industrialization and urbanization, Tilled terrain use in Heilongjiang Province is facing increasingly severe pressures. On the one hand, the non-agricultural conversion of cultivated land caused by the expansion of construction land persists, leading to a reduction in high-quality cultivated land resources. On the other hand, the non-grain production trend brought about by agricultural structure adjustment and the problem of black soil degradation caused by long-term intensive use have become increasingly prominent, including thinning soil layers, decreasing organic matter content, and intensified soil erosion, which restrict regional sustainable agricultural development and comprehensive grain production capacity. In this context, systematically analyzing the spatiotemporal evolution characteristics of the Tilled soil pattern in Heilongjiang Province over the past 20 years and identifying its main driving mechanisms are of great practical significance for deepening the understanding of land use processes, promoting high-quality regional agricultural development, and implementing the national food security strategy.

Domestic and foreign research on the evolution of cultivated land patterns and their driving forces has formed a relatively systematic theoretical and methodological system. Early studies mainly focused on the quantitative analysis alterations in the quantum and composition of arable land, often using methods such as land use dynamic degree and land use transfer matrix to evaluate the rate of cultivated land change and the type conversion relationship. As Remote Sensing (RS) and Geographic Information System (GIS) technologies advance, research has gradually expanded to the spatial dimension. The gravity center migration model has been used to analyze the spatial movement direction and change trend of cultivated land, and landscape pattern indices such as patch density, edge density, and shape index have been widely applied to characterize the degree of fragmentation, aggregation characteristics, and morphological complexity of Tilled terrain, thereby revealing the dynamic evolution process of the cultivated land spatial pattern. The

research paradigm of driving forces has undergone a transformation from qualitative analysis to quantitative modeling. Traditional statistical models, such as multiple linear regression and Logistic regression, have certain advantages in exploring the significance and direction of impact of driving factors, but they are difficult to effectively address the problems of multicollinearity and spatial autocorrelation among independent variables. To this end, researchers have introduced spatial dynamic simulation methods such as the CLUE-S model and cellular automata model to simulate the land use change process and predict future trends. In recent years, the Geographical Detector model has been widely used in the analysis of driving forces of land use change due to its advantages of no linear assumption, ability to handle type variables, and overcoming multicollinearity. By analyzing spatial stratified heterogeneity, this model quantitatively evaluates Each factor's capacity to elucidate the spatial disparities in geographical occurrences. and can identify the type and intensity of interactive effects among different driving factors, thus providing an effective means to reveal the multi-factor action mechanism of complex land systems.

Based on this, This investigation focuses on Heilongjiang Province. as the research area, aiming to systematically reveal the spatiotemporal evolution characteristics of the cultivated land pattern from 2000 to 2020 and quantitatively identify its dominant driving factors and interactive mechanisms. The main research contents include: (1) Using RS and GIS technologies to extract the spatial distribution information of cultivated land in 2000, 2010, and 2020, analyze the characteristics of Fluctuations in the extent of cultivated land, construct two phases of land use transfer matrices (2000-2010 and 2010-2020), and analyze the main transfer-in sources and transfer-out directions of cultivated land; (2) Using the factor detector of the Geographical Detector to quantitatively evaluate the explanatory power of natural and socioeconomic factors on the spatial differentiation of cultivated land; (3) Analyzing the type and intensity of interactive effects among different driving factors through the interaction detector, and revealing the comprehensive impact mechanism of multi-factor coupling on the evolution of the cultivated land pattern. This study aims to deepen the understanding of the spatiotemporal evolution laws and driving processes of cultivated land in Heilongjiang Province, providing a scientific basis and technical support for the optimal allocation of regional land resources, cultivated land protection, and the formulation of national food security policies.

2 COMPREHENSIVE OVERVIEW OF RESEARCH DOMAIN & INFO REPOSITORIES

2.1 Comprehensive Survey of the Research Region

Located in northeastern China, Heilongjiang Province has complex landforms, known as "five parts mountains, one part water, one part grass, and three parts farmland". The Sanjiang Plain and Songnen Plain are distributed in the northeastern and western parts, with fertile soil, abundant water resources, and synchronized rain and heat in summer, resulting in a high grain self-sufficiency rate and strong commodity grain output capacity. In 2023, The aggregate grain yield amounted to a substantial 155.76 billion kilograms., accounting for 11.2% of the national total grain output, ranking first in the country for 14 consecutive years, and achieving a bumper harvest for 20 consecutive years [3]. As the province with the largest cultivated land area in China, Heilongjiang Province serves as a pivotal commodity grain hub and stands out as a leading producer of rice., soybeans, and corn, with rich black soil resources and a solid agricultural foundation [4]. In 2018, grain production in Heilongjiang Province achieved a "15-year consecutive bumper harvest", with a total output reaching 7.5×10^11 kg. The total output, commodity volume, and transfer volume all ranked first in the country [5,6], making tremendous contributions to ensuring national food security. However, long-term intensive development has made the region face the dual pressures of black soil resource degradation and ecological environment protection.

2.2 Data Sources

The dataset employed in this research primarily encompasses land utilization resources., natural factor data, socio-economic factor data, and basic geographic data. Land utilization data is primarily sourced Derived from the China Land Cover Dataset (CLCD), which is based on Landsat series satellite imagery (TM/ETM+/OLI) and constructed using a random forest classification algorithm. The spatial resolution is 30 meters, with temporal coverage spanning 2000,2010, and 2020. The classification system includes categories such as arable land, forest land, grassland, water bodies, construction land, and bare land, demonstrating high classification accuracy.

Table 1 Data Source

Data Source	Data Name	Spatial Resolution	Data Description
Geospatial Data Cloud (SRTM)(http://www.gscloud.cn/)	China Land Cover Dataset (CLCD)	30m	-
Geospatial Data Cloud (SRTM)(http://www.gscloud.cn/)	elevation	90m	Extract topographic relief features
Calculated based on SRTMDEM	Slope	90m	Characterize topographic impact

Data Source	Data Name	Spatial Resolution	Data Description
NOAANCEI meteorological station data (https://www.ncei.nou.gov)	precipitation interpolation results	approximately 1km	Characterize climate humidity features
Chinese Academy of Sciences Resource and Environmental Science Data Center (http://www.resdc.cn/n)	Farmland production potential	1km	Characterize natural productivity level of cultivated land
WorkdPop dataset (https://www.worldpop.org)	Population	1km	Reflect population distribution density
2000: DMSP/OLS 2022: NPP/VHIRS	Nighttime lighting	approximately 1km	Characterize human activity intensity and urbanization level
TiantuMap (https://www.tianditu.gov.cn/)	administrative boundary	-	for the scope of the study area

Natural factor data include four categories: elevation, slope, precipitation, and farmland production potential. Among them, elevation data (DEM) are sourced from SRTM data provided by The Geospatial Data Cloud, boasting a spatial resolution of 90 meters,; slope data are calculated using ArcGIS spatial analysis tools based on DEM; precipitation data are sourced from meteorological station data of The National Oceanic and Atmospheric Administration (NOAA) of the United States of America, and spatially continuous precipitation distribution maps are generated using Kriging interpolation; The data on farmland production potential are sourced from the Resource and Environmental Science Data Center of the Chinese Academy of Sciences. This data comprehensively considers the impact of natural Elements such as illumination, temperature, water, and soil on crop yield to reflect the natural productivity level of cultivated land. Socioeconomic factor data include population and night-time light. Population figures are derived from the WorldPop database, boasting a spatial resolution of one kilometer., selecting two phases (2000 and 2020) to characterize population distribution and density. For night-time light data, DMSP/OLS stable night-time light images are used for 2000, utilizing NPP/VIIRS night-time light imagery for the year 2020. To ensure the comparability of the two phases of data, correction, denoising, and saturation correction processes are performed to reflect the intensity of human activities and urbanization level. In addition, indicators such as county-level GDP, total agricultural mechanization power, and urbanization rate from statistical yearbooks are integrated and spatially processed. To meet the requirements of model operation, all continuous variables are resampled to a 1km grid and discretized into 5 levels using the natural breaks method.

3 RESEARCH METHODS

3.1 Analysis of the Evolution of Cultivated Land Use Pattern

The land use transfer matrix serves as an esteemed approach for methodically assessing shifts in the composition and flow of regional land utilization patterns. It meticulously and thoroughly illustrates the magnitude and trend of interconversion among diverse land categories over the course of the study period. By constructing transfer matrices for two periods (2000-2010 and 2010-2020), the transfer-in sources (i.e., which land types are converted to cultivated land) and transfer-out directions (i.e., which land types cultivated land is converted to) of cultivated land in Heilongjiang Province can be clearly revealed, thereby providing a quantitative basis for understanding the specific process of dynamic changes in cultivated land.

3.2 Geographical Detector

This research primarily employs the stratified differentiation factor analyzer and interaction analyzer to conduct a quantitative examination of the driving forces behind the spatiotemporal dynamics of cultivated land utilization in Heilongjiang Province, as well as the interplay between these influencing elements. [7]. The Geographical Detector serves as a robust statistical technique designed to discern the spatial disparities among geographical entities and unravel the underlying factors that drive these variations, which is extensively utilized in the exploration of ecological and environmental transformations, as well as in the study of socioeconomic progression[8-10]. The specific model is as follows:

$$q=1-\frac{\sum_{i=1}^{L} N_i \sigma_i^2}{N\sigma^2}=1-\frac{SSW}{SST} \quad (1)$$

$$SSW=\sum_{i=1}^{L} N_i \sigma_i^2, \quad SST=N\sigma^2 \quad (2)$$

In the given equations, SSW represents the aggregate of intralayer variances, while SST denotes the comprehensive variance across the entire domain. L signifies the categorization of variable Y or factor X.; Nh is the number of units in layer h, and N is the number of units in the entire region; σ is the variance of Y values in layer h, and σ^2 is the variance

of Y values in the entire region. The range of q is [0,1]. A higher q value signifies a more pronounced spatial differentiation in the transition of cultivated land Y. Should the categorization be attributed to factor X, an elevated q value points to a greater capacity of factor X to elucidate the characteristic Y of cultivated land change, and conversely.
This research employs the Geographical Detector model to quantitatively assess the impact of various driving factors on the spatial variability of the cultivated land pattern, as well as to explore their interplay. According to the model requirements, the dependent variable (Y) needs to be a numerical type, and the independent variables (X) need to be type or categorical variables. This study selects the spatial distribution of cultivated land in two years (2000 and 2020) as the dependent variable and processes it into a binary variable based on 1 km grid units: if the sampling point in the grid falls within the cultivated land patch, it is assigned a value of 1, otherwise 0. Based on data availability and relevance to the research theme, this study constructs a driving factor index system including 6 factors in two categories (natural and socioeconomic): natural factors include X1 (elevation), X2 (slope), X3 (annual average precipitation), and X4 (farmland production potential); socioeconomic factors include X5 (population density) and X6 (night-time light intensity). To meet the model requirements, continuous independent variable data such as elevation and slope need to be discretized into type variables. This study adopts the natural breaks method, which can minimize within-group differences and maximize between-group differences, thereby better reflecting the natural clustering characteristics of the data. Each continuous variable is divided into 5 levels.

4 RESULTS

4.1 Spatiotemporal Pattern Evolution of Cultivated Land in Heilongjiang Province

4.1.1 Spatiotemporal change characteristics

Figure 1 Spatiotemporal Change Characteristics of Cultivated Land in Heilongjiang Province from 2000 to 2020

As shown in Figure 1, drawn by ArcGIS, from the spatiotemporal change characteristics of the three phases of cultivated land spatial distribution maps in Heilongjiang Province (2000, 2010, and 2020), over the past 20 years, the spatial scope and distribution form of cultivated land in the province have shown obvious dynamic evolution. The spatial distribution of prime agricultural land within the central region has maintained a consistent pattern, whereas the boundaries of cultivated land at the periphery have experienced periodic expansions and contractions in their delineation, showing an overall spatiotemporal change law of "stable core and active edge".

4.1.2 Spatial distribution characteristics

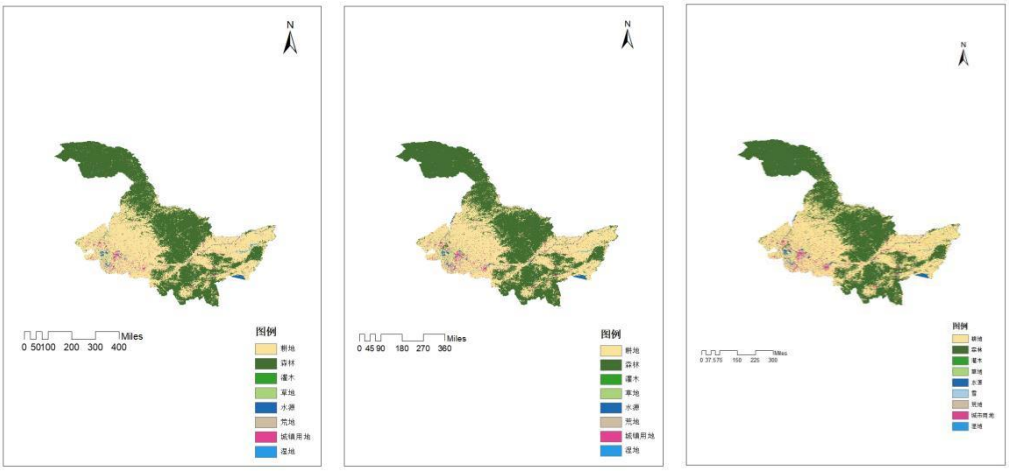

Figure 2 Changes in the Spatial Distribution Characteristics of Cultivated Land in Heilongjiang Province from 2000 to 2020

As shown in Figure 2, Rendered by ArcGIS, the spatial dispersion of cultivated land across Heilongjiang Province from 2000 to 2020 exhibits a pattern marked by "central concentration and peripheral oscillation." In the heartland of agriculture, such as the Songnen and Sanjiang Plains, the cultivated land has historically been densely packed, maintaining a consistent expanse. Conversely, at the province's periphery, particularly in mountainous regions and forest-grass transition zones, the cultivated land has undergone periodic fluctuations of expansion and retraction. This overarching spatial configuration not only sustains the agrarian edge of the central grain-growing regions but also manifests the adaptability in land utilization at the margins.

4.1.3 Analysis of cultivated land use transfer

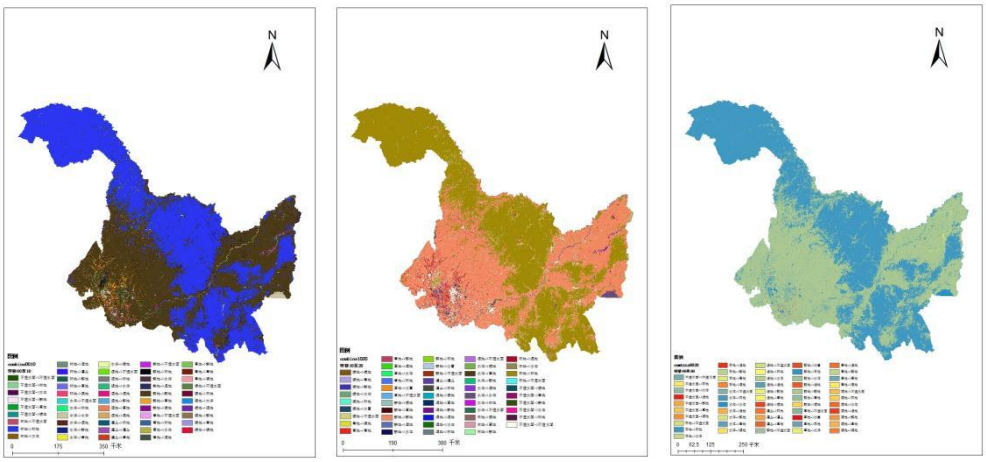

Figure 3 Analysis of Cultivated Land Use Transfer in Heilongjiang Province from 2000 to 2010, 2010 to 2020, and 2000 to 2020

As shown in Figure 3, Rendered by ArcGIS, the dynamics of cultivated land use in Heilongjiang Province between 2000 and 2020 are marked by a "bidirectional flux and categorical diversification." During the initial decade from 2000 to 2010, there was extensive interconversion among cultivated land, forestland, and grassland. This period witnessed, on one hand, the conversion of some forest and grassland into cultivated fields, indicative of the critical need for enhanced grain production at the time; conversely, the Grain for Green initiative led to the transformation of certain substandard cultivated areas into ecological lands. As the decade of 2010 to 2020 commenced, the pace of urbanization hastened, leading to a notable rise in the conversion of cultivated land into construction land. This trend was particularly pronounced in the vicinity of urban centers like Harbin and Daqing, where the encroachment upon prime cultivated land was especially evident. In sum, the trajectory of cultivated land distribution has shifted from a phase dominated by natural ecological interactions—primarily between agriculture, forestry, and grassland—to one characterized by construction encroachment and structural changes driven by socioeconomic factors.

4.2 Analysis of Driving Forces for the Evolution of Cultivated Land Pattern

4.2.1 Detection of spatial differentiation of driving factors and differences in their explanatory power

Drawing on the findings from the Geographical Detector, the degree of influence that geographical factors exert on the spatial variability of cultivated land in Heilongjiang Province has been quantitatively assessed. Analyzing the statistical

outcomes, it is observed that there exists a pronounced hierarchy in the explanatory prowess (q-value) of each contributing factor regarding the distribution of cultivated land, with the influence ranking as follows: farmland production potential (0.1546) > slope (0.0901) > precipitation (0.0645) > elevation (0.0487). The farmland production potential stands out with the highest q-value, successfully passing the 1% significance level test ($p<0.01$), suggesting that the composite natural attributes represented by this indicator—encompassing light, temperature, water, and soil—are pivotal in dictating the spatial configuration of cultivated land in the region, fundamentally shaping its macro distribution. Following as the predominant contributory element, the slope exhibits exceptional statistical significance ($p<0.01$), aligning closely with Heilongjiang Province's characteristics as a vast plain dedicated to agricultural production, and highlighting the direct impact of topography on agricultural mechanization and soil and water conservation efforts. Conversely, the explanatory strength of precipitation and elevation factors is relatively subdued, failing to meet the 0.05 significance threshold in univariate statistical analysis. This indicates that, at the provincial macro scale, altitude or precipitation alone are not adequate to account for the intricate patterns of cultivated land distribution, with their influences typically realized through synergistic interactions with other environmental gradients.

4.2.2 Multi-factor interaction and synergistic driving mechanism

The analysis results of the interaction detector further confirm that the evolution of the cultivated land use pattern in Heilongjiang Province is driven by the complex coupling of multiple natural factors, rather than the linear superposition of a single factor. The explanatory power (q-value) after the interaction of any two driving factors is significantly better than that of a single factor, showing a significant "two-factor enhancement" or "nonlinear enhancement" effect, revealing the integrity and synergy of the natural geographical system. Specifically, the interaction explanatory power between farmland production potential and slope is the strongest (q=0.2466), which is close to the sum of the single powers of the two factors, indicating that the matching of high-production potential soil and suitable terrain is the core driving force for the aggregation of cultivated land. More importantly, although the single-factor explanatory power of the precipitation factor is weak (q=0.0645), its q-value after interaction with slope jumps to 0.2094, which is significantly greater than the sum of the q-values of the two factors, showing a strong nonlinear enhancement effect. This finding profoundly clarifies the coupling mechanism of water and soil elements: the effectiveness of precipitation resources is significantly regulated by terrain slope, and their synergistic effect greatly improves the explanatory power for the spatial distribution of cultivated land. In addition, the interaction results between farmland production potential and precipitation (q=0.2199) and between farmland production potential and elevation (q=0.2191) also show high explanatory levels, further confirming that the environmental combination of multi-factor synergy optimization is the key foundation for the formation of high-quality cultivated land in Heilongjiang Province.

4.2.3 Suitability intervals and risk detection of cultivated land distribution

By analyzing the average value of cultivated land distribution under different factor classifications, the risk detector accurately identified the optimal environmental suitability intervals conducive to the aggregation of Tilled terrain. The statistical findings indicate that the allocation of cultivated land exhibits distinct threshold impacts and selective preferences across diverse influencing factors, with variations between different categories being statistically significant as evidenced by the t-test. In terms of farmland production potential, the average value of cultivated land distribution in the 2nd partition is the highest, and the medium and high-grade production potential areas are the main bearing spaces for cultivated land, reflecting the dependence of agricultural development on the natural background. Among the precipitation factors, the 1st partition shows an extremely high degree of cultivated land aggregation, which is significantly different from other precipitation gradients, indicating the absolute leading role of specific humid climate zones in the distribution of cultivated land. In terms of topographic factors, the 5th partition of the slope factor and the 4th partition of the elevation factor are the dominant distribution intervals in their respective dimensions. This nonlinear distribution characteristic reflects the adaptive choice of human activities within a specific range of altitude and slope. Overall, the cultivated land in Heilongjiang Province is not randomly distributed but highly aggregated in specific environmental combination intervals with high farmland production potential, abundant hydrothermal conditions, and suitable terrain. This distinctive feature of spatial concentration is a consequence of the interplay between the inflexible confines of the natural setting and the strategic adaptions made throughout the extensive history of agricultural progress.

5 CONCLUSION AND DISCUSSION

While this investigation has yielded significant insights, it is not without its constraints, which warrant further exploration in subsequent studies. The 1km resolution data used in this study can effectively reveal the pattern and driving forces at the macro scale, but may not capture more detailed changes at the micro scale, such as rural residential land consolidation and the occupation of facility agriculture. In the future, higher-resolution remote sensing images can be used for more detailed analysis. At the same time, the index system selected in this study mainly covers natural and socioeconomic factors, but fails to effectively quantify important driving factors such as policies, technologies, and transportation accessibility. For example, policies such as the Grain for Green project and agricultural subsidy policies have a direct and profound impact on changes in cultivated land, but it is challenging to spatialize them and incorporate them into the Geographical Detector model. The Geographical Detector model has significant advantages in revealing spatial heterogeneity and driving mechanisms of ecosystem services.

COMPETING INTERESTS

The authors have no relevant financial or non-financial interests to disclose.

FUNDING

This work was supported by the Jiamusi University Doctoral Special Research Fund Proiect(JMSUBZ2019-11). Heilongjiang Provincial Universities Basic Scientific Research Project(2019-KYYWF-1399). The authors are grateful to the editor and anonymous reviewers for their helpful comments and also acknowledge helpful comments by Chenglin Gu.

REFERENCES

[1] Sun L, Wei J, Duan D H, et al. Impact of land-use and land-cover change on urban air quality in representative cities of China. Journal of Atmospheric and Solar-Terrestrial Physics, 2016, 142: 43-54.
[2] Zhao Ruifeng, Wang Fuhong, Zhang Lihua, et al. Dynamic of farmland landscape and its socioeconomic driving forces in the middle reaches of the Heihe River. Scientia Geographica Sinica, 2017, 37(6): 920-928.
[3] Wang Shiyu, Liu Xuewei, Liu Qian, et al. Spatiotemporal change analysis of cultivated land resources in Heilongjiang Province from the perspective of food security. Heilongjiang Grain, 2024, (11): 53-55.
[4] Wei Dan, Kuang Enjun, Chi Fengqin, et al. Status and protection strategy of black soil resources in Northeast of China. Heilongjiang Agricultural Sciences, 2016(1): 158-161.
[5] Zhang Qingwei. Deepening agricultural supply-side reform. Heilongjiang Daily, 2019-3-13.
[6] Yan Bo, Hu Wenguo, Zhou Zhujun, et al. A survey on the position of Heilongjiang Province in ensuring national food security and the development direction of the grain industry. China's Grain Economy, 2019(4): 41-48.
[7] Wang Jinfeng, Xu Chengdong. Geodetector: Principle and prospective. Acta Geographica Sinica, 2017, 72(1): 116-134.
[8] Li Fan, Qiang Wenli, Liu Xiaojie, et al. Spatio-temporal evolution of meat production in China's counties and its influencing factors. Journal of Natural Resources, 2021, 36(5): 1224-1237.
[9] Zhong Yun, Zhao Beilei, Li Han. Co-agglomeration and spatial similarity: Based on the analysis of manufacturing and producer services in Guangzhou, China. Scientia Geographica Sinica, 2021, 41(3): 437-445.
[10] Guo Fuyou, Tong Lianjun, Qiu Fangdao, et al. Spatiotemporal differentiation characteristics and influencing factors of green development in the eco-economic corridor of the Yellow River Basin. Acta Geographica Sinica, 2021, 76(03): 726-739.